# Molecular mechanisms orchestrating the dynamics of secretory vesicle pools

by

Victor A. Cazares

A dissertation submitted in partial fulfillment
of the requirements for the degree of
Doctor of Philosophy
(Neuroscience)
in the University of Michigan
2015

Doctoral Committee:

Professor Edward L. Stuenkel, Chair
Professor Ronald W. Holz
Professor Leslie S. Satin
Associate Professor Michael M.A. Sutton
Professor Lois S. Weisman

Acknowledgements

First and foremost thanks to my adviser Edward Stuenkel who was an excellent mentor, friend and role model. Thanks also to members of the Stuenkel lab: Arasakumar Subramani, Antionette Williams, Widmann Hoerauf, Johnny Saldate, Meredith Njus, Sam Wing and Jason Shiau.

I would like to acknowledge the funding sources supporting my doctoral training and professional development: Ruth L. Kirschstein National Research Service Award (F31 NS 77810-4), National Institutes of Health; Rackham Merit Fellowship, Rackham School of Graduate Studies, University of Michigan; Neuroscience Scholars Fellowship, Society for Neuroscience, National Institutes of Health.

Special thanks to the dissertation committee members: Dr. Ronald Holz, Dr. Leslie Satin, Dr. Michael Sutton, Dr. Lois Weisman and the committee chair Dr. Edward Stuenkel.

I owe great gratitude to the following personal and professional mentors: Dr. Phil Corrado, Dr. Henry Schlinger, Dr. Jill Becker and especially Dr. William Martin. Also thanks to Dr. Michael Sutton, Dr. Geoff Murphy, Dr. Robert Thompson, Dr. Michael Uhler, and Dr. Asim Beg for intellectually stimulating discussions that advanced my professional training.

Thanks to the students and faculty associated with the Neurobiology course at the Marine Biological Laboratory in 2011. In addition, thanks to students and faculty associated with my research experiences in Trinity College, Dublin; specifically, Luke Healy and Donal Carney. These two experiences most prominently shaped my scientific outlook and allowed me to form a very strong network of enduring friendships in the neuroscience community. Thanks again to Ed Stuenkel for encouraging and supporting these activities.

Chapter 2 of this dissertation was previously published in the journal *Traffic* (http://www.ncbi.nlm.nih.gov/pubmed/24909540) copyrighted by John Wiley & Sons. The following are contributing authors: Arasakumar Subramani, Johnny Saldate, Widmann Hoerauf and Edward Stuenkel. This work was supported by NIH grant RO1 NIDDK-DK077050 to Edward Stuenkel. We also thank Dr. Yanan Hou for critical discussions related to the experiments and specific research reagents.

The following authors contributed to the work presented in Chapter 3 of this dissertation: Meredith Njus, Amanda Manly, Kumar Subramani, Yoav Ben-Simon, Dr. Michael Sutton, Dr. Uri Ashery and Dr. Edward Stuenkel. We also thank Christian Althaus, Cynthia Carruthers and Frederick Henry for critical discussions related to the experiments and specific research reagents.

Finally, I would like to acknowledge Caroline Walsh, Irene Cazares and Victor Cazares. As a lifelong career goal I strive to become an impactful scientist, but day-to-day I aim to make these three people, whom I care most for, proud of my efforts.

Table of Contents

Acknowledgements …… ii

List of Figures ……v

Abstract ……vii

Chapter

I. Introduction: The molecular machines that define $Ca^{2+}$-mediated exocytosis……1

II. Distinct actions of Rab3 and Rab27 GTPases on late stages of exocytosis of insulin……40

III. Dynamic partitioning of synaptic vesicle pools by the SNARE protein Tomosyn……98

IV. Discussion: Rab GTPases and SNARE proteins: The dynamic duo orchestrating vesicles to tune $Ca^{2+}$-mediated exocytosis……161

List of Figures

Figure

2.1: Adeno viral infection of pancreatic islet slices and electrophysiological identification of **β**-cells……70

2.2: Expression of Rab GAPs transitions Rab3 and Rab27 into GDP-bound states……72

2.3: Overexpression of Rab GAP proteins does not alter density of SGs adjacent to plasma membrane……74

2.4: Mobility of membrane adjacent SGs is unaffected by overexpression of GAP proteins……76

2.5: Determination of IRP and RRP size to sequentially applied step-depolarization pulse protocols in EGFP-infected **β**-cells……78

2.6: Rab27A is essential to development of IRP and key to defining RRP size in **β**-cells……80

2.7: Rab3 exerts a central role in rapid refilling of RRP in **β**-cells……82

2.8: Rab3 actions on rapid refilling of RRP are downstream of cAMP enhancement of IRP and RRP size……84

2.9: Summary of Chapter 2 findings……86

3.1: Tomo1 localizes to presynaptic boutons and inhibits evoked neurotransmitter release in cultured hippocampal neurons……136

3.2: Effects of Tomo1 expression on distribution of SVs among functionally defined presynaptic SV pools……138

3.3: Tomo1 serves as Cdk5 interacting partner and catalytic substrate with Cdk5 activation sensitive to neural activity……140

3.4: Tomosyn and Cdk5 share common signaling pathway regulating the TRP……142

3.5: Tomo1 interacts with Rab3A-GTP……144

3.6: Tomo1 interaction with Rab3A and Synapsin1 is regulated by Cdk5……146

3.7: Activity dependent phosphorylation of Tomo1 and its role in synaptic……148

4.1: Potential effects of Tomo on spine density and silent synapses……179

4.2: β-phorbol esters induce translocation of Munc13-1 and RIM2……181

4.3: Evidence for an interaction between Tomo1 and Ra27A ……183

Abstract

The secretion of chemical messengers via $Ca^{2+}$-dependent exocytosis of vesicles is fundamental to a wide-range of physiological events. Rab GTPases and SNARE proteins govern the temporal and spatial precision of transmitter release. Yet, little is known about their role in specifying the size and filling kinetics of functionally defined vesicle pools, which impact the strength and efficiency of exocytosis.

We first sought to delineate the distinct vs. overlapping roles of highly homologous Rab GTPase proteins, Rab3 and Rab27, which display high sequence homology, share protein-effectors, and may functionally compensate. To define their actions, we overexpressed Rab3GAP and/or EPI64A GTPase-activating protein in wild-type or Rab27-null cells to transit the Rab3 family or Rab27A to a GDP-bound inactive state. We found Rab27A is essential for generation of the functionally defined immediately releasable pool, Rab3 is essential for a kinetically rapid filling of the RRP, and both cooperate in populating the readily releasable granule pool (RRP). We conclude that while Rab3 and Rab27A cooperate to generate release-ready vesicles in β-cells, they also direct unique kinetic and functional properties of the exocytotic pathway.

We also investigated how the SNARE Tomosyn1 (Tomo1) regulates the partitioning of synaptic vesicle (SV) pools in hippocampal neurons. Tomo1 inhibits SV priming at the plasma membrane. Yet, its localization to SVs and cytosol uniquely positions it to

coordinate SV pool partitioning. We that find that Tomo1 controls SV transition between the Resting Pool and Total Recycling Pool (TRP), and modulates the RRP size. Tomo1's regulation of SV distribution between pools is sensitive to neural activity and requires Cdk5. We provide novel evidence for an interaction between Tomo1 and Rab3A-GTP, and through this with Synapsin1 proteins, known regulators of SV recruitment. In addition, Tomo1 regulatory control over the TRP occurred independent of its C-terminal SNARE domain. Hence, Tomo1 actions on neurotransmission extend beyond its known inhibition of SV priming into the RRP and may involve other effector proteins. Altogether, our results advance the understanding of how Rab and Tomosyn proteins coordinate steps of the vesicle cycle that lead to functional heterogeneity among vesicles and thus may determine modes of transmitter release.

# Chapter I:

# Introduction: The molecular machines that define $Ca^{2+}$-mediated exocytosis

## 1.1 Introduction

The secretion of chemical messengers via $Ca^{2+}$-dependent exocytosis of vesicles or dense core granules is a highly specialized and dynamic process occurring with high temporal and spatial precision. This process is fundamental to a wide-range of physiological processes and cell types, these include: the secretion of insulin from pancreatic β-cells, which regulates blood glucose level [1-3]; or the secretion of lytic granules from cytotoxic T-lymphocytes, which is important for destroying target cells during protective immune responses [4,5]. One of most complex secretory systems is that of the nervous system, which secretes dozens of classes of neurotransmitters, hormones and peptides from distinct neuronal cell types with differing stimulus coupling, modes of release and with functions ranging from sensory/motor processing to learning and cognition [6,7]. While these secretory systems diverge greatly in function and modes of secretion, many commonalities exist. This is best illustrated by studies that show how perturbations of molecules involved in $Ca^{2+}$-dependent exocytosis lead to deleterious conditions affecting many physiological systems and often impacting different species [8-14].

$Ca^{2+}$-dependent exocytosis can be described as a multi-step process culminating when a cell membrane depolarizes and triggers the opening of voltage-gated $Ca^{2+}$ channels (VGCC) causing a brief and local elevation in $Ca^{2+}$ concentrations. The opening of a VGCC causes the $Ca^{2+}$ concentration to rise to ~100mM within a 20 nm nanodomain at the site of the VGCC but this concentration then decreases within mS as the VGCCs close; at 200 nm from the VGCC the concentration is closer to ~10mM rising and falling within the order of 10 ms [15]. This transient elevation activates the release apparatus, which mediates the fusion of vesicles containing soluble as well as membrane-integral proteins and signaling lipids with the plasma membrane. During fusion of the two lipid bilayers, an aqueous channel termed the fusion pore (with a approximate 4nm diameter) develops allowing the soluble protein messengers within the vesicle to be released into the extracellular space. Opening of the fusion pore can be followed by the full-collapse of the vesicle into the plasma membrane thus becoming contiguous; or fusion pore opening can be transient without full-collapse. Subsequent to fusion and release, vesicles are recycled via one of two major routes, often depending on the cell-type. (1) Membranes and proteins can be retrieved via clathrin-mediated endocytosis and shuttled through an endosomal recycling pathway or, (2) locally recycled and refilled with transmitter for immediate reuse. In some cases, vesicles bypass conventional routes of endocytosis as they never collapse; subsequent to fusion pore opening and closing they remain near the plasma membrane in a release-ready state, referred to as 'kiss-and-stay' fusion; or they undock from the plasma and are locally recycled, known as 'kiss-and-run'.

*SNARE complex formation*

The fusion of vesicles is catalyzed by the formation of an ATP-dependent heterotrimeric SNARE (soluble *N*-ethylmaleimide-sensitive factor attachment protein receptor) protein complex, with formation of this SNARE complex constituting a process referred to as priming. SNARE proteins are classified as such in accordance to a conserved coiled-coil stretch of ~70 residues known as the SNARE motif. They are further subdivided as R, Qa, Qb or Qc types based on the positioning of the SNARE motif within a four-helix bundle. All SNARE complexes contain one member of each class forming into multiple layers of hydrophobic side chains and one central polar layer (called the zero ionic layer) in which R-SNAREs contribute arginine residues and each Q-SNARE a glutamine [16]. In neurosecretory systems and in insulin release the SNAREs are: VAMP2 which contains an R-SNARE, Syntaxin1A which contains a Qa; and SNAP25 which contains both a Qb and Qc. However, there are multiple variants within these SNARE protein families and in certain cell secretory processes or phases of secretion different family members participate to drive membrane fusion. In general, vesicle-associated proteins contain R-SNAREs while plasma membrane proteins contain Q-SNAREs. The formation of a fusiogenic SNARE complex is believed to be initiated when cognate SNAREs bind in *trans* at the N-terminal ends of each of the four SNARE motifs forming a highly stable four-helical bundle. The SNARE bundle then progressively zippers from N- to C-terminus bringing the membranes into closer apposition until fusion is catalyzed [17]. After fusion, the fully zippered *cis*-SNARE complex emanating from the plasma membrane is recycled by NSF and its adaptor protein, $\alpha$-SNAP, using ATP-hydrolysis.

*Calcium-mediated triggering of fusion*

Crucial to regulated exocytosis are mechanisms that clamp vesicle fusion (or said another way, halt the progression of SNARE complex formation from *trans* to *cis*) until a signal discharges or triggers it. The temporal precision of vesicle release then becomes directly proportional to the kinetics of signal onset and the sensitivity of the trigger to the signal. The best-characterized molecular trigger thus far has been the Synaptotagmin1 (Syt1), which contains an N-terminal transmembrane region coupling it onto vesicles and two cooperative C2 calcium/phospholipid-binding regions (C2A and C2B) at its C-terminus [18]. In addition, Syt1 has the ability to bind to Syntaxin1 and SNARE complexes [19]. Upon VGCC opening, 4-5 calcium ions bind to the Syt1 C2 domains within ~200-300 mS triggering its association to the plasma membrane and zippering of SNARE proteins [20]. Moreover, Syt1 function appears to be critical for limiting spontaneous vesicle release in neurons [21]. The affinity for calcium of sensors utilized in exocytosis are critical to the overall function, for example the release of small synaptic vesicles (SV) from neuronal cells and exocytosis of large-dense core vesicles (LDCV) in endocrine cells occurs in distinct kinetic phases largely determined by the sensitivity of the calcium sensors and their positioning with respect to the $Ca^{2+}$ entry site. With some exceptions, in both systems, Syt1 predominantly mediates the fast or immediate phase of release as it is a low affinity sensor, while Syt7 accounts for the slow component of LDCV fusion [22,23]. The slower component of SV release in neuronal cells is termed asynchronous and does not seem to depend on Syt1 function, alternative calcium sensors have been hypothesized including Syt2, Syt7 and Syt9; however the vesicle pools they affect and the specific characteristics they confer onto release modes are not well established [24,25].

Recent studies have suggested that the protein Complexin (Cpx) serves as another clamp for SV fusion. In this model, Cpx inserts an accessory α-helix into the partially zippered SNARE complex to prevent its full assembly and clamp spontaneous fusion. Upon VGCC activation, Syt1 is proposed to displace the Cpx clamp; but interestingly, a distinct N-terminal portion of Cpx then interacts with the membrane-insertion sequence of SNARE proteins and is believed critical for activating the force transfer of SNAREs [26,27]. In this model, the coordinated activities of Syt and Cpx proteins constitute a central clamping and triggering mechanism [24,28].

*Protein regulators essential for SNARE complex formation and fusion*

In addition to SNAREs, Munc13 and Munc18 protein families are also essential for $Ca^{2+}$-mediated exocytosis, though the precise reasons why remains unknown. The absence of either of these proteins results in near complete abrogation of neurotransmitter release [29-32]. The homologs of Munc18 and Munc13 in *C. elegans* are part of a large family of genes initially identified by a forward genetic screen for paralytic phenotypes ("UNCoordinated") with concomitant accumulations in acetylcholine suggesting deficits in neurotransmitter release [33]. Subsequently, the mammalian unc18 (Munc18) was found in affinity-purified Syntaxin from brain lysates [34] and shortly after Munc13 was identified as being present in neuronal synapses [35]. Although, their mechanisms are not well understood they are generally accepted to be essential for SNARE assembly and fusion. Munc18 binds to Syntaxin in two distinct conformations, (1) a self-inhibited 'closed' conformation, in which the N-terminal Habc-domain of Syntaxin folds over and binds to the SNARE motif, thus hindering SNARE complex formation; (2) an 'open' conformation, that is

receptive to SNARE complex formation. Early studies of Munc18 concluded that it served an inhibitory role as it stabilized Syntaxin in a closed non-fusiogenic conformation [36,37]. However, other studies showed that not only is Munc18 necessary, but that it facilitates release contradicted this notion [38,39]. It is now recognized that Munc18 remains in complex with Syntaxin located at the plasma membrane as SNARE complexes nucleate (though it appears it may change its binding sites and conformational structure) [34,40-42]. Thus, current models suggest that it may serve to select the right R-SNARE helix and prevent premature SNARE-assembly [43]. Munc13 is thought to be essential for switching Syntaxin from the closed to open conformations in order to relieve autoinhibition. While, the binding affinity between Munc13 domains and various Syntaxin domains are weak, most studies suggest that the central MUN domain of Munc13 stimulates opening of Syntaxin by extracting the SNARE motif. In fact, site-directed point mutations that stabilize Syntaxin in an open conformation rescue the SV release deficits seen in *C. elegans* unc13 mutants {[44,45]. In addition, NMR and fluorescence experiments show that expression of the MUN domain can accelerate the transition from the Munc18-1/closed Syntaxin-1 complex to the Munc18-1/SNARE-complex [46]. Moreover, evidence suggests that Munc13 proteins also play other roles, which coordinate the trafficking, tethering and positioning of vesicles with SNARE complex formation near VGCCs via interaction with scaffolding proteins like RIM and vesicle-associated proteins like RabGTPases.

*RIM proteins coordinate vesicles, SNARE complexes and VGCCs*

Since stimulus-dependent calcium elevations are brief and restricted to micro or nanodomains (50-100uM), the positioning of primed vesicles near calcium channels is

necessary to achieve the levels of synchronicity between VGCC activation and vesicle fusion onset observed in neuronal and endocrine exocytosis. As previously stated, while the calcium affinity of the sensor largely affects this coupling (i.e. Syt2 leads to much faster release than than Syt1 which is faster than Syt7); another site of potent regulation is the positioning of the sensor relative to the calcium source. At large synapses like the Calyx of held, VGCC—sensor coupling distance was estimated to be ~100 nm, suggesting that coupling is loose but can likely be compensated by the large number of SVs in a readily-releasable pool (~1,750 SVs)[47-49]; while at smaller cortical or hippocampal-type synapses (containing ~5-10 readily-releasable SVs) coupling is much tighter with only 10-20 nm distances [50,51]. One of the major scaffolding proteins that can spatially organize these molecules and processes are proteins of the RIM gene family. RIMs are endowed with the capability to bind and thus determine $Ca^{2+}$ channel density at a release site [52,53]. In fact, loss of RIM proteins in *Drosophila* leads to significant reductions in number of $Ca^{2+}$ channels at presynaptic active zones and concomitant decrease in $Ca^{2+}$ influx [54]. They were initially identified in a Rab3 binding screen (RabGTPase-interacting molecule) and proposed to be, and subsequently shown to be important in docking of vesicles [55,56]. Moreover, they have also been proposed to initiate a priming cascade via an interaction with Munc13 via an N-terminal zinc-finger motif. This interaction is thought to then relieve Munc13 from autoinhibitory homodimer conformations that consequently promotes Munc13—Syntaxin interactions; which then switches Syntaxin from autoinhibited—closed to open SNARE complex-receptive conformations [56-59]. The capability of RIM proteins to regulate multiple steps of the secretory pathway positions them to strongly change the strength and efficiency of secretion. In agreement with this notion, it is known that the

level of RIM proteins in neurons are strongly regulated by the ubiquitin-proteosome system in response to neural activity [60]; and its functions are critical for the expression of several types of presynaptic neural plasticity, though the precise mechanisms have yet to be identified [61-63].

*Vesicle recruitment to release sites and/or active zones*

The sites of exocytotic activity in neuronal cells of the mammalian hippocampus are localized to an axon terminal site or 'en passant' axonal swellings (termed boutons). These are distinctly characterized in electron micrographs by an accumulation or cluster of synaptic vesicles adjacent to an electron dense region apposed to the plasma membrane called the active zone (AZ). The AZ demarcates the presynaptic release sites of neurons; it is where VGCCs are actively localized to and it maintains a network of molecules (including RIM) that coordinates with vesicle-recruitment factors in order to dock and prime vesicles for release. In fact some AZs, such as the photoreceptor 'ribbon' synapses or the *Drosophila* neuromuscular junction contain additional specialized structures (ribbons or T-bars, respectively) which accelerate the rate at which synaptic vesicles can be recruited into the AZ [64]. Comparatively, endocrine or neuroendocrine release sites do not contain strong morphologically apparent AZ's even though they contain most of the same molecules found in AZs and these often appear to be spatially segregated on the PM. Perhaps, this reflects a morphological specialization of neuronal cells since the release of chemical messengers is highly restricted to small regions (0.2-0.5 mm diameter) directly opposite the post-synaptic receptor signaling region (postsynaptic density) and deviations from this strongly impact its excitability [65]. Despite lacking an active zone, endocrine cells do display

dynamic transport of LDCVs to sites of release, in fact, recent studies have suggested that continued recruitment of so-called “newcomer” granules which display minimal residence at the plasma membrane largely account for the sustained phase of insulin release, reviewed in ([66]).

Rabs are a class of small G-proteins belonging to the Ras superfamily, of which there exist many variants (>60 mammalian Rabs) and which are differentially distributed across many organelles and known to regulate membrane trafficking between different subcellular compartments in organisms from yeast to humans [67]. The central regulatory feature of Rabs is their ability to cycle between a GTP-active to a GDP inactive state, which often determines their ability to bind effectors and associate with vesicle membranes. Two additional regulatory proteins drive GTPase activity: Rab GTPase activating protein (GAP) accelerates the intrinsic rate of GTP hydrolysis and Rab GTP exchange factor (GEF) stimulates GTP binding [68]. From the Rab family, Rab3A is predominantly expressed in neurons and secretory cells accounting for ~25% of GTPase activity in the brain [69]. Rab3 has four protein isoforms (A-D), which appear to compensate for one another functionally; deletion of three isoforms leads to lethality if Rab3A is one of the deleted genes in mice [70]. Astonishingly, Rab3 proteins can be found on all synaptic vesicles in a nerve terminal at rest, each vesicle containing approximately 10 copies, but it is completely absent from the plasma membrane [71,72]. To explain this, studies have now shown via optical and biochemical methods that Rab3 proteins undergo GTPase activity during stimulated secretion and consequently are displaced from the vesicle membrane [73-75]. Furthermore, one recent report suggests that this is due to the ability of Syt1 to bind and sequester Rab3-GAP, thus reducing GTPase activity—only upon calcium binding does Syt1

release Rab3-GAP which can then stimulate the Rab3 GTP-GDP transition [76]. All studies to date suggest two major though seemingly contradictory roles for Rab3: (1) Recruitment of vesicle to release sites following stimulated depletion and (2) a molecular clamp or inhibitor of vesicle priming. Early evidence for these conclusions emanated from studies in neurosecretory cells showing that overexpression or microinjection of Rab3A or a constitutively GTP-bound mutant inhibits regulated exocytosis in chromaffin cells and PC12 cells [77-80]. In agreement with this, knock-out of the Rab3A gene in hippocampal neurons led to an enhancement in $Ca^{2+}$-dependent exocytosis with no changes in the number of vesicles that are docked, and/or primed release-ready [69,81]. Yet, quadruple knock-out of Rab3 led to approximately a 30% reduction in evoked release, with no changes in spontaneous release or number of primed readily-releasable vesicles [70]. Thus, it was not clear, was Rab3A facilitating or clamping secretion? Recent studies have offered some clarification of these discrepancies. Four separate studies confirmed that Rab3A was critical for recruitment of vesicles to release sites in isolated nerve terminals (synaptosomes), clonal pancreatic β-cells, mammalian chromaffin cells and photoreceptor cells of the tiger salamander (*Ambystoma tigrinum*) [56,82-84]. One revelatory conclusion from these studies was that the GTPase cycling of Rab3 serves as a regulatory gate during the transitions from docking to priming. Specifically, Rab3-GTP is critical for recruiting and docking vesicles presumably via its interaction with RIM proteins since point mutations in RIM (E36A/R37S), which abrogate Rab-binding lead to significant reductions in the number of docked granules [56]. Moreover, it is known that Rab3A can form a tripartite complex with Rim and Munc13 and also binds Munc18 directly when it is associated with the closed form of Syntaxin [58,85]. Thus, vesicles can be recruited to sites of SNARE

complex formation via sequencing of effector interactions [86]. One of the most critical observations was that Rab mutants inhibited the subsequent Munc13-induced transitions of Syntaxin from a closed to open state [56]. Though not explicitly tested, it is perceived that Rab3A cycling from GTP to GDP removes the clamp on priming via displacing a yet to be identified repressor protein and permitting SNARE complex formation {Muller:2011jv}. Moreover, these findings could also partly explain why not all granules docked at the plasma membrane are primed and release-ready.

Some of the early controversy surrounding Rab3's inhibitory vs. enhancing roles in secretion likely stemmed from the compensatory actions of other Rabs. For one, Rab3 has four distinct isoforms, which as previously stated, are able to functionally compensate for one another. Thus, early work in *C elegans,* which contains only one Rab3 protein more clearly distinguished Rab3's role in vesicle recruitment. This study observed that Rab3 null mutants in *C. elegans* have fewer vesicles near the active zone suggesting an involvement in transport and docking [87]. Further complicating the study of Rab3 was that another highly homologous Rab, which also appears to functionally compensate has been identified in both neuronal and endocrine secretory cells. Rab27 comes in two distinct isoforms (A,B); Rab27B is predominantly localized on neuronal SVs, while Rab27A is mainly on endocrine and neuroendocrine LDCVs . Very few studies have detailed the role of Rab27B in exocytosis, though it was discovered that Rab3A and Rab27B reside on distinct SV pools, although a degree of overlap was also demonstrated [75]. Furthermore, while Rab3A has been observed to readily disassociate from vesicles upon calcium induced exocytosis, Rab27(A,B) persists for a longer time on the membrane, suggesting that they have

overlapping but distinct functions [75,88]. In addition, Rab27 is rather unique as it has been found to bind effectors in both its GTP and GDP bound states [89-91].

The study of neuronal and secretory Rabs has been recently reinvigorated following the discovery of a second partially compensatory Rab. Subsequent to the discovery of SNARE proteins, a significant amount of enthusiasm was generated for discovering the 'bridge' linking vesicle recruitment/docking to the release machinery. This enthusiasm was furthered fueled by the exciting developments in model systems like yeast, wherein among many other discoveries, mutations of the GTPase Sec4 caused lethality and was associated with an accumulation of vesicles that were randomly distributed throughout the cell, implying that Sec4p is needed for the polarized delivery of secretory vesicles to budding sites [92]. Thus the initial genetic studies conducted in mice lacking all forms of the neuronal GTPase Rab3 (e.g. quadruple knock-out) were met with a certain degree of disappointment when it caused very mild phenotypes [70]. More recently, the identification of Rab GAP, GEF and the factor that dissociates Rabs from vesicles GDI (GTPase-dissociation inhibitor) has rekindled the excitement since their perturbation affects all Rab3 proteins and/or Rab27 and causes severe phenotypes. First, mutations in the Rab GDI gene that cause either a premature stop-codon or a reduction in Rab3 binding were found to be directly responsible for X-linked non-specific mental retardation in humans [93]. Next Rab3 GAP was identified and mutations were found to cause Warburg Micro syndrome and Martsolf syndrome, both of which exhibit mental retardation [94-99]. Importantly, these perturbations mainly affect Rab3 since Rab27 is paired with different GAPs (EPI64A/EPI64B) and is not as sensitive to disassociation from vesicles by Rab3 GDI. Therefore, these studies suggest that Rab3 may have some unique function, which cannot

be compensated by Rab27. In contrast, both Rab3 and Rab27 share the same GEF [100]. Studies conducted in mice deficient in Rab3 GEF were found to be perinatal lethal and showed a ~10-fold reduction in the number of vesicles and were found to have defective neuromuscular transmission, whereas post-synaptic function was normal [101]. In accordance, studies in *C. elegans* found that mutations in the Rab3 GEF homolog, AEX-3, caused a more severe synaptic transmission defect not seen in Rab-3 mutants alone—further study determined that Rab27 was also present and localized to nerve terminals and accounted for the non-Rab3 related deficits [102]. Altogether these data suggest significant roles for Rab GTPases in regulated $Ca^{2+}$ evoked secretion, yet given the number of Rabs present and the number of effectors they share, distinguishing unique and overlapping roles has remained a challenge.

*Vesicles coalesce into distinct functionally defined pools*

All discoveries in the field of secretion and neurotransmitter release can be traced back to the discoveries by Bernard Katz and his colleagues as they established that neurotransmitters are released in discrete "quanta" [103,104]. Since its initial development it has been shown that this theory does suffer some limitations, for example, there is some controversy regarding the variability in quantal size with coefficients of variation ranging from 0.22-0.6—but, these studies are technically challenging and more clarification is needed [105-109]. Nonetheless, the quantal model has been extremely useful and furthermore, these early studies determined that $Ca^{2+}$ regulates neurotransmitter release since reduction of extracellular [$Ca^{2+}$] significantly reduced the number of quanta released and increased the rate of failure in release. In addition, they hypothesized that presynaptic

terminals contained a pool of many quanta and that stimulation leads to the synchronous release of only a portion of this pool. Subsequent, electron-microscopic analysis of release sites discovered that what was referred to as "quanta" corresponded to vesicular membranes and determined that neurotransmitter presynaptic boutons contain up to ~500,000 vesicles at a frog NMJ [110]! In contrast, small release sites in the mammalian CNS (e.g. cortical, hippocampal) contain usually only ~100 but up to ~500 [111-115]. Functional studies then began to observe that repetitive stimulation led to a diminution in the amplitude of the post-synaptic response, suggesting that only a fraction of vesicles is 'release-ready' [116-118]. This was early evidence that not all vesicles share the same propensity for release and thus may be functionally categorized into distinct pools. Today, the functional categorization of vesicles has expanded to many different pools some of which are highly specialized. The following review will discuss only what are considered as the three major pools: Readily-releasable pool (RRP), Reserve Pool (RP) and the Resting Pool (ResP) [119]. For a full account of other SV pools refer to: [51,120]

*RRP*- The readily-releasable pool is composed of a small subset of vesicles (5-9 at small-central synapses, ~5% of the total vesicle pool) docked in the AZ. They have the highest probability of release (Pr) of all vesicles at the bouton and thus most significantly impact the strength of neurotransmitter release [121]. The RRP can be depleted with only few (5-15) high-frequency stimuli or via 1s exposure to a hypertonic solution (e.g. adding 0.5 mOsm / L Sucrose), the latter, by mechanisms that are not well understood [122-124]. Full replenishment of the RRP is variable and is modulated by the intracellular calcium concentration, it has a time constant of ~10-30 sec [125]. The size of the RRP scales proportionally with the size of the AZ, as do the number of docked vesicles and the relative

levels of immunogold-labeled Rim1/2 proteins and Cav2.1 VGCCs, leading many to hypothesize the existence of a limited number of RRP 'slots' [126-128]. Although it is generally assumed that each vesicle in the RRP has an equal probability of release, some studies at central synapses have shown otherwise[129,130]. This is certainly the case in chromaffin and β-cells, which have an immediately-releasable pool that sustains much faster kinetics than RRP vesicles [131-134]. The kinetics of secretory response were best described by membrane capacitance recordings in bovine chromaffin cells with millisecond time resolution following step-depolarizations or the flash photolysis of caged $Ca^{2+}$ [135,136]. These studies uncovered that the secretory response could be characterized by a double-exponential fit with time constants of 20–40 ms and ~300 ms constituting the RRP and Slowly Releasable Pool (SRP), respectively [137]. Depletion of these pools was followed by a sustained phase that is proportional to the rate of vesicle refilling [138,139].

*RP*- The recycling pool is often referred to as depot pool as it constitutes the reservoir from which depleted RRP vesicles are refilled. The size of the RP and the kinetics at which an RP vesicle can transition into an RRP can impose a direct limit on the rate of release from the RRP [140]. Thus, during periods of repetitive stimulation a limited or small recycling pool can significantly constrain rates of quantal neurotransmission [125,140]. In the CNS, the RP has been best characterized for hippocampal neurons where on average it accounts for ~40-50% of the total pool [111,141-143]. Transitions from the RP to the RRP can be defined by the rates at which any given vesicle can be reversibly docked and primed, a process that can be accelerated by increases in $[Ca^{2+}]$ [125,144-146]. In hippocampal neurons and in chromaffin cells, the time constant for refilling the RRP ranges from 5-10 s [140,147]. Though, not discussed here it should be noted that

alternative mechanisms have been suggested which may compensate for a small RP during a bout of activity, for example, rapid retrieval and reuse of SVs by mechanisms including kiss-and-run (~1s) or ultrafast endocytosis (50-100 ms) [148,149]. Moreover, others have suggested that what is rate-limiting during high rates of activity is not the number of vesicles or the rate of recycling but the number of 'slots' available for priming [127].

*ResP*- The RRP + RP fraction of vesicles are designated the Total Recycling Pool (TRP) and account for all vesicles actively going through repeated bouts of exocytosis and endocytosis. Interestingly, the TRP, on average only accounts for half the releasable quanta in neuronal cells. The remaining vesicles are recalcitrant to release even during prolonged stimulation that is sufficient to deplete the TRP. Interest and study of the ResP has increased significantly especially as optical tools have facilitated their study. Most commonly used are the pH-sensitive fluorescent probes termed pHluorins, which can be subcloned into lumenal domains of vesicle proteins, for example, VGLUT, VAMP, VMAT, Synaptophysin [150-152]. Expression of these reporters in neuronal or neuroendocrine cells leads to minimal fluorescence at rest. This is because the fluorescence of pHluorin is quenched in acidic compartments like the vesicle lumen (pH ~5.5). During spontaneous or stimulated fusion vesicles expose their intralumenal proteins to the neutral extracellular space (pH ~7.3) causing a conformational change in the pHluorin molecule and a 20-fold increase in fluorescence [153]. In addition, Styryl dyes, such as FM1-43, which are amphipathic compounds that can be used to label recycling synaptic vesicle membranes have been used extensively [154]. Some of these can also be photoconverted into an electron-dense material for further high-resolution structural analysis via electron microscopy [115,155]. From these studies it has been discovered that the ResP scales

dynamically in response to many physiological stimuli and to counteract strong perturbations. For example, blocking endocytosis elicits an unlocking of ResP vesicles into the RP [156]. Vesicle are also shifted between the ResP and RP to strengthen or reduce the amount of neurotransmitter release [141,157-159].

*Brief overview of modes of release in neuronal and insulin-secreting β-cells*

Despite the fact that neuronal tissue is derived from an embryonic germ layer distinct from that of β-cells (i.e. ectoderm, endoderm, respectively), they contain 15% of the conserved β-cell markers [160]. Nonetheless, it stands that these are not derived from common tissue, which has lead some to speculate that strong similarities in physiology, development and gene expression are a case of convergent evolution [161]. These commonalities, especially as they relate to the physiology of exocytosis, provide significant experimental advantages as they permit the study of how shared molecules function and form complexes that can produce strikingly different release modes that suit an evolutionary purpose.

Chemical transmission at small excitatory synapses (~1mm$^3$) of the central nervous system occurs when an action potential (AP) invades a bouton. The resulting membrane depolarization leads to the opening of VGCCs (primarily P/Q and N-type) and subsequent $Ca^{2+}$ influx [162]. This triggers the fusion of synaptic vesicles containing approximately 200mM glutamate which then activate AMPA (α-amino-3-hydroxy-5-methylisoxazole-4-propionic acid) receptors of a post-synaptic cell ~0.6 ms after the AP [20,163]. Important to note, AP firing is not a pre-requisite to SV release, for example, in hippocampal neurons spontaneous release of a quantum occurs on ~1-2 times per second. Their mechanism for

release, calcium sensor or vesicle pool source is still being determined [164,165]. However, compared to spontaneous release, upon opening of VGCC's, the rate of vesicle release is increased supralinearly, over 100,00 fold [43]. Evoked release of neurotransmitters occurs in two distinct phases, synchronous release occurring within milliseconds after the AP (and accounting for >90% of release); while asynchronous persist tens of millisecond and event up to tens of seconds [166]. During trains of APs the ratio of synchronous to asynchronous release can shift to a point where asynchronous dominates [167]. Interestingly, studies done in the Calyx of held revealed that both types of release exhibit similar $Ca^{2+}$ affinities (~40mM) but have different $Ca^{2+}$ cooperativity, which is a measure of the sensitivity of neurotransmitter release rate to changes in the synaptic $Ca^{2+}$ current [168,169]. This has led to a dual calcium sensor theory, though other explanations include: functional heterogeneity among vesicle pools, distance of vesicles from VGCCs, number of formed SNARE complexes and differences in the size of single quanta [168]. Finally, it is important to note that the firing of an AP does not always lead to vesicle fusion. In fact, in hippocampal neurons the probability that a single AP will elicit the fusion of at least one SV, termed neurotransmitter release probability (Pr) is generally very low < 0.3 [170]. Moreover, Pr can be highly variable between individual release sites from any given neuron, several electrophysiological and imaging studies have shown that synaptic terminals can individually and dynamically set their Pr through local feedback regulation [65,123,141,170-173].

Pancreatic β-cells produce insulin and store it in LDCVs. Single β-cells are approximately 10-12 micrometers in diameter and associate in clusters in a structure called the islet of Langerhans (named after the discoverer) [174]. As in neurons, exocytosis

is stimulated by membrane depolarization but in this case induced by the closing of a $K_{ATP}$ channel in response to elevations in extracellular glucose concentrations (~10mM). Specifically, increased glucose uptake by GLUT2 transporters leads to metabolic degradation and consequent shifts in the intracellular ATP/ADP ratio. The subsequent membrane depolarization causes the activation of L-type VGCC (Cav1.3) triggering a transient first-phase of insulin secretion lasting ~10 minutes. The first-phase of insulin secretion is thought to stem from release of RRP vesicles. Next, a second, prolonged phase of insulin secretion, which can last up to hours is thought to be supplied by RP vesicles that are mobilized only by metabolizable stimuli and ATP-dependent reactions. The second phase of insulin is thought to act independently but in synergy with the $K_{ATP}$-channel pathway. Interestingly, type-II diabetes is associated with a specific loss of insulin secretion during the first-phase. Like neurons, the RRP of β-cells is thought to only constitute ~5% of the total pool (~13,000 LDCVs). Moreover, within the RRP, a subset of more highly calcium-sensitive LDCVs releases with faster kinetics. The distribution of LDCVs has been examined by electron microscopy and found that 10% of granules are docked at the plasma membrane while up to 30% are within one granule diameter, suggesting that only half of the docked granules are primed [174]. Despite an abundance of LDCVs near the plasma membrane, many of which appear to be docked, recent experiments using live cell TIRF microscopy have uncovered that glucose stimulation leads to fusion of vesicles that are newly recruited and show minimal residence at the plasma membrane. In contrast, depolarization by Hi $K^+$ elicits fusion from the pool of vesicles that is already docked at the plasma membrane [56,175]. Altogether this suggests the existence of distinct stimulus-

secretion coupling mechanism that may involve the function of distinct Rab proteins and SNARE regulators [176].

*Preview to the dissertation: Molecular mechanisms that regulate the strength of exocytosis*

Priming a vesicle into a releasable state may at first glance seem as a straightforward process based on the SNARE hypothesis; however, if one considers the great number of molecules that have to act in the right time and place the challenge then becomes formidable and highly sensitive to molecular regulation. This concept is best illustrated by work done using *in vitro* reconstituted systems, which have shown that pairing of cognate SNAREs while sufficient to fuse membranes, fails to replicate rates and extent of vesicle fusion seen in cells. Interestingly, a recent *in vitro* study has more closely approximated 'cellular' fusion by reconstituting a Rab5 GTPase together with SNAREs thus forming more efficient machinery. They conclude that Rab proteins are required for and confer additional specificity and efficiency to SNARE complex formation [177]. Nonetheless, even in this study, only a set of 17 reconstituted human proteins were used together with a limited lipid composition in comparison with in-cell systems in which a synaptic vesicle contains ~80 different integral proteins and when docked is associated with up to ~269 proteins [72,178].

The goals of these investigations are to identify some of the critical membrane organizers, which can confer molecular specificity and thus coordinate docking and priming. Given the fundamental role of Rab GTPases in targeting and recruiting vesicles to sites of release, one of the main focuses of this dissertation was to try to resolve the distinct vs. overlapping roles of Rab3 and Rab27 proteins in vesicle exocytosis (Chapter 1). These

studies were conducted using membrane capacitance measurement of exocytosis from insulin secreting β-cells. This model allowed us to precisely dissect the kinetic contributions of each Rab GTPase on vesicle recruitment and in setting the size of vesicle pools. Moreover, results gleaned from these studies offer a significant mechanistic contribution that may eventually help explain deficits in the first-phase of insulin release associated with type-II diabetes.

The next set of studies (Chapter 2) was aimed at characterizing the functions of an R-SNARE protein termed Tomosyn. Unlike most SNARE proteins Tomosyn is not membrane anchored by a C-terminal transmembrane region [179]. It is not completely unique in this, for example SNAP25 also does not have a C-terminal transmembrane region but it does associate with membranes by palmitoylation [180]. Moreover, Tomosyn is a very large protein relative to most SNAREs, which don't carry many other protein binding domains outside of the SNARE motif. Tomosyn's R-SNARE motif is highly homologous to that of VAMP2 and thus can compete for the formation of trimeric SNARE complexes [181-183]. In contrast to, VAMP2/Synataxin/SNAP25 complexes, those containing Tomosyn instead of VAMP2 are non-fusiogenic [181,183,184]. Moreover, the larger N-terminal domain of Tomosyn is enriched with WD40-repeats that are predicted to form into twin β-propeller structures [179]. Tomosyn proteins are predicted to be highly homologous to the structure of the yeast Sro7 [179,185]. Interestingly, mutations in the yeast Sro7 lead to lethality and growth defects caused by clustering of what appears as non-fusiogenic vesicles [14]. Many studies have concluded that Sro7p coordinates with the Rab GTPase Sec4p to target vesicles to fusion sites via interactions with the SNARE Sec9p [14,186-188]. In mammals, two genes Tomosyn1 and Tomosyn2 encode 7 differentially spliced proteins

and have been localized to the cytosol, plasma membrane and both synaptic as well as insulin-containing vesicles [189-193]. Functional studies in mammalian and invertebrate models indicate that Tomosyn1 is an inhibitor of priming, though the specific mechanism by which it does this has not been defined [8,182,194-201]. Studies done using *in vitro* reconstituted fusion assays or lipid mixing have established that Tomosyn does compete with VAMP to limit the formation of SNARE complexes [183,184]. However, in cellular systems this mechanism has not been established as necessary or sufficient to inhibit exocytosis as expression of mutants lacking the C-terminal domain still inhibit [179,198]. In *C. elegans,* Tomosyn has been established as a direct functional competitor with Unc13 since the deficits caused by Unc13 mutations can be rescued by removing Tomosyn [197,202]. This suggest that Tomosyn has a central role in vesicle priming, a conclusion which was further strengthened by studies in chromaffin cells, which show clearly that Tomosyn1 expression leads to a reduction in the RRP size; however in addition they find that refilling of the RRP is also strongly reduced [194]. Thus it remains unclear, how does Tomosyn inhibit and does it inhibit only RRP formation via SNARE mediated clamping? Or is it an active regulator of vesicle recruitment upstream of SNARE complex formation?

To answer some of these questions we conducted a series of studies in rat hippocampal release sites where vesicle pool sizes have been well characterized and measurements of the dynamics of each pool are accessible via fluorescent reporters. By studying the role of Tomosyn in vesicle pool partitioning we are able to uncover whether its regulation is limited to only the final steps is SV priming. Moreover, based on the high homology with the yeast protein Sro7p, our experiments sought to uncover if Tomosyn proteins can also coordinate with Rab GTPases and may account for how Tomosyn proteins

can render vesicles recalcitrant to release. Finally, given the dynamic nature of neuronal neurotransmission we investigated the role of Tomosyn in the activity-dependent tuning of neurotransmitter release strength.

## 1. 2 Bibliography


1. MacDonald PE, Rorsman P. Oscillations, intercellular coupling, and insulin secretion in pancreatic beta cells. PLoS Biol 2006;4:e49.

2. Porte D, Kahn SE. beta-cell dysfunction and failure in type 2 diabetes: potential mechanisms. Diabetes 2001;50 Suppl 1:S160–3.

3. Henquin JC. Triggering and amplifying pathways of regulation of insulin secretion by glucose. Diabetes 2000;49:1751–1760.

4. Neumann H, Medana IM, Bauer J, Lassmann H. Cytotoxic T lymphocytes in autoimmune and degenerative CNS diseases. Trends in Neurosciences 2002;25:313–319.

5. Hong W. Cytotoxic T lymphocyte exocytosis: bring on the SNAREs! Trends Cell Biol 2005;15:644–650.

6. Südhof TC. Neurotransmitter release: the last millisecond in the life of a synaptic vesicle. 2013;80:675–690.

7. Südhof TC, Malenka RC. Understanding synapses: past, present, and future. 2008;60:469–476.

8. Barak B, Okun E, Ben-Simon Y, Lavi A, Shapira R, Madar R, Wang Y, Norman E, Sheinin A, Pita MA, Yizhar O, Mughal MR, Stuenkel E, van Praag H, Mattson MP, Ashery U. Neuron-specific expression of tomosyn1 in the mouse hippocampal dentate gyrus impairs spatial learning and memory. Neuromolecular medicine 2013;15:351–363.

9. Kumar R, Corbett MA, Smith NJC, Jolly LA, Tan C, Keating DJ, Duffield MD, Utsumi T, Moriya K, Smith KR, Hoischen A, Abbott K, Harbord MG, Compton AG, Woenig JA, Arts P, Kwint M, Wieskamp N, Gijsen S, Veltman JA, Bahlo M, Gleeson JG, Haan E, Gecz J. Homozygous mutation of STXBP5L explains an autosomal recessive infantile-onset neurodegenerative disorder. Hum Mol Genet 2015;24:2000–2010.

10. Davis LK, Meyer KJ, Rudd DS, Librant AL, Epping EA, Sheffield VC, Wassink TH. Novel copy number variants in children with autism and additional developmental anomalies. J Neurodev Disord 2009;1:292–301.

11. Bhatnagar S, Oler AT, Rabaglia ME, Stapleton DS, Schueler KL, Truchan NA, Worzella SL, Stoehr JP, Clee SM, Yandell BS, Keller MP, Thurmond DC, Attie AD. Positional cloning of a type 2 diabetes quantitative trait locus; tomosyn-2, a negative regulator of insulin secretion. PLoS Genet 2011;7:e1002323.

12. Ye S, Huang Y, Joshi S, Zhang J, Yang F, Zhang G, Smyth SS, Li Z, Takai Y, Whiteheart SW. Platelet secretion and hemostasis require syntaxin-binding protein STXBP5. J

Clin Invest 2014;124:4517–4528.

13. Barak B, Shvarts-Serebro I, Modai S, Gilam A, Okun E, Michaelson DM, Mattson MP, Shomron N, Ashery U. Opposing actions of environmental enrichment and Alzheimer's disease on the expression of hippocampal microRNAs in mouse models. Transl Psychiatry 2013;3:e304.

14. Rossi G, Brennwald P. Yeast homologues of lethal giant larvae and type V myosin cooperate in the regulation of Rab-dependent vesicle clustering and polarized exocytosis. Mol Biol Cell 2011;22:842–857.

15. Neher E. Vesicle Pools and Ca2+ Microdomains: New Tools for Understanding Their Roles in Neurotransmitter Release. 1998;20:389–399.

16. Antonin W, Fasshauer D, Becker S, Jahn R, Schneider TR. Crystal structure of the endosomal SNARE complex reveals common structural principles of all SNAREs. Nat Struct Biol 2002;9:107–111.

17. Hanson PI, Roth R, Morisaki H, Jahn R, Heuser JE. Structure and conformational changes in NSF and its membrane receptor complexes visualized by quick-freeze/deep-etch electron microscopy. Cell 1997;90:523–535.

18. Chapman ER. How does synaptotagmin trigger neurotransmitter release? Annu Rev Biochem 2008;77:615–641.

19. Vrljic M, Strop P, Ernst JA, Sutton RB, Chu S, Brunger AT. Molecular mechanism of the synaptotagmin-SNARE interaction in Ca2+-triggered vesicle fusion. Nat Struct Mol Biol 2010;17:325–331.

20. Lisman JE, Raghavachari S, Tsien RW. The sequence of events that underlie quantal transmission at central glutamatergic synapses. Nat Rev Neurosci 2007;8:597–609.

21. Littleton JT, Stern M, Schulze K, Perin M, Bellen HJ. Mutational analysis of Drosophila synaptotagmin demonstrates its essential role in Ca(2+)-activated neurotransmitter release. Cell 1993;74:1125–1134.

22. Schonn J-S, Maximov A, Lao Y, Südhof TC, Sørensen JB. Synaptotagmin-1 and -7 are functionally overlapping Ca2+ sensors for exocytosis in adrenal chromaffin cells. Proceedings of the National Academy of Sciences 2008;105:3998–4003.

23. Xu J, Mashimo T, Südhof TC. Synaptotagmin-1, -2, and -9: Ca(2+) sensors for fast release that specify distinct presynaptic properties in subsets of neurons. 2007;54:567–581.

24. Sun J, Pang ZP, Qin D, Fahim AT, Adachi R, Südhof TC. A dual-Ca2+-sensor model for neurotransmitter release in a central synapse. Nature 2007;450:676–682.

25. Saraswati S, Adolfsen B, Littleton JT. Characterization of the role of the Synaptotagmin family as calcium sensors in facilitation and asynchronous neurotransmitter release. Proc Natl Acad Sci U S A 2007;104:14122–14127.

26. Giraudo CG, Garcia-Diaz A, Eng WS, Chen Y, Hendrickson WA, Melia TJ, Rothman JE. Alternative zippering as an on-off switch for SNARE-mediated fusion. Science 2009;323:512–516.

27. Maximov A, Tang J, Yang X, Pang ZP, Südhof TC. Complexin controls the force transfer from SNARE complexes to membranes in fusion. Science 2009;323:516–521.

28. Huntwork S, Littleton JT. A complexin fusion clamp regulates spontaneous neurotransmitter release and synaptic growth. Nat Neurosci 2007;10:1235–1237.

29. Richmond JE, Davis WS, Jorgensen EM. UNC-13 is required for synaptic vesicle fusion in C. elegans. Nat Neurosci 1999;2:959–964.

30. Augustin I, BETZ A, Herrmann C, Jo T, Brose N. Differential expression of two novel Munc13 proteins in rat brain. Biochem J 1999;337 ( Pt 3):363–371.

31. Verhage M, Maia AS, Plomp JJ, Brussaard AB, Heeroma JH, Vermeer H, Toonen RF, Hammer RE, van den Berg TK, Missler M, Geuze HJ, Südhof TC. Synaptic assembly of the brain in the absence of neurotransmitter secretion. Science 2000;287:864–869.

32. Varoqueaux F, Sigler A, Rhee J-S, Brose N, Enk C, Reim K, Rosenmund C. Total arrest of spontaneous and evoked synaptic transmission but normal synaptogenesis in the absence of Munc13-mediated vesicle priming. Proc Natl Acad Sci U S A 2002;99:9037–9042.

33. Brenner S. The genetics of behaviour. Br Med Bull 1973;29:269–271.

34. Hata Y, Slaughter CA, Südhof TC. Synaptic vesicle fusion complex contains unc-18 homologue bound to syntaxin. Nature 1993;366:347–351.

35. Brose N, Hofmann K, Hata Y, Südhof TC. Mammalian Homologues of Caenorhabditis elegans unc-13 Gene Define Novel Family of C2-domain Proteins. J Biol Chem 1995;270:25273–25280.

36. Yang B, Steegmaier M, Gonzalez LC, Scheller RH. nSec1 binds a closed conformation of syntaxin1A. J Cell Biol 2000;148:247–252.

37. Dong Y, Wan Q, Yang X, Bai L, Xu P. Interaction of Munc18 and Syntaxin in the regulation of insulin secretion. Biochemical and Biophysical Research Communications 2007;360:609–614.

38. Toonen RFG, Verhage M. Munc18-1 in secretion: lonely Munc joins SNARE team and

takes control. Trends in Neurosciences 2007;30:564–572.

39. Jorgacevski J, Potokar M, Grilc S, Kreft M, Liu W, Barclay JW, Bückers J, Medda R, Hell SW, Parpura V, Burgoyne RD, Zorec R. Munc18-1 Tuning of Vesicle Merger and Fusion Pore Properties. J Neurosci 2011;31:9055–9066.

40. Dulubova I, Sugita S, Hill S, Hosaka M, Fernandez I, Südhof TC, Rizo J. A conformational switch in syntaxin during exocytosis: role of munc18. EMBO J 1999;18:4372–4382.

41. Khvotchev M, Dulubova I, Sun J, Dai H, Rizo J, Südhof TC. Dual modes of Munc18-1/SNARE interactions are coupled by functionally critical binding to syntaxin-1 N terminus. J Neurosci 2007;27:12147–12155.

42. D'Andrea-Merrins M, Chang L, Lam AD, Ernst SA, Stuenkel EL. Munc18c interaction with syntaxin 4 monomers and SNARE complex intermediates in GLUT4 vesicle trafficking. J Biol Chem 2007;282:16553–16566.

43. Jahn R, Fasshauer D. Molecular machines governing exocytosis of synaptic vesicles. Nature 2012;490:201–207.

44. Richmond JE, Weimer RM, Jorgensen EM. An open form of syntaxin bypasses the requirement for UNC-13 in vesicle priming. Nature 2001;412:338–341.

45. Madison JM, Nurrish S, Kaplan JM. UNC-13 interaction with syntaxin is required for synaptic transmission. Curr Biol 2005;15:2236–2242.

46. Ma C, Li W, Xu Y, Rizo J. Munc13 mediates the transition from the closed syntaxin–Munc18 complex to the SNARE complex. Nat Struct Mol Biol 2011;18:542–549.

47. Sakaba T, Neher E. Calmodulin Mediates Rapid Recruitment of Fast-Releasing Synaptic Vesicles at a Calyx-Type Synapse. 2001;32:1119–1131.

48. Sätzler K, Söhl LF, Bollmann JH, Borst JGG, Frotscher M, Sakmann B, Lübke JHR. Three-dimensional reconstruction of a calyx of Held and its postsynaptic principal neuron in the medial nucleus of the trapezoid body. J Neurosci 2002;22:10567–10579.

49. Meyer AC, NEHER E, Schneggenburger R. Estimation of quantal size and number of functional active zones at the calyx of Held synapse by nonstationary EPSC variance analysis. J Neurosci 2001;21:7889–7900.

50. Vyleta NP, Jonas P. Loose coupling between Ca2+ channels and release sensors at a plastic hippocampal synapse. Science 2014;343:665–670.

51. Rizzoli SO, Betz WJ. Synaptic vesicle pools. Nat Rev Neurosci 2005;6:57–69.

52. Kaeser PS, Deng L, Wang Y, Dulubova I, Liu X, Rizo J, Südhof TC. RIM proteins tether

Ca2+ channels to presynaptic active zones via a direct PDZ-domain interaction. Cell 2011;144:282–295.

53. Han Y, Kaeser PS, Südhof TC, Schneggenburger R. RIM determines $Ca^2$+ channel density and vesicle docking at the presynaptic active zone. 2011;69:304–316.

54. Liu KSY, Siebert M, Mertel S, Knoche E, Wegener S, Wichmann C, Matkovic T, Muhammad K, Depner H, Mettke C, Bückers J, Hell SW, Müller M, Davis GW, Schmitz D, Sigrist SJ. RIM-binding protein, a central part of the active zone, is essential for neurotransmitter release. Science 2011;334:1565–1569.

55. Wang Y, Okamoto M, Schmitz F, Hofmann K, Südhof TC. Rim is a putative Rab3 effector in regulating synaptic-vesicle fusion. Nature 1997;388:593–598.

56. Yasuda T, Shibasaki T, Minami K, Takahashi H, Mizoguchi A, Uriu Y, Numata T, Mori Y, Miyazaki J-I, Miki T, Seino S. Rim2α Determines Docking and Priming States in Insulin Granule Exocytosis. Cell Metab 2010;12:117–129.

57. Deng L, Kaeser PS, Xu W, Südhof TC. RIM Proteins Activate Vesicle Priming by Reversing Autoinhibitory Homodimerization of Munc13. 2011;69:317–331.

58. Dulubova I, Lou X, Lu J, Huryeva I, Alam A, Schneggenburger R, Südhof TC, Rizo J. A Munc13/RIM/Rab3 tripartite complex: from priming to plasticity? EMBO J 2005;24:2839–2850.

59. Koushika SP, Richmond JE, Hadwiger G, Weimer RM, Jorgensen EM, Nonet ML. A post-docking role for active zone protein Rim. Nat Neurosci 2001;4:997–1005.

60. Jiang X, Litkowski PE, Taylor AA, Lin Y, Snider BJ, Moulder KL. A Role for the Ubiquitin-Proteasome System in Activity-Dependent Presynaptic Silencing. Journal of Neuroscience 2010;30:1798–1809.

61. Müller M, Liu KSY, Sigrist SJ, Davis GW. RIM Controls Homeostatic Plasticity through Modulation of the Readily-Releasable Vesicle Pool. J Neurosci 2012;32:16574–16585.

62. Castillo PE, Schoch S, Schmitz F, Südhof TC, Malenka RC. RIM1alpha is required for presynaptic long-term potentiation. Nature 2002;415:327–330.

63. Nicoll RA, Schmitz D. Synaptic plasticity at hippocampal mossy fibre synapses. Nat Rev Neurosci 2005;6:863–876.

64. Südhof TC. The presynaptic active zone. 2012;75:11–25.

65. Branco T, Staras K. The probability of neurotransmitter release: variability and feedback control at single synapses. Nat Rev Neurosci [Internet] 2009;10:373–383. Available from: http://www.nature.com/doifinder/10.1038/nrn2634

66. Gaisano HY. Here come the newcomer granules, better late than never. Trends in Endocrinology & Metabolism 2014;:1–8.

67. Hutagalung AH, Novick PJ. Role of Rab GTPases in membrane traffic and cell physiology. Physiol Rev 2011;91:119–149.

68. Barr F, Lambright DG. Rab GEFs and GAPs. Curr Opin Cell Biol 2010;22:461–470.

69. Geppert M, Bolshakov VY, Siegelbaum SA, Takei K, De Camilli P, Hammer RE, Südhof TC. The role of Rab3A in neurotransmitter release. Nature 1994;369:493–497.

70. Schlüter OM, Schmitz F, Jahn R, Rosenmund C, Südhof TC. A complete genetic analysis of neuronal Rab3 function. J Neurosci 2004;24:6629–6637.

71. Matteoli M, Takei K, Cameron R, Hurlbut P, Johnston PA, Südhof TC, Jahn R, De Camilli P. Association of Rab3A with synaptic vesicles at late stages of the secretory pathway. J Cell Biol 1991;115:625–633.

72. Takamori S, Holt M, Stenius K, Lemke EA, Grønborg M, Riedel D, Urlaub H, Schenck S, Brügger B, Ringler P, Müller SA, Rammner B, Gräter F, Hub JS, De Groot BL, Mieskes G, Moriyama Y, Klingauf J, Grubmüller H, Heuser J, Wieland F, Jahn R. Molecular anatomy of a trafficking organelle. Cell 2006;127:831–846.

73. Fischer von Mollard G, Südhof TC, Jahn R. A small GTP-binding protein dissociates from synaptic vesicles during exocytosis. Nature 1991;349:79–81.

74. Fischer von Mollard G, Stahl B, Khokhlatchev A, Südhof TC, Jahn R. Rab3C is a synaptic vesicle protein that dissociates from synaptic vesicles after stimulation of exocytosis. J Biol Chem 1994;269:10971–10974.

75. Pavlos NJ, Grønborg M, Riedel D, Chua JJE, Boyken J, Kloepper TH, Urlaub H, Rizzoli SO, Jahn R. Quantitative analysis of synaptic vesicle Rabs uncovers distinct yet overlapping roles for Rab3a and Rab27b in Ca2+-triggered exocytosis. J Neurosci 2010;30:13441–13453.

76. Cheng Y, Wang J, Wang Y, Ding M. Synaptotagmin 1 directs repetitive release by coupling vesicle exocytosis to the Rab3 cycle. Elife 2015;4.

77. Holz RW, Brondyk WH, Senter RA, Kuizon L, Macara IG. Evidence for the involvement of Rab3A in Ca(2+)-dependent exocytosis from adrenal chromaffin cells. J Biol Chem 1994;269:10229–10234.

78. L Johannes PMLMRJDVJPHFD. The GTPase Rab3a negatively controls calcium-dependent exocytosis in neuroendocrine cells. EMBO J 1994;13:2029.

79. Lin CG, Pan CY, Kao L-S. Rab3A delayed catecholamine secretion from bovine adrenal chromaffin cells. Biochemical and Biophysical Research Communications

1996;221:675–681.

80. Schlüter OM, Khvotchev M, Jahn R, Südhof TC. Localization versus function of Rab3 proteins. Evidence for a common regulatory role in controlling fusion. J Biol Chem 2002;277:40919–40929.

81. Geppert M, Goda Y, Stevens CF, Südhof TC. The small GTP-binding protein Rab3A regulates a late step in synaptic vesicle fusion. Nature 1997;387:810–814.

82. Leenders AG, Lopes da Silva FH, Ghijsen WE, Verhage M. Rab3a is involved in transport of synaptic vesicles to the active zone in mouse brain nerve terminals. Mol Biol Cell 2001;12:3095–3102.

83. van Weering JRT, Toonen RF, Verhage M. The Role of Rab3a in Secretory Vesicle Docking Requires Association/Dissociation of Guanidine Phosphates and Munc18-1. PLoS ONE 2007;2:e616.

84. Tian M, Xu CS, Montpetit R, Kramer RH. Rab3A Mediates Vesicle Delivery at Photoreceptor Ribbon Synapses. J Neurosci 2012;32:6931–6936.

85. Graham ME, Handley MTW, Barclay JW, Ciufo LF, Barrow SL, Morgan A, Burgoyne RD. A gain-of-function mutant of Munc18-1 stimulates secretory granule recruitment and exocytosis and reveals a direct interaction of Munc18-1 with Rab3. Biochem J 2008;409:407–416.

86. Südhof TC. Function of Rab3 GDP-GTP exchange. 1997;18:519–522.

87. Nonet ML, Staunton JE, Kilgard MP, Fergestad T, Hartwieg E, Horvitz HR, Jorgensen EM, Meyer BJ. Caenorhabditis elegans rab-3 mutant synapses exhibit impaired function and are partially depleted of vesicles. Journal of Neuroscience 1997;17:8061–8073.

88. Handley MTW, Haynes LP, Burgoyne RD. Differential dynamics of Rab3A and Rab27A on secretory granules. Journal of Cell Science 2007;120:973–984.

89. Lam AD, Ismail S, Wu R, Yizhar O, Passmore DR, Ernst SA, Stuenkel EL. Mapping dynamic protein interactions to insulin secretory granule behavior with TIRF-FRET. Biophys J 2010;99:1311–1320.

90. Fukuda M, Kanno E. Analysis of the role of Rab27 effector Slp4-a/Granuphilin-a in dense-core vesicle exocytosis. Meth Enzymol 2005;403:445–457.

91. Fukuda M. Versatile Role of Rab27 in Membrane Trafficking: Focus on the Rab27 Effector Families. J Biochem 2005;137:9–16.

92. Salminen A, Novick PJ. A ras-like protein is required for a post-Golgi event in yeast secretion. Cell 1987;49:527–538.

93. D'Adamo P, Menegon A, Nigro Lo C, Grasso M, Gulisano M, Tamanini F, Bienvenu T, Gedeon AK, Oostra B, Wu S-K, Tandon A, Valtorta F, Balch WE, Chelly J, Toniolo D. Mutations in GDI1 are responsible for X-linked non-specific mental retardation. - PubMed - NCBI. Nat Genet 1998;19:134–139.

94. Clabecq A. Biochemical characterization of Rab3-GTPase-activating protein reveals a mechanism similar to that of Ras-GAP. J Biol Chem 2000;275:31786–31791.

95. Sakane A, Miyoshi J, Takai Y, Sasaki T. Analysis on the Emerging Role of Rab3 GTPase-Activating Protein in Warburg Micro and Martsolf Syndrome. In: Small GTPases in Disease, Part A. Elsevier; 2008. p. 131–139.

96. Fukui K, Sasaki T, Imazumi K, Matsuura Y, Nakanishi H, Takai Y. Isolation and characterization of a GTPase activating protein specific for the Rab3 subfamily of small G proteins. J Biol Chem 1997;272:4655–4658.

97. Nagano F, Sasaki T, Fukui K, Asakura T, Imazumi K, Takai Y. Molecular cloning and characterization of the noncatalytic subunit of the Rab3 subfamily-specific GTPase-activating protein. J Biol Chem 1998;273:24781–24785.

98. Aligianis IA, Johnson CA, Gissen P, Chen D, Hampshire D, Hoffmann K, Maina EN, Morgan NV, Tee L, Morton J, Ainsworth JR, Horn D, Rosser E, Cole TRP, Stolte-Dijkstra I, Fieggen K, Clayton-Smith J, Mégarbané A, Shield JP, Newbury-Ecob R, Dobyns WB, Graham JM, Kjaer KW, Warburg M, Bond J, Trembath RC, Harris LW, Takai Y, Mundlos S, Tannahill D, Woods CG, Maher ER. Mutations of the catalytic subunit of RAB3GAP cause Warburg Micro syndrome. Nat Genet 2005;37:221–224.

99. Aligianis IA, Morgan NV, Mione M, Johnson CA, Rosser E, Hennekam RC, Adams G, Trembath RC, Pilz DT, Stoodley N, Moore AT, Wilson S, Maher ER. Mutation in Rab3 GTPase-activating protein (RAB3GAP) noncatalytic subunit in a kindred with Martsolf syndrome. Am J Hum Genet 2006;78:702–707.

100. Figueiredo AC, Wasmeier C, Tarafder AK, Ramalho JS, Baron RA, Seabra MC. Rab3GEP is the non-redundant guanine nucleotide exchange factor for Rab27a in melanocytes. J Biol Chem 2008;283:23209–23216.

101. Tanaka M, Miyoshi J, Ishizaki H, Togawa A, Ohnishi K, Endo K, Matsubara K, Mizoguchi A, NAGANO T, Sato M, Sasaki T, Takai Y. Role of Rab3 GDP/GTP exchange protein in synaptic vesicle trafficking at the mouse neuromuscular junction. Mol Biol Cell 2001;12:1421–1430.

102. Mahoney TR, Liu Q, Itoh T, Luo S, Hadwiger G, Vincent R, Wang Z-W, Fukuda M, Nonet ML. Regulation of synaptic transmission by RAB-3 and RAB-27 in Caenorhabditis elegans. Mol Biol Cell 2006;17:2617–2625.

103. FATT P, KATZ B. Spontaneous subthreshold activity at motor nerve endings. J Physiol (Lond) 1952;117:109–128.

104. del CASTILLO J, KATZ B. Quantal components of the end-plate potential. J Physiol (Lond) [Internet] 1954;124:560–573. Available from: http://www.ncbi.nlm.nih.gov/pmc/articles/PMC1366292/

105. Scheuss V, Neher E. Estimating Synaptic Parameters from Mean, Variance, and Covariance in Trains of Synaptic Responses. Biophys J 2001;81:1970–1989.

106. Glavinović MI, Vitale ML, Trifaró JM. Comparison of vesicular volume and quantal size in bovine chromaffin cells. Neuroscience 1998;85:957–968.

107. Ulrich D, Luscher HR. Miniature excitatory synaptic currents corrected for dendritic cable properties reveal quantal size and variance. Journal of Neurophysiology 1993;69:1769–1773.

108. Faber DS, Korn H. Applicability of the coefficient of variation method for analyzing synaptic plasticity. Biophys J 1991;60:1288–1294.

109. Bekkers JM, Richerson GB, Stevens CF. Origin of variability in quantal size in cultured hippocampal neurons and hippocampal slices. Proc Natl Acad Sci U S A 1990;87:5359–5362.

110. Heuser JE, Reese TS. Evidence for recycling of synaptic vesicle membrane during transmitter release at the frog neuromuscular junction. J Cell Biol 1973;57:315–344.

111. Micheva KD, Smith SJ. Strong effects of subphysiological temperature on the function and plasticity of mammalian presynaptic terminals. J Neurosci 2005;25:7481–7488.

112. Shepherd GM, Harris KM. Three-dimensional structure and composition of CA3-->CA1 axons in rat hippocampal slices: implications for presynaptic connectivity and compartmentalization. Journal of Neuroscience 1998;18:8300–8310.

113. Schikorski T, Stevens CF. Morphological correlates of functionally defined synaptic vesicle populations. Nat Neurosci 2001;4:391–395.

114. Harris KM, Sultan P. Variation in the number, location and size of synaptic vesicles provides an anatomical basis for the nonuniform probability of release at hippocampal CA1 synapses. Neuropharmacology 1995;34:1387–1395.

115. Harata N, Pyle JL, Aravanis AM, Mozhayeva M, Kavalali ET, Tsien RW. Limited numbers of recycling vesicles in small CNS nerve terminals: implications for neural signaling and vesicular cycling. Trends in Neurosciences 2001;24:637–643.

116. LILEY AW, NORTH KA. An electrical investigation of effects of repetitive stimulation on mammalian neuromuscular junction. Journal of Neurophysiology 1953;16:509–527.

117. Elmqvist D, Quastel DM. A quantitative study of end-plate potentials in isolated human muscle. J Physiol (Lond) 1965;178:505–529.

118. Elmqvist D, HOFMANN WW, KUGELBERG J, Quastel DM. AN ELECTROPHYSIOLOGICAL INVESTIGATION OF NEUROMUSCULAR TRANSMISSION IN MYASTHENIA GRAVIS. J Physiol (Lond) 1964;174:417–434.

119. Alabi AA, Alabi AA, Tsien RW, Tsien RW. Synaptic vesicle pools and dynamics. Cold Spring Harbor Perspectives in Biology 2012;4:a013680.

120. Denker A, Rizzoli SO. Synaptic vesicle pools: an update. Front Syn Neurosci 2010;2:135.

121. Dobrunz L. Release probability is regulated by the size of the readily releasable vesicle pool at excitatory synapses in hippocampus. International Journal of Developmental Neuroscience 2002;20:225–236.

122. Rosenmund C, Stevens CF. Definition of the readily releasable pool of vesicles at hippocampal synapses. 1996;16:1197–1207.

123. Dobrunz LE, Stevens CF. Heterogeneity of release probability, facilitation, and depletion at central synapses. 1997;18:995–1008.

124. Ariel P, Ryan TA. Optical mapping of release properties in synapses. Front Neural Circuits 2010;4.

125. Stevens CF, Wesseling JF. Activity-dependent modulation of the rate at which synaptic vesicles become available to undergo exocytosis. 1998;21:415–424.

126. Holderith N, Lorincz A, Katona G, Rózsa B, Kulik A, Watanabe M, Nusser Z. Release probability of hippocampal glutamatergic terminals scales with the size of the active zone. Nat Neurosci 2012;

127. Neher E. What is Rate-Limiting during Sustained Synaptic Activity: Vesicle Supply or the Availability of Release Sites. - PubMed - NCBI. Front Syn Neurosci 2010;2:144.

128. Cao Y-Q, Tsien RW. Different relationship of N- and P/Q-type Ca2+ channels to channel-interacting slots in controlling neurotransmission at cultured hippocampal synapses. J Neurosci 2010;30:4536–4546.

129. Schlüter OM, Basu J, Südhof TC, Rosenmund C. Rab3 Superprimes Synaptic Vesicles for Release: Implications for Short-Term Synaptic Plasticity. J Neurosci 2006;26:1239–1246.

130. Ryan TA, Li L, Chin L-S, Greengard P, Smith SJ. Synaptic vesicle recycling in synapsin I knock-out mice. J Cell Biol 1996;134:1219–1227.

131. Horrigan FT, Bookman RJ. Releasable pools and the kinetics of exocytosis in adrenal chromaffin cells. Neuron 1994;13:1119–1129.

132. Merrins MJ, Stuenkel EL. Kinetics of Rab27a-dependent actions on vesicle docking and priming in pancreatic beta-cells. J Physiol (Lond) 2008;586:5367–5381.

133. Yang Y, Gillis KD. A highly Ca2+-sensitive pool of granules is regulated by glucose and protein kinases in insulin-secreting INS-1 cells. J Gen Physiol 2004;124:641–651.

134. Alvarez YD, Marengo FD. The immediately releasable vesicle pool: highly coupled secretion in chromaffin and other neuroendocrine cells. J Neurochem [Internet] 2011;116:155–163. Available from: http://eutils.ncbi.nlm.nih.gov/entrez/eutils/elink.fcgi?dbfrom=pubmed&id=21073467&retmode=ref&cmd=prlinks

135. Heinemann C, Chow RH, NEHER E, Zucker RS. Kinetics of the secretory response in bovine chromaffin cells following flash photolysis of caged Ca2+. Biophysj 1994;67:2546–2557.

136. Voets T. Dissection of three Ca2+-dependent steps leading to secretion in chromaffin cells from mouse adrenal slices. 2000;28:537–545.

137. Stevens DR, Schirra C, Becherer U, Rettig J. Vesicle pools: lessons from adrenal chromaffin cells. Front Syn Neurosci 2011;3:2.

138. Neves G, Lagnado L. The kinetics of exocytosis and endocytosis in the synaptic terminal of goldfish retinal bipolar cells. J Physiol (Lond) 1999;515 ( Pt 1):181–202.

139. S rensen J. Formation, stabilisation and fusion of the readily releasable pool of secretory vesicles. Pflugers Arch - Eur J Physiol 2004;448.

140. Gersdorff von H, Matthews G. Depletion and replenishment of vesicle pools at a ribbon-type synaptic terminal. Journal of Neuroscience 1997;17:1919–1927.

141. Ratnayaka A, Marra V, Bush D, Burden JJ, Branco T, Staras K. Recruitment of resting vesicles into recycling pools supports NMDA receptor-dependent synaptic potentiation in cultured hippocampal neurons. J Physiol (Lond) 2012;590:1585–1597.

142. Fernández-Alfonso T, Ryan TA. A heterogeneous “resting” pool of synaptic vesicles that is dynamically interchanged across boutons in mammalian CNS synapses. Brain Cell Bio 2008;36:87–100.

143. Li Z, Burrone J, Tyler WJ, Hartman KN, Albeanu DF, Murthy VN. Synaptic vesicle recycling studied in transgenic mice expressing synaptopHluorin. Proc Natl Acad Sci U S A 2005;102:6131–6136.

144. Smith C, Moser T, Xu T, NEHER E. Cytosolic Ca2+ acts by two separate pathways to modulate the supply of release-competent vesicles in chromaffin cells. 1998;20:1243–1253.

145. Wang LY, Kaczmarek LK. High-frequency firing helps replenish the readily releasable pool of synaptic vesicles. Nature 1998;394:384–388.

146. Gomis A, Burrone J, Lagnado L. Two actions of calcium regulate the supply of releasable vesicles at the ribbon synapse of retinal bipolar cells. Journal of Neuroscience 1999;19:6309–6317.

147. Voets T, Neher E, Moser T. Mechanisms Underlying Phasic and Sustained Secretion in Chromaffin Cells from Mouse Adrenal Slices. 1999;23:607–615.

148. Valtorta F, Meldolesi J, Fesce R. Synaptic vesicles: is kissing a matter of competence? Trends Cell Biol 2001;11:324–328.

149. Zhou L, McInnes J, Verstreken P. Ultrafast Synaptic Endocytosis Cycles to the Center Stage. Dev Cell 2014;28:5–6.

150. Miesenböck G, De Angelis D. Visualizing secretion and synaptic transmission with pH-sensitive green fluorescent proteins : Abstract : Nature. Nature 1998;

151. Voglmaier SM, Kam K, Yang H, Fortin DL, Hua Z, Nicoll RA, Edwards RH. Distinct endocytic pathways control the rate and extent of synaptic vesicle protein recycling. 2006;51:71–84.

152. Royle SJ, Granseth B, Odermatt B, Derevier A, Lagnado L. Imaging phluorin-based probes at hippocampal synapses. Methods Mol Biol 2008;457:293–303.

153. Sankaranarayanan S, De Angelis D, Rothman JE, Ryan TA. The Use of pHluorins for Optical Measurements of Presynaptic Activity. Biophys J 2000;79:2199–2208.

154. Kavalali ET, Jorgensen EM. Visualizing presynaptic function. Nat Neurosci 2013;17:10–16.

155. Harata N, Ryan TA, Smith SJ, Buchanan J, Tsien RW. Visualizing recycling synaptic vesicles in hippocampal neurons by FM 1-43 photoconversion. Proc Natl Acad Sci U S A 2001;98:12748–12753.

156. Poskanzer KE, Davis GW. Mobilization and fusion of a non-recycling pool of synaptic vesicles under conditions of endocytic blockade. Neuropharmacology 2004;47:714–723.

157. Rose T, Schoenenberger P, Jezek K, Oertner TG. Developmental refinement of vesicle cycling at schaffer collateral synapses. 2013;77:1109–1121.

158. Kim SH, Ryan TA. CDK5 serves as a major control point in neurotransmitter release.

2010;67:797–809.

159. Virmani T, Atasoy D, Kavalali ET. Synaptic vesicle recycling adapts to chronic changes in activity. J Neurosci 2006;26:2197–2206.

160. Eberhard D. Neuron and beta-cell evolution: learning about neurons is learning about beta-cells. Bioessays 2013;35:584–584.

161. Arntfield ME, van der Kooy D. β-Cell evolution: How the pancreas borrowed from the brain: The shared toolbox of genes expressed by neural and pancreatic endocrine cells may reflect their evolutionary relationship. Bioessays 2011;33:582–587.

162. Iwasaki S, Momiyama A, Uchitel OD, Takahashi T. Developmental changes in calcium channel types mediating central synaptic transmission. J Neurosci 2000;20:59–65.

163. Burger PM, Mehl E, Cameron PL, Maycox PR, Baumert M, Lottspeich F, De Camilli P, Jahn R. Synaptic vesicles immunoisolated from rat cerebral cortex contain high levels of glutamate. Neuron 1989;3:715–720.

164. Schneggenburger R, Rosenmund C. Molecular mechanisms governing Ca2+ regulation of evoked and spontaneous release. Nat Neurosci 2015;18:935–941.

165. Truckenbrodt S, Rizzoli SO. Spontaneous vesicle recycling in the synaptic bouton. Frontiers in Cellular Neuroscience 2014;8.

166. Kaeser PS, Regehr WG. Molecular mechanisms for synchronous, asynchronous, and spontaneous neurotransmitter release. Annu Rev Physiol 2014;76:333–363.

167. Neher E, Sakaba T. Multiple roles of calcium ions in the regulation of neurotransmitter release. 2008;59:861–872.

168. Pang ZP, Südhof TC. Cell biology of Ca2+-triggered exocytosis. Curr Opin Cell Biol 2010;22:496–505.

169. Matveev V, Bertram R, Sherman A. Calcium cooperativity of exocytosis as a measure of Ca2+ channel domain overlap. Brain Res 2011;1398:126–138.

170. Murthy VN, Sejnowski TJ, Stevens CF. Heterogeneous release properties of visualized individual hippocampal synapses. 1997;18:599–612.

171. Zucker RS, Regehr WG. Short-term synaptic plasticity. Annu Rev Physiol 2002;64:355–405.

172. Abbott LF, Regehr WG. Synaptic computation. Nature 2004;431:796–803.

173. Mitra A, Mitra SS, Tsien RW. Heterogeneous reallocation of presynaptic efficacy in

recurrent excitatory circuits adapting to inactivity. Nat Neurosci 2012;15:250–257.

174. Rorsman P, Eliasson L, Renström E, Gromada J, Barg S, Göpel S. The Cell Physiology of Biphasic Insulin Secretion. News Physiol Sci 2000;15:72–77.

175. Shibasaki T, Sunaga Y, Fujimoto K, Kashima Y, Seino S. Interaction of ATP sensor, cAMP sensor, Ca2+ sensor, and voltage-dependent Ca2+ channel in insulin granule exocytosis. J Biol Chem 2004;279:7956–7961.

176. Izumi T. Heterogeneous modes of insulin granule exocytosis: molecular determinants. Front Biosci (Landmark Ed) 2011;16:360–367.

177. Ohya T, Miaczynska M, Coskun U, Lommer B, Runge A, Drechsel D, Kalaidzidis Y, Zerial M. Reconstitution of Rab- and SNARE-dependent membrane fusion by synthetic endosomes. Nature 2009;459:1091–1097.

178. Boyken J, Grønborg M, Riedel D, Urlaub H, Jahn R, Chua JJE. Molecular Profiling of Synaptic Vesicle Docking Sites Reveals Novel Proteins but Few Differences between Glutamatergic and GABAergic Synapses. 2013;78:285–297.

179. Williams AL, Bielopolski N, Meroz D, Lam AD, Passmore DR, Ben-Tal N, Ernst SA, Ashery U, Stuenkel EL. Structural and functional analysis of tomosyn identifies domains important in exocytotic regulation. Journal of Biological Chemistry 2011;

180. Lang T, Jahn R. Core proteins of the secretory machinery. Handb Exp Pharmacol 2008;:107–127.

181. Pobbati AV, Razeto A, Böddener M, Becker S, Fasshauer D. Structural basis for the inhibitory role of tomosyn in exocytosis. J Biol Chem [Internet] 2004;279:47192–47200. Available from: http://www.jbc.org/content/279/45/47192.full

182. Gladycheva SE, Lam AD, Liu J, D'Andrea-Merrins M, Yizhar O, Lentz SI, Ashery U, Ernst SA, Stuenkel EL. Receptor-mediated regulation of tomosyn-syntaxin 1A interactions in bovine adrenal chromaffin cells. J Biol Chem 2007;282:22887–22899.

183. Hatsuzawa K, Lang T, Fasshauer D, Bruns D, Jahn R. The R-SNARE motif of tomosyn forms SNARE core complexes with syntaxin 1 and SNAP-25 and down-regulates exocytosis. J Biol Chem 2003;278:31159–31166.

184. Yu H, Rathore SS, Gulbranson DR, Shen J. The N- and C-terminal domains of tomosyn play distinct roles in soluble N-ethylmaleimide-sensitive factor attachment protein receptor binding and fusion regulation. Journal of Biological Chemistry 2014;289:25571–25580.

185. Hattendorf DA, Andreeva A, Gangar A, Brennwald PJ, Weis WI. Structure of the yeast polarity protein Sro7 reveals a SNARE regulatory mechanism. Nature

2007;446:567–571.

186. Lehman K, Rossi G, Adamo JE, Brennwald P. Yeast homologues of tomosyn and lethal giant larvae function in exocytosis and are associated with the plasma membrane SNARE, Sec9. J Cell Biol 1999;146:125–140.

187. Grosshans BL, Novick P. Identification and Verification of Sro7p as an Effector of the Sec4p Rab GTPase. In: Small GTPases in Disease, Part A. Elsevier; 2008. p. 95–108.

188. Rossi G, Watson K, Demonch M, Temple B, Brennwald P. In vitro reconstitution of Rab GTPase-dependent vesicle clustering by the yeast lethal giant larvae/tomosyn homolog, Sro7. Journal of Biological Chemistry 2015;290:612–624.

189. Fujita Y, Shirataki H, Sakisaka T, Asakura T, Ohya T, Kotani H, Yokoyama S, Nishioka H, Matsuura Y, Mizoguchi A, Scheller RH, Takai Y. Tomosyn: a syntaxin-1-binding protein that forms a novel complex in the neurotransmitter release process. 1998;20:905–915.

190. Yokoyama S, Shirataki H, Sakisaka T, Takai Y. Three splicing variants of tomosyn and identification of their syntaxin-binding region. Biochemical and Biophysical Research Communications 1999;256:218–222.

191. Widberg CH, Bryant NJ, Girotti M, Rea S, James DE. Tomosyn interacts with the t-SNAREs syntaxin4 and SNAP23 and plays a role in insulin-stimulated GLUT4 translocation. J Biol Chem 2003;278:35093–35101.

192. Groffen AJA, Jacobsen L, Schut D, Verhage M. Two distinct genes drive expression of seven tomosyn isoforms in the mammalian brain, sharing a conserved structure with a unique variable domain. J Neurochem 2005;92:554–568.

193. Cheviet S, Bezzi P, Ivarsson R, Renström E, Viertl D, Kasas S, Catsicas S, Regazzi R. Tomosyn-1 is involved in a post-docking event required for pancreatic beta-cell exocytosis. Journal of Cell Science 2006;119:2912–2920.

194. Yizhar O, Matti U, Melamed R, Hagalili Y, Bruns D, Rettig J, Ashery U. Tomosyn inhibits priming of large dense-core vesicles in a calcium-dependent manner. Proc Natl Acad Sci U S A 2004;101:2578–2583.

195. Zhang W, Lilja L, Mandic SA, Gromada J, Smidt K, Janson J, Takai Y, Bark C, Berggren P-O, Meister B. Tomosyn is expressed in beta-cells and negatively regulates insulin exocytosis. Diabetes 2006;55:574–581.

196. Gracheva EO, Burdina AO, Holgado AM, Berthelot-Grosjean M, Ackley BD, Hadwiger G, Nonet ML, Weimer RM, Richmond JE. Tomosyn inhibits synaptic vesicle priming in Caenorhabditis elegans. PLoS Biol 2006;4:e261.

197. McEwen JM, Madison JM, Dybbs M, Kaplan JM. Antagonistic regulation of synaptic vesicle priming by Tomosyn and UNC-13. 2006;51:303–315.

198. Yizhar O, Lipstein N, Gladycheva SE, Matti U, Ernst SA, Rettig J, Stuenkel EL, Ashery U. Multiple functional domains are involved in tomosyn regulation of exocytosis. J Neurochem 2007;103:604–616.

199. Gracheva EO, Burdina AO, Touroutine D, Berthelot-Grosjean M, Parekh H, Richmond JE. Tomosyn negatively regulates CAPS-dependent peptide release at Caenorhabditis elegans synapses. J Neurosci 2007;27:10176–10184.

200. Gracheva EO, Burdina AO, Touroutine D, Berthelot-Grosjean M, Parekh H, Richmond JE. Tomosyn negatively regulates both synaptic transmitter and neuropeptide release at the C. elegans neuromuscular junction. J Physiol (Lond) 2007;585:705–709.

201. Chen K, Richlitzki A, Featherstone DE, Schwärzel M, Richmond JE. Tomosyn-dependent regulation of synaptic transmission is required for a late phase of associative odor memory. Proceedings of the National Academy of Sciences 2011;108:18482–18487.

202. Hu Z, Tong X-J, Kaplan JM. UNC-13L, UNC-13S, and Tomosyn form a protein code for fast and slow neurotransmitter release in Caenorhabditis elegans. Elife 2013;2:e00967.

## Chapter II

## Distinct actions of Rab3 and Rab27 GTPases on late stages of exocytosis of insulin

### 2.1 Abstract

Rab GTPases associated with insulin-containing secretory granules (SGs) are key in targeting, docking and assembly of molecular complexes governing pancreatic β-cell exocytosis. Four Rab3 isoforms along with Rab27A are associated with insulin granules, yet elucidation of the distinct roles of these Rab families on exocytosis remains unclear. To define specific actions of these Rab families we employ Rab3GAP and/or EPI64A GTPase-activating protein overexpression in β-cells from wild-type or Ashen mice to selectively transit the entire Rab3 fam- ily or Rab27A to a GDP-bound state. Ashen mice carry a sponta- neous mutation that eliminates Rab27A expression. Using membrane capacitance measurements we find that GTP/GDP nucleotide cycling of Rab27A is essential for generation of the functionally defined immediately releasable pool (IRP) and central to regulating the size of the eadily releasable pool (RRP). By comparison, nucleotide cycling of Rab3 GTPases, but not of Rab27A, is essential for a kinetically rapid filling of the RRP with SGs. Aside from these distinct functions, Rab3 and Rab27A GTPases demonstrate considerable functional overlap in building the readily releasable granule pool. Hence,

while Rab3 and Rab27A cooperate to generate release-ready SGs in β-cells, they also direct unique kinetic and functional properties of the exocytotic pathway.

## 2.2 Introduction

Insulin secretion from endocrine pancreatic β-cells is essential in regulating blood glucose levels. Key to this secretion is highly regulated membrane trafficking and exocytotic pathways of insulin-containing secretory granules (SGs). Defects in the process of insulin production, trafficking and secretion can lead to profound metabolic disorders and diabetes mellitus (1). Physiologically, insulin secretion is typically triggered from β-cells in response to elevated blood glucose concentrations, which raises the intracellular ATP/ADP concentration ratio and drives closure of KATP channels leading to a depolarization of the plasma membrane. Depolarization of the β-cell membrane then triggers activation of voltage-gated Ca2+ channels, wherein Ca2+ influx results in an induction of exocytosis of the insulin SGs (2). Prolonged glucose activation of β-cells induces a second sustained phase of exocytotic insulin secretion, the mechanisms of which are less well understood (3 – 6). In addition, incretins such as glucagon-like peptide-1 and glucose-dependent insulinotropic polypeptide strongly potentiate insulin secretion via cAMP signaling. Central to exocytosis of insulin SGs is the assembly/disassembly of molecular complexes that direct SG membrane targeting, tethering and biochemical competency for undergoing membrane fusion (7–9). While evolutionarily conserved SNARE pro- teins and regulators of SNARE complex assembly define the priming and fusion process, Rab GTPases are believed to be critical determinants of organelle identity, vesicle targeting, membrane tethering and SNARE complex formation (10,11).

Rab3A was the first Rab GTPase identified on insulin-containing SGs (12). Genetic studies using Rab3A knockout mice (13,14) as well as investigations examining the effects of overexpression of Rab3A mutants (15 – 19) demonstrate that Rab3A is required for normal levels of insulin secretion and control of plasma glucose levels. More recently, Rab27A, a close evolutionary relative of Rab3, has also been found to be associated with these SGs (20 – 22). Similarly, functional studies of Rab27A-deficient mice (13,23,24) and overexpression of Rab27A mutants (21,25) have determined that Rab27A exerts regulatory activity over the exocytotic release of insulin. Although recent studies have confirmed that Rab3 and Rab27 are commonly colocalized on SGs and neuronal synaptic vesicles (26), the precise mechanisms by which they regulate late stages of exocytosis and the degree to which they exert functional overlap during vesicle priming and exocytosis remain poorly defined. Assigning specific roles to these Rabs has been complicated by their high structural homology and the promiscuity of effectors between the Rab3/Rab27 families. Moreover, knockout mice where three Rab3 isoforms are deleted do not survive when Rab3A is one of the deleted isoforms (14), further complicating studies assigning specific actions of Rab3 proteins versus Rab27 within the exocytotic pathway.

The subfamily of Rab3 consists of four isoforms (Rab3A–D), with each being present in pancreatic β-cells and in part associated with SGs (27). By comparison, Rab27 consists of two isoforms (Rab27A,B), but only Rab27A is expressed and targeted to insulin-containing SGs (24). The activity of Rab3 and Rab27 family proteins, like other GTPases, is determined by their cycling between a GDP-bound mostly inactive and cytosolic form and a GTP-bound active and membrane-bound form. Transitions between GTP/GDP states are mediated by guanine nucleotide exchange factors (GEFs) that stimulate the binding of GTP, and by

GTPase-activating proteins (GAPs) that accelerate the intrinsic rate of Rab-GTP hydrolysis and return the Rab protein to an inactive state (28). While greater than 60 Rab proteins have been identified in mammalian cells, comparatively fewer regulatory Rab GEFs and Rab GAPs have been identified. Indeed, GTP binding of both Rab3 and Rab27 families is promoted by a single Rab GEF, termed Rab3GEP (29), suggesting a potential for commonality in their activation. Yet, return to a GDP-bound state for these Rabs is driven by distinct GAPs (Rab3GAP and EPI64, respectively) (30,31). Differences in regulated GAP inactivation likely lead to characteristic rates of GTP/GDP cycling and granule residency. Notably, fluorescence imaging of Rab3A and Rab27A on SGs has demonstrated that they exhibit kinetic differences in granule membrane association (26,32). For example, activation of secretion is often accompanied by rapid dissociation of Rab3A from the exocytic vesicles, while Rab27A appears to be largely maintained on SGs throughout fusion and early stages of endocytosis (33,34). These results are consistent with studies showing that association between Rab3 and the SG membrane is rigorously correlated with Rab3's GTP-bound state, while Rab27 appears to be able to associate with granules in both GDP- and GTP-bound states (35,36).

Multiple effectors have been reported for the Rab3 and Rab27 GTPases, which fall largely within four groups including, Rab-interacting molecules (RIMs and RIM-like proteins); synaptotagmin-like proteins (Slp and rabphilin); Slp-like proteins lacking C2 homologous regions (Slac and Noc2); and a vesicle priming protein Munc13-4 (37,38). For these effector families, RIM proteins interact with all isoforms of Rab3 but apparently not Rab27. Conversely, Slp1, Slp2-a, Slp3-a, Slp5 and Slac2-a–c interact specifically with Rab27A/B but not Rab3. By comparison, Slp4A, rabphilin and no C2 domain protein (Noc2)

interact with Rab27A/B, Rab3s and Rab8 *in vitro*; however, binding affinities suggest preference for interaction with Rab27s *in vivo* (38,39). Finally, Munc13-4, a member of the Munc13 family that participates in exocytotic priming, has been reported to interact specifically with Rab27 (40). Importantly, Rab effectors may show cycling on/off membranes that differ kinetically from the Rabs themselves, suggesting that effector interactions with Rab GTPases may exhibit temporal and spatial differences and support distinct roles in the exocytic pathway (41). Although Rab3 and Rab27 are important regulators of secretory activity their functional specificity remains poorly understood, in part as a result of effector overlap.

In this study, we identify distinct roles of Rab3 and Rab27 family proteins in the final stages of the exocytotic pathway for insulin secretion from pancreatic β-cells. The investigations are novel in employing selective overexpression of the catalytic subunit of Rab3GAP and/or EPI64A to specifically activate GTP hydrolysis and respectively deactivate Rab3 and/or Rab27 family proteins. Whole-cell capacitance measurements were used to evoke and measure exocytotic activity and to assign specific actions of the Rab families on functionally distinct vesicle pools of β-cells in pancreatic islet slices. Furthermore, we employed total internal reflection fluorescence (TIRF) microscopy of fluorescently tagged insulin-containing SGs to examine GAP overexpression effects on SG plasma membrane targeting and on juxtamembrane mobility. Our results provide the first quantitative evidence to distinguish largely differential roles of these Rab GTPase families in the priming of SGs into the immediately and readily releasable SG pools.

## 2.3 Results

To determine the sites of action and to differentiate distinct roles of Rab3 and Rab27 proteins on exocytosis in β-cells, experiments were performed using pancreatic islet slices from wild-type (wt) or Ashen mice. In addition, overexpression of GAPs, specifically Rab3GAP or EPI64A, was used to deactivate all isoforms of the Rab3 and/or Rab27 family, respectively. Islet slices, as opposed to isolated β-cells, were used to (i) retain the spatial and physiological characteristics of the exocytotic machinery and gap junctions of β-cells found in intact islet tissue; (ii) facilitate the maintenance of glucose responsiveness and electrical and secretory characteristics through organotypic tissue culture, while allowing efficient viral infection; and (iii) promote a tissue platform allowing stable long-term recording of membrane capacitance measurements from β-cells under a whole-cell voltage-clamp configuration.

As shown in Figure 1, cultured pancreatic islet slices allow effective infection with adenovirus for protein expression and provide excellent visualization of individual islet cells. The islet cell type specific to each electrophysiological recording was distinguished by measuring steady-state voltage-dependent inactivation properties of voltage-gated Na+ channels. Mouse β-cells contain a voltage-gated Na+ current whose steady-state inactivation properties are strongly left voltage shifted with respect to the inactivation properties of Na+ currents of α- and δ-cells (Figure 1B) (42,43). The use of pancreatic islet slices also allows electrophysiological current-clamp recording of oscillations in electrical activity from individual β-cells, termed bursting, when the slices are exposed to stimulatory levels of glucose in the bathing media. Notably, this glucose-induced electrical bursting behavior was retained for at least 3 days in cultured slices, suggesting that normal

phenotypic characteristics are maintained during organotypic slice culture on supported membranes (Figure 1C). Moreover, this glucose-induced bursting behavior was observed in cultures of slices from both wt and Ashen mice.

Rab3GAP and EPI64A have been characterized to exhibit Rab GAP activity specific to members of the Rab3 family and Rab27A (31,44). The effectiveness of overexpression of these GAPs to selectively shift the nucleotide-bound state of Rab3 or Rab27 proteins in insulin-secreting cells (Min6) was confirmed using a series of fluorescent imaging experiments (Figure 2). Notably, CFP-Rab3A or CFP-Rab27A expression exhibited punctate patterning of fluorescence that colocalized with a SG luminal reporter [neuropeptide Y (NPY)-mCH, Figure 2A] as confirmed by colocalization analysis (Figure 2B). Importantly, the punctate pattern of CFP-Rab3A or CFP-Rab3D was completely eliminated upon co-expression of mYFP-Rab3GAP but not with mYFP-EPI64A (Figure 2C). By comparison, punctate localization of CFP-Rab27A was retained upon co-expression of Rab GAPs (Rab3GAP or EPI64A, Figure 2D), a result consistent with reports indicating that Rab27A associates with SGs in both GDP- and GTP-bound states (35,36). To confirm that GAP over-expression effectively transitions these Rab GTPases into their GDP-bound state, irrespective of subcellular distribution, we next determined the effect of GAP overexpression on GTP-dependent Rab3A and Rab27A effector interactions (35). RIM2α(1-179) is a splice variant that specifically interacts with GTP-bound Rab3 (18), whereas Slp4A(AGAAAY) is a mutant that interacts exclusively with the GTP-bound form of Rab27A (35). As shown in Figure 2E, co-expression of CFP-Rab3 and cYFP-RIM2α(1-179) results in colocalization of punctate fluorescence, which was lost when mCH-Rab3GAP was co-expressed. Co-expression of CFP-Rab27A with cYFP-Slp4A(AGAAAY) also demonstrated

overlapping punctate fluorescence, which was lost with the added expression of mCH-EPI64A (Figure 2F). Taken together these results confirm that (i) Rab3GAP and EPI64A transition Rab3 and Rab27A, respectively, into their GDP-bound states; (ii) Rab27A localization to granules can be retained even in its GDP-bound form; and (iii) overexpression of GAPs strongly reduces Rab3 and Rab27A GTP-dependent effector interactions.

Docking of SGs at the plasma membrane is a key step in regulated exocytosis, as this is proposed necessary for the formation of *trans*-SNARE core complexes (vesicle priming). Not surprisingly, Rab3 and, more recently, Rab27 GTPases have been reported as central to targeting and docking secretory vesicles in β-cells (19,24), yeast (45), neuroendocrine cells [PC12 (46) and chromaffin cells (47)] and synaptic vesicles in *Caenorhabditis elegans* (48) and mammalian nerve terminals (49,50). Therefore, we next determined whether overexpression of the Rab GAP proteins exerted specific actions on insulin granule docking or on the mobility of insulin SGs directly adjacent to the plasma membrane. To assess effects of GAP over- expression on docking we used TIRF microscopy of a co-expressed SG luminal tag (NPY-mCH) in Min6 cells to visualize single SGs and quantify their density just beneath the plasma membrane. Min6 cells were used as they retain glucose-induced insulin secretion, aggregate in cell clusters and TIRF microscopy of β-cells in islet slices was not achievable. Representative images of NPY-mCH-tagged insulin SGs expressing only NPY-mCH or when co-expressed with Rab3GAP, EPI64A or with both Rab GAPs are shown in Figure 3A. As evident from the micrographs, no differences were observed in individual SG size or shape upon expression of the GAPs. In addition, SG density exhibited no significant differences between the different expression conditions (Figure 3B). These data differ from

reported differences in SG docking observed with Rab3 and/or Rab27A knockdown (46,51,52) and suggest that Rab GAP overexpression, while strongly shifting nucleotide equilibrium of the associated GTPases to a GDP-bound state, may not completely preclude rapid pas- sage of the GTPases through GTP-bound states to drive certain effector interactions important for SG docking.

Rab3 GTPases are believed to remain associated with docked SGs up until the final exocytotic steps leading to membrane fusion. By comparison, Rab27 may remain associated with vesicles throughout the exo-endocytotic process with its GTP/GDP nucleotide state being selectively regulated during passage through the exocytotic fusion and subsequent membrane recycling (35,36). While the functional role(s) of Rabs following granule tethering/ docking are poorly understood, progression of vesicle priming following docking is commonly believed to lead to stable membrane association and an associated strong reduction in granule motion. Indeed, TIRF imaging of SGs immediately adjacent to the plasma membrane has repeatedly demonstrated that they are highly constrained in motion (53–57). To determine if a shift in nucleotide state equilibrium of Rabs may alone modulate motion of docked SGs we next performed time-lapse TIRF imaging of control and Rab GAP-transfected Min6 cells. Imaging was performed on cells held in physiological saline containing 3mM glucose to reduce effects of secretion and activated granule recruitment on measures of docked granule mobility. The $x$–$y$ $(\Delta R)2$ and axial $(\Delta Z)2$ mobility of individual docked SGs for each condition was determined. As shown in Figure 4, the measured $(\Delta R)2$ and $(\Delta Z)2$ cumulative probability of SG mobility in cells co-transfected with Rab3GAP, EPI64A or Rab3GAP + EPI64A, as well as NPY-mCH showed no significant differences from those of control cells (NPY-mCH only). These data suggest that Rab–

effector interactions are not essential to maintenance of the stable and largely immobile population of docked SGs.

To identify specific Rab3 and Rab27A GTPase activities during the final steps of the regulated exocytotic pathway we employed highly time-resolved membrane capacitance (*C*m) measurements from β-cells within islet tissue slices of wt control (C3H/He) or Ashen mice as well as from β-cells in the slices infected with Rab3GAP or EPI64A. Pancreatic β-cells contain well-described SG pools, including a large reserve pool (RP), a readily releasable pool (RRP), a small subset of the RRP termed the immediately releasable pool (IRP) and a highly calcium-sensitive pool (4,13,58 – 62). The IRP size is small and immediately released in response to a stimulus. If the stimulus is strong or prolonged and the IRP is depleted release then occurs from the RRP. The IRP is refilled from the RRP and the RRP from the RP. To elicit release and measure the size of the IRP and RRP a succession of step depolarizations (−80 mV holding potential to 0 mV step potential) was applied under whole-cell voltage clamp. Release and depletion of the IRP was accomplished by a series of five 50-millisecond step depolarizations, while the RRP was released using 10 500-millisecond step depolarizations, with each series using 100-millisecond inter- step intervals. As Rab GTPases have been reported key for vesicle targeting, docking and priming we also deter- mined the actions that Rab3 and Rab27A proteins exert on refilling of the IRP and RRP following their depletion. To measure Rab protein effects on refilling of the IRP and RRP a second train of successive step depolarizations was applied 20 seconds following cessation of the initial train of depolarizing stimuli.

In wt control β-cells, the first train of step depolarizations resulted in an averaged Δ*C*m of 20 fF (fempto-Farads) corresponding to the IRP and 250 fF for the RRP (Figure

5A,C, black). Based on estimates of 1.7 fF per granule these Δ*C*m values indicate IRP in control conditions to be ≈12 granules and the RRP to be ≈147 granules. Interestingly, these values for the IRP and RRP are approximately twice those we previously reported from isolated pancreatic β-cells (13), indicating that the more integrative character of islet slices likely retains more physiologically robust secretory responses in culture. Importantly, Δ*C*m responses to a second train of step depolarizations applied 20 seconds after completion of the first train demonstrated only 45% recovery of the IRP while the RRP recovered to 85% of its initial value (Figure 5B,C, gray). This 20-second refilling interval, whereby incomplete refilling of the IRP and RRP was demonstrated in wt control cells, is used in the following experiments as a reference when evaluating effects of Rab protein nucleotide state on their capacities to direct SG pool refilling.

To confirm that the voltage-step-evoked Δ*C*m of the β-cells reflect Ca2+-dependent exocytotic activity we also tested for Δ*C*m to successive step depolarizations from a −80 mV holding potential to +40 mV, a value closer to the expected Ca2+ equilibrium potential and strongly reduced voltage-gated Ca2+ current. As shown (Figure 5A – C, blue) steps to this potential resulted in significantly smaller evoked averaged Δ*C*m response (9 fF IRP and 20 fF RRP).

Figure 5D compares representative macroscopic β-cell currents in response to the initial 50-millisecond voltage step during the first (black) and second (red) train of step depolarizations from −80 to 0mV. Note that the current responses to each applied train were equivalent, suggesting that differences in Δ*C*m responses between the trains are not the result of inadequate recovery or of rundown of the evoked current. Most of the β-cells demon- strated a rapid inward followed by a strongly reduced sustained inward current

following the step depolarizations that likely reflect voltage-gated Na+ and Ca2+ current components (Figure 5D, lower). Interestingly, in a small subset of β-cells only the sustained current, most likely representing Ca2+ influx, was observed, which also demonstrated complete recovery during the intertrain interval (Figure 5D, upper). Indeed, voltage steps to 0mV from a −50mV holding poten- tial, where voltage-gated Na+ channels in β-cells are inactivated, resulted in a sustained inward Ca2+ cur- rent with amplitudes close to that of the sustained current observed upon steps to 0mV from a −80mV holding potential (Figure 5E).

Insulin-containing SGs in wt control β-cells possess both Rab27A and the four isoforms of Rab3 (A, B, C and D) GTPases (20 – 22, 63, 27). As a test for distinct as well as complimentary actions of these GTPases we initially examined the effects of Rab27A on IRP and RRP sizes and on pool refilling using three separate experimental conditions. These conditions include exocytotic measurements from β-cells in islet slices of the Ashen mouse (i.e. Rab27A-deficient) and of β-cells following EPI64A adenoviral infection of islet slices isolated from Ashen and wt mice. As shown in Figure 6, the averaged initial IRP and RRP exocytotic responses measured from β-cells under each of these three conditions were significantly reduced from those of wt mice (control response, dashed line, Figure 6B). The IRP from β-cells of Ashen mice was most strongly affected (~90% reduction), whereas overexpression of EPI64A in β-cells of Ashen or wt control slices resulted in an approximately 50% reduction in IRP from control. The reduced effect on IRP size with EPI64A over- expression in Ashen β-cells suggests that EPI64A exerts Rab27A-independent effects on secretion. Indeed, EPI64A has also been characterized as a binding protein of EBP50, which participates in actin bundling at the cell periphery (64). By comparison to

the substantial reduction of the IRP from wt control with loss of Rab27 or Rab27-GTP, the RRP for each condition (Ashen, Ashen + EPI64A and control + EPI64A) was significantly reduced, but only by approximately 25%. Note that measured differences in IRP and RRP pool sizes of control and Ashen β-cells were not associated with changes in voltage-gated integrated Ca2+ influx (Figure 6C). Moreover, while expression of EPI64A resulted in a reduced Ca2+ influx, diminution in Δ*C*m responses was not greater than observed for Ashen-only β-cells.

Rab27A effects on refilling of the IRP and RRP were determined through application of a second train of step depolarizations following a 20-second recovery interval. Measurement of the Δ*C*m responses showed that in Ashen β-cells the reduced IRP completely refilled, while the RRP refilled to approximately the same percentage as observed for wt β-cell controls (Figure 6B). By comparison, Ashen β-cells overexpressing EPI64A demonstrated complete refilling of both the IRP and RRP, whereas the overexpression of EPI64A in control cells led to incomplete refilling of the IRP and RRP. EPI64A facilitation of RRP pool refilling in the absence of Rab27A, but not in Rab27A containing control cells, suggests that alternative actions of EPI64A in the exocytotic pathway may be enhanced when functional competition with Rab27A is absent. Overall, the data indicate that Rab27A-GTP is critically important in enhancing the size of the IRP and that this is independent of effects on the rate of IRP pool refilling. Rab27A-GTP was also observed integral to setting the overall RRP size, but without substantial effect on pool refilling.

As a test for distinct functional effects between Rab27A and the Rab3 GTPase family we next determined the effects of overexpression of Rab3GAP on IRP and RRP sizes and on

pool refilling in pancreatic β-cells. As demonstrated above, Rab3GAP specifically targets the Rab3 isoforms without notable effect on Rab27A-GTP. As shown in Figure 7A,C, overexpression of Rab3GAP in wt β-cells results in an approximately 50% reduction in the IRP from wt control. By comparison, Rab3GAP overexpression exerted little effect on the RRP when compared with control wt β-cells (Figure 7C). Importantly, the predominate shift in Rab3 isoforms to the GDP-bound state through Rab3GAP overexpression resulted in a substantial deficit in refilling of the IRP and RRP as defined by Δ*C*m responses to the subsequent train of step depolarizations (Figure 7A,C). Therefore, it is clear that the GTP-bound state of Rab3 isoforms, but not of Rab27A, are key to rapid refilling of both the IRP and RRP. Although Rab3GAP overexpression reduced integrated Ca2+ influx from levels of wt β-cell controls no significant differences were observed on the influx between Rab3GAP-overexpressing control or Ashen cells (Figure 7E), or with EPI64A-overexpressing β-cells (Figure 6C). These data suggest that the specific deficit in pool refilling upon Rab3GAP overexpression is not attributable to reduced Ca2+ influx.

To identify potential compensatory functions of Rab27A and Rab3 isoforms in the final stages of exocytosis we next evaluated the effects of combined deficit of Rab27A activity and GTP-bound Rab3 isoforms through overexpression of Rab3GAP in the Ashen β-cells. Ashen cells were used instead of EPI64A co-expression to mitigate alternative actions of EPI64A in the exocytotic pathway. Under these conditions we again observed a reduction in the IRP similar to that seen upon independent reduction of the GTP-bound state of Rab3 isoforms by Rab3GAP overexpression in wt β-cells (Figure 7B,C). Notably, overexpression of Rab3GAP in Ashen cells demonstrated an increased IRP size relative to Ashen alone. This paradoxical result may indicate that enhanced Rab3GAP GTP/GDP

cycling of Rab3s may partially offset a Rab27 deficit on the IRP. By comparison, RRP size in the absence of Rab3-GTP and Rab27A was observed to exhibit a substantial and significant reduction greater than that exhibited by Ashen cells or Rab3GAP overexpression alone. In addition, loss of functionally active Rab3-GTP and Rab27A resulted in strongly reduced refilling of the IRP and RRP (Figure 7C). When considered with the findings above, these data demonstrate that GAP overexpression targeting either or both Rab27A or Rab3 proteins reduces IRP size by approximately 50% of wt control. In comparison, individual expression of Rab27A or Rab3 GAP proteins resulted in a smaller effect on the initial size of the RRP, while combined loss of Rab27A and Rab3-GTP isoforms strongly reduced the size of the RRP. A likely interpretation is that Rab27A and Rab3 perform compensatory roles in filling of the IRP and RRP pools. Yet, comparison of the kinetics of refilling of the IRP and RRP pools following depletion indicates that Rab3-GTP isoforms, but not Rab27A, drive rapid refilling of exocytotic SG pools.

Ca2+-triggered insulin secretion from β-cells is potently amplified by increased subplasma membrane cAMP. In addition, the insulinotropic actions of glucagon and incretin hormones are largely mediated via increased cAMP levels, with protein kinase A (PKA) and cAMP-regulated GEF cAMP-GEFII (also termed Epac2) serving as primary downstream cAMP effectors (65–69). Rab3GAP, but not EPI64A, overexpression strongly dimin- ished the rapid refilling of the IRP and RRP following initial depletion. Therefore, we next tested if GTP-bound Rab3 isoforms were required for cAMP to enhance the initial secretory response, and if cAMP signaling was able to offset the Rab3GAP-induced deficit in rapid refilling of the IRP and RRP. For this analysis, the whole-cell recording patch pipettes contained 100 μM cAMP and evaluation of β-cell SG pool parameters of Rab3GAP-

overexpressing cells commenced, as above, 90 seconds after attaining the whole-cell configuration. As shown in Figure 8, inclusion of cAMP resulted in a significant increase in initial $\Delta C$m responses associated with the IRP and RRP compared with Rab3GAP overexpression in wt β-cells. In spite of this cAMP-driven increase in IRP and RRP size, refilling of the pools remained significantly incomplete to the standard 20-second recovery period. Also, although cAMP treatment increased integrated Ca2+ influx relative to cells treated with Rab3GAP alone (39.3±6.1 pC, Rab3GAP; 84.1±15.9 pC, Rab3GAP+cAMP) the enhanced influx did not overcome a Rab3GAP-mediated deficit in IRP and RRP pool refilling.

## 2.4 Discussion

The results of this study are among the first to identify and establish unique functional activities of Rab3 and Rab27 proteins on late stages of the exocytotic pathway, while also identifying functional overlap. Notably, we find that establishment of an IRP is completely dependent upon the presence of Rab27A GTPase in β-cells maintained in an islet architecture, as the IRP was completely lacking in Ashen β-cells. Rab27A was also found to participate in setting the RRP size under steady-state conditions, as the RRP response to an initial evoked secretory response was significantly reduced in size in Ashen β-cells as well as in wt β-cells overexpressing the Rab27A GAP EPI64A. By comparison, overexpression of Rab3GAP exerted little effect on RRP size under steady-state conditions, although Rab3 GTPases appeared to cooperate with Rab27A in setting the IRP size. Remarkably, however, Rab3, but not Rab27A, GTPases exert a key and prominent role to rapidly refill the IRP and RRP. Assignment of this kinetic effect to Rab3 GTPases resulted

from an observed strong deficit in rapid refilling of the RRP upon overexpression of Rab3GAP, and because neither Ashen β-cells nor overexpression of EPI64A in wt β-cells demonstrated a kinetic deficit in IRP and RRP refilling. Interestingly, the kinetic deficit in Rab3GAP-overexpressing β-cells did not mitigate cAMP from strongly potentiating the steady-state IRP and RRP size, although notably, refilling of these pools following depletion remained incomplete. Our experimental conditions do not exclude the possibility that the Rab3GAP-mediated slowing of refilling is independent of Rab3. However, previous studies have demonstrated that loss of Rab3GAP results in no changes in the levels of key exocytotic proteins or morphology of release sites (70,71). Moreover, Müller et al. showed that Rab3 specifically mediated a deficit in compensatory synaptic exocytosis in Rab3GAP mutant synapses. Taken together, these data support that Rab3GAP actions on secretion being directly related to perturbations in the activity of Rab3 GTPases. Finally, the combined loss of active Rab3 GTPases with Rab27A resulted in an RRP size that was more severely reduced than observed in Ashen β-cells. Notably, the present results complement our initial report that established incomplete refilling of the RRP following its evoked depletion in isolated and cultured Ashen β-cells (13). In addition, we reported that β-cells lacking only the Rab3A isoform displayed normal IRP and RRP refilling, which together with the present results suggest that other Rab3 isoforms are able to fully compensate for loss of Rab3A. The present data demonstrate distinct functional and kinetic regulatory activities of Rab3 and Rab27A GTPases on SG transition to fusion competency, while also providing evidence that full development of β-cell secretory activity requires convergent actions of Rab3 and Rab27A GTPases.

An important feature of this study is that we have identified unique roles for Rab27 and Rab3 GTPases. Rab27 GTPases are necessary for the formation of an IRP. This was a surprising result given the extensive literature linking Rab3/RIM complexes with docking near calcium channels, as required for the IRP (19,72 – 74). Nonetheless, our results suggest that Rab27 is a limiting factor for the formation of the IRP, which could be mediated by Rab27 unfettering of Rab3-clamped granules through stimulation of GTPase activity (75), or via Rab27 complexes with Slp4A/Munc18-1/Syntaxin (76). Rab3A GTPases exert a unique role on the rapid repopulation of the IRP and RRP in pancreatic β-cells. Yet, the mechanism by which Rab3 GTPases exert this action remains unanswered. Bio-chemical, genetic and live cell imaging have demonstrated that targeting/docking and priming functions of Rab GTPases involve a sequencing of effector interactions (77). In addition, multiple lines of evidence have indicated that docked SGs may be the primary location of Rab3 GTPase priming actions, because Rab3GAP hydrolyzes Rab3-GTP to Rab3-GDP concurrently with Ca2+ -triggered vesicle fusion (77 – 79). This catalytic event is believed to occur after vesicle docking/tethering but prior to endocytosis, as Rab3 is absent from clathrin-containing vesicles (80). Rab effectors interact directly, or in molecular scaffolds, with other mediators of vesicle priming and membrane fusion. For example, Rab3 GTPase effectors include rabphilin (17), Noc2 (39), Slp4 (35), Munc18-1 (81) and RIM1α/2α (18). Notably, RIM1α/2α bind with the priming factor Munc13-1 and nuclear magnetic resonance spectroscopy has established that Rab3-GTP, Rim2α and Munc13-1 can assemble into a tripartite complex (82). RIM has been established to exert a key role in insulin secretion (83) and be associated with both Rab3-GTP on the insulin granule (19) and L-type Ca2+ channels on the plasma membrane (84). In addition to effector interaction

with RIM, Rab3-GTP interactions with Munc18-1 or rabphilin may serve as the link between granule docking and priming reactions with SNARE proteins (81,85). These results have led to a model whereby a secretory stimulus enhances GTP hydrolysis to elicit disassembly of the GTP-bound Rab–effector complexes, thereby allowing the spatially localized interaction of Rab effectors with downstream mediators required for vesicle priming/fusion and formation of the SNARE complex (77, 78, 86, 87). Moreover, recent reconstitution of Rab5 with its cognate SNARE-dependent membrane fusion pathway has demonstrated that Rab and SNARE machineries act coordinately to facilitate the process of membrane tethering/docking and fusion (88). Importantly, although Rab3 GTPases may serve as gatekeepers regulating transition of docked SGs into primed releasable pools, the specific SGs on which Rab3 acts to rapidly refill the RRP remain unknown, particularly as insulin SGs are subject to rapid recruitment and priming during sustained glucose-stimulated insulin secretion (89,90).

Glucose-stimulated β-cell secretion is biphasic, consisting of a rapid and a slower more prolonged phase of insulin release. The initial phase has generally been equated with the IRP, which is completely released over milliseconds in response to step depolarization under voltage clamp (91). This association is based on the number of SGs released, and on timing differences between the direct electrical- and glucose-evoked release resulting from the immedi- acy of membrane potential changes versus glucose diffusion, uptake and metabolism and insulin diffusion from an intact tissue. In addition, molecular scaffolding of a small set of SGs to voltage-gated calcium channels, and of insensitivity of fusion of the IRP by the Ca2+ chelator EGTA, but not the kinetically faster chelator BAPTA, have strongly indicated that the IRP consists of docked SGs. Moreover, TIRF imaging of insulin SGs has

demonstrated that the initial rapid fusion events result largely from membrane adjacent/docked SGs (92 – 94). Taken together, release from the IRP is likely to be completely accounted for by fusion of membrane-docked SGs.

By comparison, the source of SGs that comprise the RRP (generally assigned to the second phase of glucose-stimulated insulin secretion) is less concretely identified. This pool likely is composed of docked (or membrane resident) SGs as well as a set of newcomer granules that have more recently been identified to cycle rapidly from the RP to undergo membrane fusion (95). Previous findings have established that Rab3 and Rab27 GTPases coordinately regulate the docking of dense core SGs (46) while also differing in membrane cycling dynamics (32). Our data demonstrate that the formation of an IRP is completely dependent upon Rab27A, with active Rab3 GTPases exerting a modulatory role. For the RRP, active Rab3 GTPases exert a critical role on rapid refilling of the RRP following initial depletion, while GTP-bound Rab27A appears important in defining the overall size of the RRP. Thus, although overexpression of Rab3GAP slowed RRP refilling it did not notably affect RRP size. The divergent actions of these Rab GTPases may correlate with differences reported in their dynamic association with SGs (32,33,96). The Rab3A pool, which likely reflects similar behavior of the other Rab3 GTPases, demonstrates a rapid exchange between the SGs and cytosol, whereas Rab27A has demonstrated little exchange associated with the exocytotic event (32,33). The rapid exchange of Rab3 GTPases may account for their ability to kinetically facilitate RRP refilling as they are able to quickly cycle onto SGs and recruit appropriate effectors that promote SG recruitment to the plasma membrane as well as subsequent tethering/docking and priming processes. Not only is rapid granule/cytosolic exchange lacking for Rab27A, fluorescence recovery after

photobleaching studies have indicated that once it associates with newly synthesized SGs it becomes non-exchangeable, perhaps as a result of low inherent GTPase activity (32). In support of its low GTPase activity, a high percentage of Rab27A has been reported to be GTP-bound and membrane-associated, even in unstimulated pituitary, platelet, pancreatic acinar and insulin-secreting Min6 cells (20,97,98). Yet, GTPase activity appears key to regulation of insulin secretion because Rab27A, unlike most GTPases, has been reported to bind effectors in both the GDP- and GTP-bound states. In its GDP-bound state, Rab27A recruits and inter- acts with Slp4A (37). Slp4A (also termed granuphilin) was originally identified in pancreatic β-cells as a protein that binds to the closed form of syntaxin1A and Rab27A-GDP to participate in docking of the insulin granules (20,99,100). Yet, this Rab27A-GDP-directed docking complex has been reported to be extremely stable and strongly inhibitory to the progression of SG priming and membrane fusion (35,101). Release of this clamp on granule priming is believed to require the transition of Rab27A to its GTP-bound state, although Rab27A-GTP retains high-affinity Slp4A binding. Interestingly, the Rab27A/granuphilin/syntaxin1A complex may also con- tain Munc18 (99), an apparent regulator with Munc13 of SNARE complex assembly, suggesting that transition of Rab27A from GDP- to GTP-bound state may also allow initiation of priming processes. Our data demonstrating a reduction in RRP size in Ashen β-cells are consistent with Rab27A promoting stability of SG tethering/docking and priming into the RRP. In addition, complete elimi- nation of the IRP in Ashen β-cells suggests that Rab27A may also be important in targeting insulin SGs to membrane nanodomains adjacent to voltage-gated calcium channels.

While glucose stimulation of β-cells may facilitate transition of Rab27A from its GDP- to GTP-bound state and pro- mote vesicle priming, it also drives Rab3-GTP binding (75), vesicle fusion and a coincident cycling of Rab27A back to a GDP-bound state. Unlike Rab3 GTPases, post-fusion membrane-associated Rab27-GDP in pancreatic β-cells does not rapidly exchange into the cytosol, but rather acts to recruit and activate the endocytotic regulators coronin3 and Cdc42-GTP-bound IQGAP1 (34,102). The interaction of Rab27A-GDP with coronin3, a promoter of F-actin bundling, in complex with IQGAP1 has been reported essential for endocytosis of insulin secretory membrane. Moreover, overexpression of EPI64A in β-cells has previously been found to reproduce glucose-dependent translocation of coronin3 (103), likely resulting from GTP hydrolysis and production of Rab27A-GDP. The negative clamp on exocytotic activity of Rab27A-GDP through Slp4A interaction, and its slow exchange into the cytosol following exocytosis may account for its kinetically slower action on refilling of the vesicle pools from newcomer granules than that of Rab3.

It is important to note that while we have identified distinct functional activities of Rab3 and Rab27 GTPases in the exocytotic pathway, these GTPases also demonstrated a high degree of functional commonality. For example, the RRP, while reduced in Ashen β-cells as well as in wt β-cells overexpressing EPI64A, remained present and rapidly refilled following the depolarization-evoked depletion protocol. Rab3 GTPases also largely compensated for Rab27 absence, as evidenced by an even stronger reduction in RRP size and pool refilling upon Rab3GAP overexpression in Ashen β-cells. Conversely, Rab27A also appears to exert substantial functional compensation when Rab3 GTPases are shifted to their GDP-bound state by Rab3GAP overexpression, as there was little effect on RRP size,

although the rate of refilling was significantly slowed. This functional overlap is likely based on the high homology between Rab3 and Rab27 (57% by amino acid sequence) that leads to sharing of a number of effectors (rabphilin, Noc2 and Slp4A). Also, even where Rab3 and Rab27A exhibit effector selectivity (Rab3, RIM1/2a, Rab27A, Slac2-C and Munc13-4) the effectors demonstrate overlap in their reported functional activities (19,21,40).

In summary, our data are novel in identifying unique func- tional activities of Rab3 and Rab27 GTPases within the exocytotic pathway. Identification of the precise pathways that govern these mechanistic differences requires further investigation. Our data further suggest that Rab3 GTPases act to rapidly refill releasable granule pools but that Rab27 may demarcate and define the quantity of releasable sites as well as be required to populate the IRP. The linear sequencing of SGs from the RRP to IRP suggests a dynamic coordination in GTPase activity and/or effector switching during secretagogue stimulation. In addition, while functional diversity is distinguishable, there remain considerable compensatory actions between these GTPases, which likely result from the cooperative use of effectors and/or specificity in effectors with functional similarity. Future investigations require evaluating whether all the isoforms of Rab3 participate in rapid refilling of the RRP and identifying which most effectively compensates for loss of Rab27A.

## 2.5 Materials and Methods

*Mice and pancreatic islet slice preparation*

All experiments were approved by the University Committee on Use and Care of Animals (UCUCA) and appropriate measures were taken to reduce the pain of experimental

animals. Mice carrying a spontaneous A to T transversion mutation in the Rab27A gene (ash/ash; C3H/He back- ground) lead to the production of a non-functional Rab27A protein that lacks critical domains of the GTP-binding pocket. These Ashen mice were initially supplied by N. A. Jenkins (National Cancer Institute) in cooperation with Jackson Laboratories. Gender- and age-matched mice of the same background strain variant (C3H/HeSnJ) were used as con- trols. Mice were sacrificed by CO2 asphyxiation, decapitated and the pancreas sterilely removed for preparation of isolated islets. Collagenase P (1mg/mL, Roche Diagnostics), soybean trypsin inhibitor (0.1mg/mL) and neutralized bovine serum albumin (2.5 mg/mL) dissolved in 5 mL of 5% CO2/95% O2 gassed F12K Nutrient Kaighn's media were immediately injected into the pancreas until well distended. Following injection, the pancreas and remaining collagenase solution were placed in a 25-mL Erlenmeyer flask, gassed with 5% CO2/95% O2 and placed into a 37◦C oscillating water bath (100 cycles/min) for 10 min. Following this period, free collagenase solution surrounding the pancreas was removed and replaced with a fresh 5-mL aliquot of collagenase solution and the flask returned to the oscillating water bath for an additional 15 min. Dispersion of the pancreas to generate isolated islets and acini was then performed by sequential passage through polypropylene pipettes of decreasing tip diameter. The resulting cell suspension was transferred to a 10-cm culture plate and individual intact islets identified using an inverted microscope were removed by hand micropipetting into a F12K media-containing collection dish. The isolated islets were then collected and placed into 37◦C liquid agarose (low melting point) and centrifuged at 1700 × $\boldsymbol{g}$ at 25◦C for 2 min. Horizontal slices (150 μm) were then cut from the islets concentrated at the tip of the solidified agarose and transferred to millicell-supported membranes (0.4 μm pore;

Millipore, Cork IRL) in culture media (DMEM, 15% heat-inactivated FBS, 0.0005% β-mercaptoethanol, 50 U/mL peni- cillin, 50 μg/mL streptomycin and 0.05 mg/mL soybean trypsin inhibitor) for 1–3 days of organ culture.

*Expression constructs and viral infection*

Expression of exogenously introduced transgenes in cells of cultured islets was accomplished using adenoviral infection. The vector pAdTrack-CMV (Addgene) was used for subcloning into and for infection and expression of the catalytic subunit of Rab3GAP (Yoshimi Takai, Kobe University), EPI64A (Open Biosystems, Thermo Scientific) or β-Gal (control). The sequence fidelity of all constructs was confirmed by DNA sequencing (University of Michigan DNA Sequencing Core). Islets were infected with viral aliquots sufficient to infect approximately 20% of the surface layer of cells within a slice. Virus was diluted in media and applied directly onto the islets and into the small volume of media resident on the millicell membrane surface. After 12 h the media were exchanged for fresh culture media. To identify infected cells the pAdTrack contained an independent CMV promoter driving expression of the fluorescent EGFP tracer.

*Islet slice electrophysiology*

Islet slices surrounded by the agarose matrix were transferred to a continuously perfused and temperature-controlled (31∘C) recording chamber (Warner Instruments) that was mounted on an upright Nikon EF-89 microscope and equipped with a 40× water immersion lens (NA 1.2) for viewing of individual cells. Whole-cell patch-clamp experiments were performed on cells within islet slices using an EPC-9 or EPC-10 amplifier

and PATCHMASTER acquisition software (HEKA Elektronik). Patch pipettes with a resistance of 3–6 MΩ when filled with the pipette solution were pulled from Schott capillary glass containing a microfiber (AM Systems) and then coated with Sylgard (Dow Corning) to reduce capacitance transients. Currents underlying test pulses and *I–V* relationships were compensated for linear leak current using a P/4 protocol.

Evoked changes in cell capacitance associated with exocytotic activity were measured using the PATCHMASTER software lock-in extension (sine + DC) with a 30-mV peak sinusoid signal applied at a frequency of 1.8 kHz. Data were analyzed only if the resulting Rs maintained <20 MΩ. Although β-cells are electrically coupled, previous reports have estab- lished that only 1.5% of the current response to the sine wave originates from neighboring cells (104). In addition, although changes in membrane capacitance reflect a net measurement of exocytotic and endocytotic activity, endocytosis operates at a significantly slower rate than exocytosis, suggesting that the rapid sequential voltage-step-evoked responses largely represent exocytotic activity. The standard extracellular solution contained (mM): 135 NaCl, 2.5 KCl, 1.25 NaH2PO4, 2 sodium pyruvate, 0.5 ascorbic acid, 1 MgCl2, 2 CaCl2, 3 glucose and 26 NaHCO3. The solution was gassed continuously with 5% CO2/95% O2 for a pH of 7.4. In experiments where glucose concentration was raised the NaCl was reduced to maintain an equivalent osmolality (290 mOsmol/L). The pipette solution used for whole-cell recording contained (mM): 120 Cs-glutamate, 10 NaCl, 10 KCl, 1 MgCl2 , 10 HEPES (pH 7.15 with CsOH), 0.05 EGTA, 3 Mg-ATP and 0.2 Na-GTP. Current-clamp recordings from β-cells in islet slices were performed using amphotericin (250 μg/mL)-perforated patch-clamp conditions with the following pipette solution (mM): 76

K2SO4, 5 NaCl, 10 KCl, 1 MgCl2, 0.2 EGTA and 10 HEPES (pH 7.35 with KOH). All reagents were from Sigma unless stated otherwise.

*Confocal microscopy*

Confocal imaging was performed on an Olympus IX81 disc-spinning con- focal microscope using a Plan-Apochromat 100× oil immersion objective (1.4 NA). Fluorescent illumination was provided by a Lambda LS 300-W xenon arc lamp (Sutter Instruments) coupled to a shuttered liquid light guide for controlled transmission of light to the microscope optics. Images were acquired using an electron multiplying charge-coupled device (EM-CCD) Hamamatsu (ImagEM) camera and a 2× optical zoom (Optem). Monomeric versions of mCH, YFP, Citrine (a YFP derivative of reduced pH sensitivity), CFP, Cerulean or EGFP N-terminal fluoroprotein-tagged fusion proteins were imaged using the following excitation/emission filter sets: Ex 472/30; 562/40; 501/18; 416/25 and Em: 520/35; 641/75; 547/31; 464/23, respectively. Prior to image acquisition the illumination intensity/camera gain of each fluorescence channel was optimized to ensure a full dynamic range (16-bit image). Once acquisition parameters were determined, identical set- tings were used for each condition being compared. Cytofluorograms for Rab GTPases versus granules (NPY-mCH), see Figure 2B, were constructed by taking background-subtracted (rolling-ball radius filter = 100 pixels) intensities of each pixel per channel and plotting them against one another. A Pearson's *r* correlation coefficient was then calculated to indicate the degree of colocalization between Rabs and granules.

*Total internal reflection fluorescence microscopy*

TIRF imaging of SG mobility in transfected MIN6 cells was performed on an Olympus IX71 microscope equipped with a 60× oil immersion objective (1.49 NA). Cells were co-transfected with Citrine (control) or a N-terminal Citrine-tagged Rab3GAP and/or EPI64A along with NPY-mCH to label the lumen of insulin-containing SGs. TIRF imaging of MIN6 cells was performed in a physiological saline containing (mM): 135 NaCl, 5 KCl, 1 MgCl2, 2 CaCl2, 3 glucose and 10 HEPES (pH7.4). For illumination, two lasers including a 50-mW diode-pumped solid-state laser operating at a fixed wavelength of 594 nm (Cobolt Mambo) and a 225-mW Argon-ion laser (National Laser Company) beam (selected 488-nm laser line) were passed through a acousto-optic tunable filter (AOTF) to select the passing laser line and adjust illumination power. Out- put of the AOTF was coupled to a unimodal fiber optic that was directed through beam expansion optics immediately prior to being reflected into the microscope body by a mirror mounted on a galvanometer to position the laser illumination in the back focal plane of the objective. The position of the 488-nm laser line in the back focal plane was adjusted to set a resulting evanescent field depth of 100 nm. An additional achromatic lens between the mirror and the microscope objective focused the laser on the back focal plane of the objective. The microscopes filter cube assembly contains a laser clean-up filter (488 ± 10 nm), dichroic mirror (z488rdc) and emitter (HQ525/50). All filters were laser grade from Chroma Technologies. Fluorescence emission images were acquired with a 16-bit, 512 × 512 pixel Photometrics QuantEM 512SC EM-CCD camera (Roper Scientific) with 16 × 16 μm pixel size. To achieve Nyquist sampling, emission was submitted to additional magnification from a 1.6× magnifier on the

IX71 and a 2.5× beam expander. The laser lines, laser powers, incident angle and camera were controlled using METAMORPH software (Molecular Devices).

Images were acquired at 20Hz and with mobility in *x*–*y* and axial (*z*) dimensions determined by tracking granules that were present through- out the entire image series in each cell using custom-written MATLAB scripts. Granule detection was accomplished by applying a binary mask to each image, with the default masking threshold set to 15 standard deviations above the mean of a background region of interest. The centroid coordinates of each granule in each masked image were determined and a comparison of granule centroids across frames was used to identify those SGs that remained throughout the complete image series. Each of these SGs was then individually tracked by applying a 2D Gaussian fit for the granule in its first frame, and then searching a 12 × 12 pixel region sur- rounding the granule's fitted center coordinates in the next frame, for a similar Gaussian fit. Specific limits were set for acceptable changes in $x - y$ position and minimum time spent at a position for a given granule to be considered the same. Granule tracking was terminated if two unique granules collided. Changes in $x - y$ position between frames for each granule were determined using its center coordinates. For axial motion, fluorescence intensity for each tracked granule per frame was determined using a granule's center coordinates to center a 3 × 3 pixel mask and mea- sure averaged intensity. The apparent interframe fluctuations in central $x - y$ positions $(\Delta R)2$ and fluorescence intensity $(\Delta Z')2$ were determined as previously described (105), with apparent integrated intensity fluctuations occurring between frames for individual granules $(\Delta Z')2$ corrected for instrumental noise (shot noise and EM-CCD camera noise) by imaging tetraspeck beads adhered to a glass coverslip to generate corrected $(\Delta Z)2$. Interframe *x*–*y* mobility

represented by $(\Delta R)2$ was calculated by: $(\Delta R)2 = ((x2 - x1)2 + (y2 - y1)2)$*83.3 nm/pixel, where $x$ and $y$ represent the centroid position between paired interframe intervals 1 and 2. Apparent interframe axial mobility $(\Delta Z')2$ is based on background-subtracted intensities ($I$) in successive frames (1 and 2) and with $z$=0 defined as the brightest intensity granule ($I$o) per cell. Characteristic TIRF depth (Dp) was set at 100nm. For each frame ($i$) the apparent intensity ($Ii'$ ) is calculated as: $Ii' = Ioe-z'i/Dp$, which upon rearranging results in: $z' = -Dpln(I'/I)$.

*Statistics*

All statistical analysis was done using GraphPad Prism. Where indicated, one-way analysis of variance (ANOVA) was used to test for significant differences (significance was set to a $p < 0.05$). *Post hoc* Bonferroni protected *t*-tests were used for comparisons between specific groups. To test whether cumulative frequency distributions of granule mobility were significantly different, we employed the Kolmogorov–Smirnov test. Statistical significance at a $p<0.05$ is noted within figures by an asterisk (*).

## 2.6 Acknowledgements

This work was supported by NIH grant RO1 NIDDK-DK077050 to E. L. S. We thank Dr. Yanan Hou for critical discussions related to the experiments and specific research reagents.

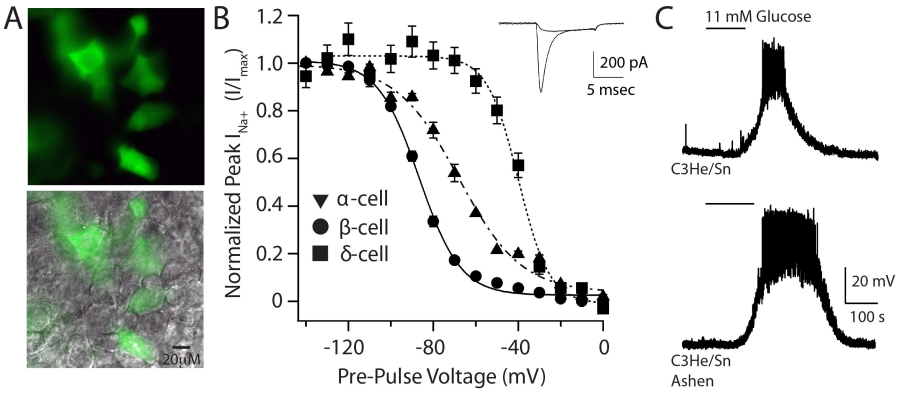
A
20μM
B
Normalized Peak $I_{Na+}$ ($I/I_{max}$)
1.2
1.0
0.8
0.6
0.4
0.2
0
-120
-80
-40
0
Pre-Pulse Voltage (mV)
α-cell
β-cell
δ-cell
200 pA
5 msec
C
11 mM Glucose
C3He/Sn
20 mV
100 s
C3He/Sn
Ashen

**Figure 2.1: Adeno viral infection of pancreatic islet slices and electrophysiological identification of β-cells.** A)Fluorescent micrograph of islet slice infected with pAdTrack-CMV-EGFP adenovirus (upper) that is overlayed on a differential interference contrast image of the slice (lower). B) Normalized averaged steady-state voltage-dependent Na+ inactivation relationships recorded under voltage clamp from infected pancreatic islet cells (mean ± SEM; N = α, 3; β, 8; δ, 3). Inactivation voltage-clamp protocol: holding potential, −70 mV; prepulse voltages of 200-millisecond duration ranged from −150 to 0 mV in 10-mV increments; pulse potential, 0 mV for 10 milliseconds; interpulse interval, 5 seconds. Inset, representative voltage-dependent current from β-cell when held at prepulse potentials of −100 and −40 mV. C) Current-clamp recordings of glucose-stimulated (11 mM) action-potential bursting behavior from β-cells in wt control (C3He/Sn) and Ashen islet slices that were subjected to 3 days organotypic tissue culture. Slices were perfused with normal extracellular solution containing 3 mM glucose for at least 5 min prior to glucose stimulation.

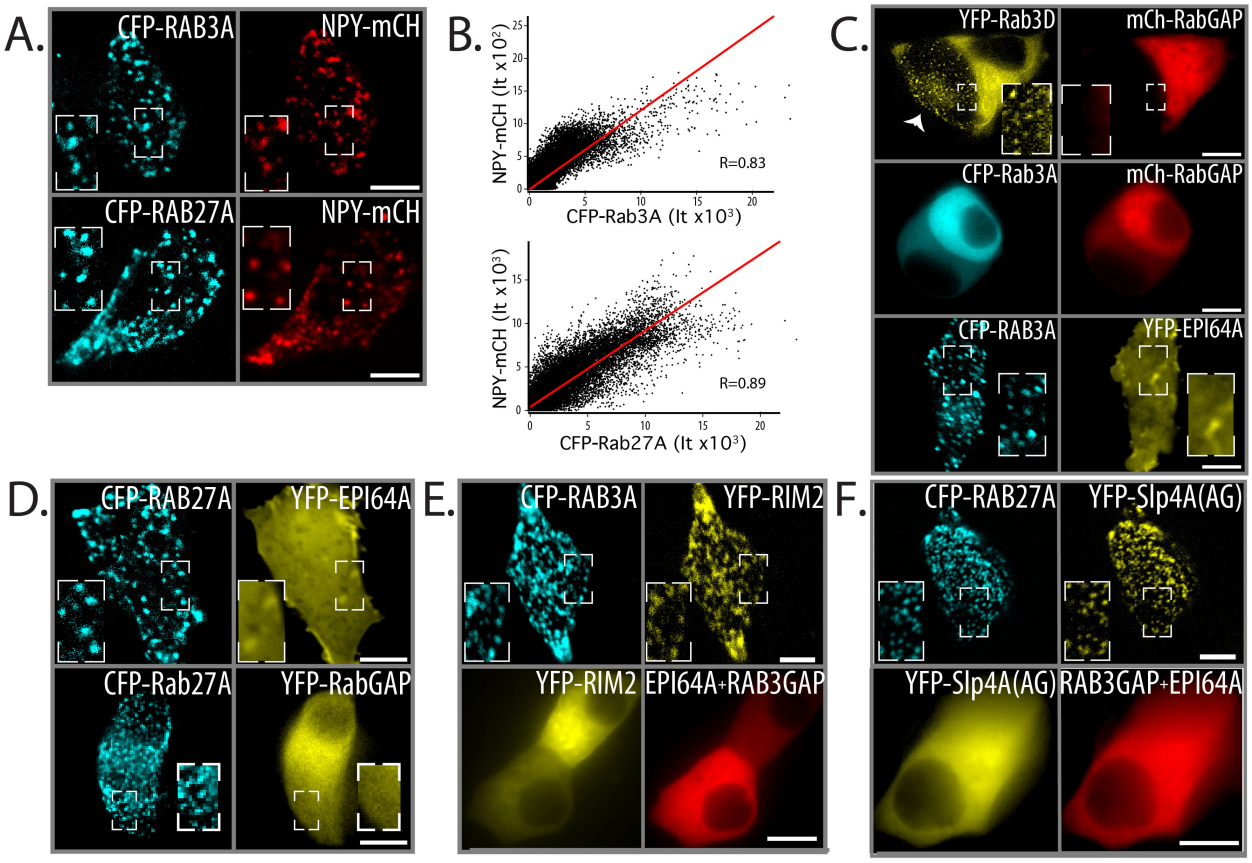
A.
CFP-RAB3A
NPY-mCH
CFP-RAB27A
NPY-mCH
B.
NPY-mCH (It x10²)
CFP-Rab3A (It x10³)
R=0.83
NPY-mCH (It x10³)
CFP-Rab27A (It x10³)
R=0.89
C.
YFP-Rab3D
mCh-RabGAP
CFP-Rab3A
mCh-RabGAP
CFP-RAB3A
YFP-EPI64A
D.
CFP-RAB27A
YFP-EPI64A
CFP-Rab27A
YFP-RabGAP
E.
CFP-RAB3A
YFP-RIM2
YFP-RIM2
EPI64A+RAB3GAP
F.
CFP-RAB27A
YFP-Slp4A(AG)
YFP-Slp4A(AG)
RAB3GAP+EPI64A

**Figure 2.2: Expression of Rab GAPs transitions Rab3 and Rab27 into GDP-bound states.** A) Confocal images of Min6 cells co-expressing CFP-Rab3A or CFP-Rab27A with a SG lumen marker (NPY-mCH). B) Cytofluorograms showing correlation of pixel by pixel intensities (It; N = 4 Rab3A; N = 5 Rab27A). C) Representative images of Rab3GAP and EPI64A co-expressed with Rab3A or Rab3D. Note that vesicular localization of Rab3D was retained in an adjacent non-Rab3GAP transfected cell (arrowhead). D) Co-expression of GAP proteins with Rab27A had no apparent effect on Rab27A's association with SGs. E) Co-expression of CFP-Rab3A + cYFP-Rim2α(1-179) demonstrates colocalization of punctate fluorescence (upper) that is lost with added expression of mCH-Rab3GAP (lower). F) Co-expression of CFP-Rab27A + cYFP-Slp4A(AGAAAY), denoted on figure as YFP-Slp4A(AG), demonstrates colocalization of punctate fluorescence (upper) that is lost with added expression of mCH-EPI64A (lower). Scale bar = 5 μm, within each figure insets show expanded view of a region of the cell (outlined in white-dashed line)

.

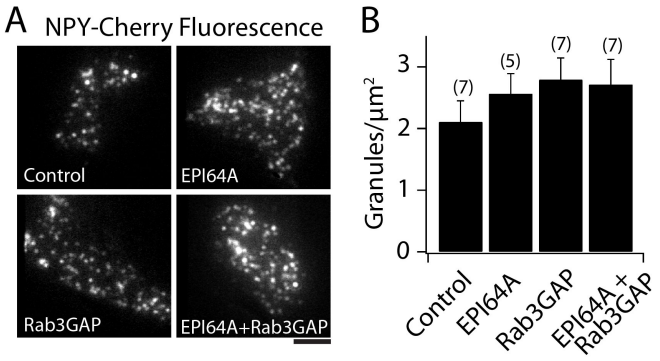
A
NPY-Cherry Fluorescence
Control
EPI64A
Rab3GAP
EPI64A+Rab3GAP
B
Granules/µm²
0
1
2
3
(7)
(5)
(7)
(7)
Control
EPI64A
Rab3GAP
EPI64A + Rab3GAP

**Figure 2.3: Overexpression of Rab GAP proteins does not alter density of SGs adjacent to plasma membrane.** A) TIRF micrographs of SGs in Min6 cells transfected with NPY-mCH, a fluorescent lumenal marker of SGs, alone (control) or in combi- nation with EPI64A (upper right), Rab3GAP (lower left) or EPI64A and Rab3GAP (lower right). B) Averaged measured density of SGs for each condition (mean ± SEM; N = number of cells). Scale bar below images = 5 μm.

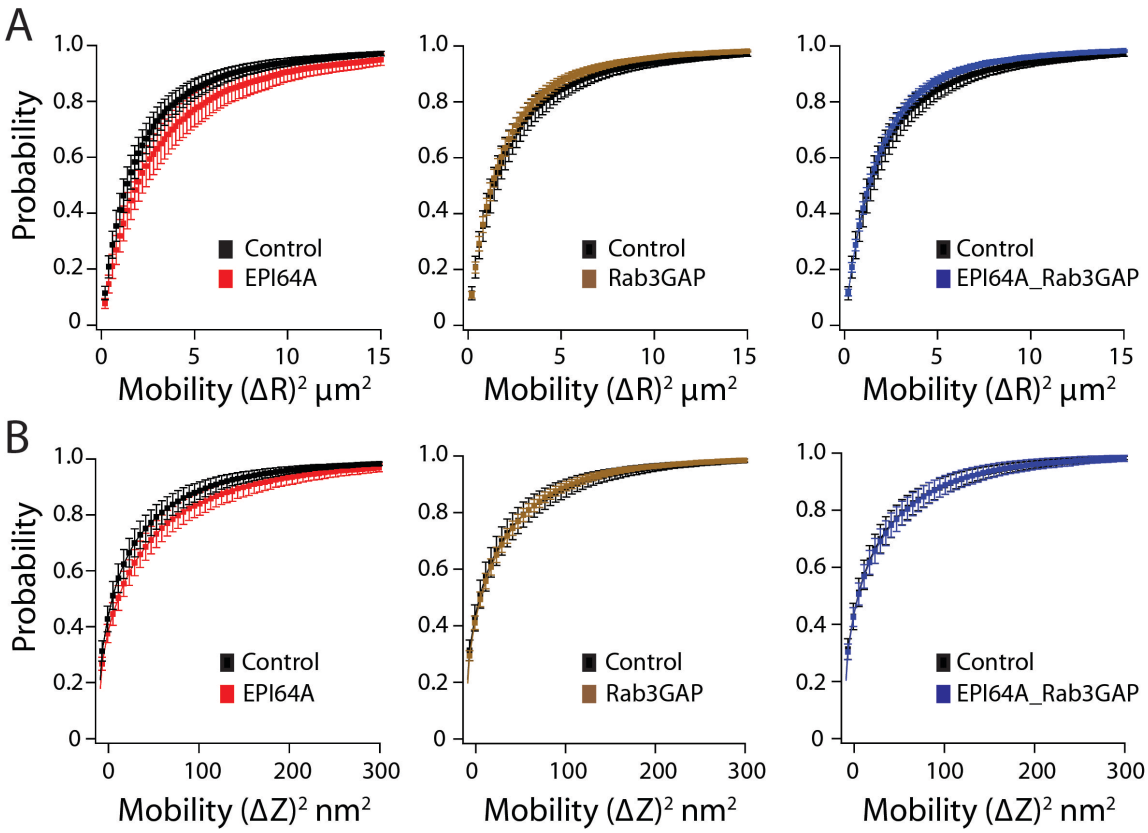
A
Probability
1.0
0.8
0.6
0.4
0.2
0
0
5
10
15
Mobility (ΔR)² µm²
Control
EPI64A
Control
Rab3GAP
Control
EPI64A_Rab3GAP
B
Probability
0
100
200
300
Mobility (ΔZ)² nm²
Control
EPI64A
Control
Rab3GAP
Control
EPI64A_Rab3GAP

**Figure 2.4: Mobility of membrane adjacent SGs is unaffected by overexpression of GAP proteins.** A and B) Averaged cumulative probability distributions of apparent interframe fluctuations in central x–y positions (ΔR)2 (A) or axial position (ΔZ)2 (B) of membrane adjacent SGs in Min6 cells transfected with the granule lumenal marker NPY-mCH and co-transfected with Citrine (control), Citrine–EPI64A, Citrine–Rab3GAP or Citrine–EPI64A+Citrine–Rab3GAP. The control (ΔR)2 and (ΔZ)2 data are included on each appropriate graph to allow comparison to the GAP treatments. Measurements made only on membrane adjacent SGs that were present throughout the entire 10-second imaging stream. Data are presented as mean ± SEM; control, 7 cells, 86 granules; EPI64A, 5 cells, 98 granules; Rab3GAP, 7 cells, 150 granules; EPI64A + RabGAP, 7 cells, 131 granules.

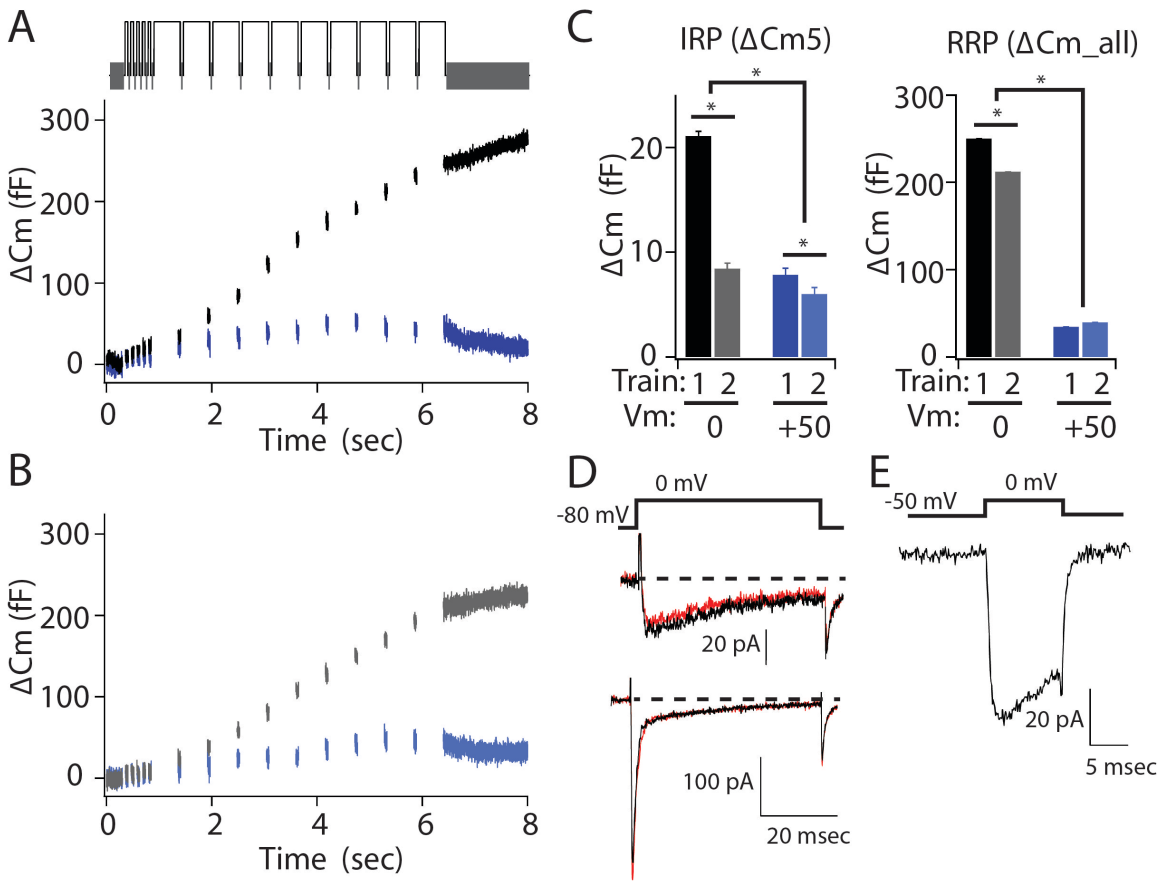
A
300
200
100
0
ΔCm (fF)
0
2
4
6
8
Time (sec)
B
300
200
100
0
ΔCm (fF)
0
2
4
6
8
Time (sec)
C
IRP (ΔCm5)
RRP (ΔCm_all)
ΔCm (fF)
20
10
0
300
200
100
0
Train: 1 2
1 2
Vm:
0
+50
D
0 mV
-80 mV
20 pA
100 pA
20 msec
E
-50 mV
0 mV
20 pA
5 msec

**Figure 2.5: Determination of IRP and RRP size to sequentially applied step-depolarization pulse protocols in EGFP-infected β-cells.** A) Averaged ΔCm to applied pulse protocol from EGFP-infected cells. Depolarization steps were from a holding potential of −80 mV to 0 mV (black) or to +50 mV (blue). Pulse protocol pattern is illustrated above ΔCm. B) Averaged ΔCm to repeat application of pulse protocols (step to 0 mV, gray; +50 mV, light blue) applied to the same cells as in part A 20 seconds following the initial protocol. C) Averaged IRP (left) and RRP (right) pool sizes and recovery of granule pools following the 20-second non-stimulus interval. Mean ± SEM; N = 19 cells, 4 animals. D) Representative inward current to first step depolarization (holding potential −80 mV, step potential 0 mV) of initial (black) and second (red) applied pulse protocols. Currents from two different β-cells are shown (upper, lower) to illustrate interpulse interval protocol allows complete recovery of voltage-gated Ca2+ current (upper) and of Na+ and Ca2+ current (lower). E) Averaged voltage-gated Ca2+ current from β-cells used for ΔCm analysis measured on step to 0 mV from a holding potential (−50 mV) where voltage-gated Na+ channels are inactivated.

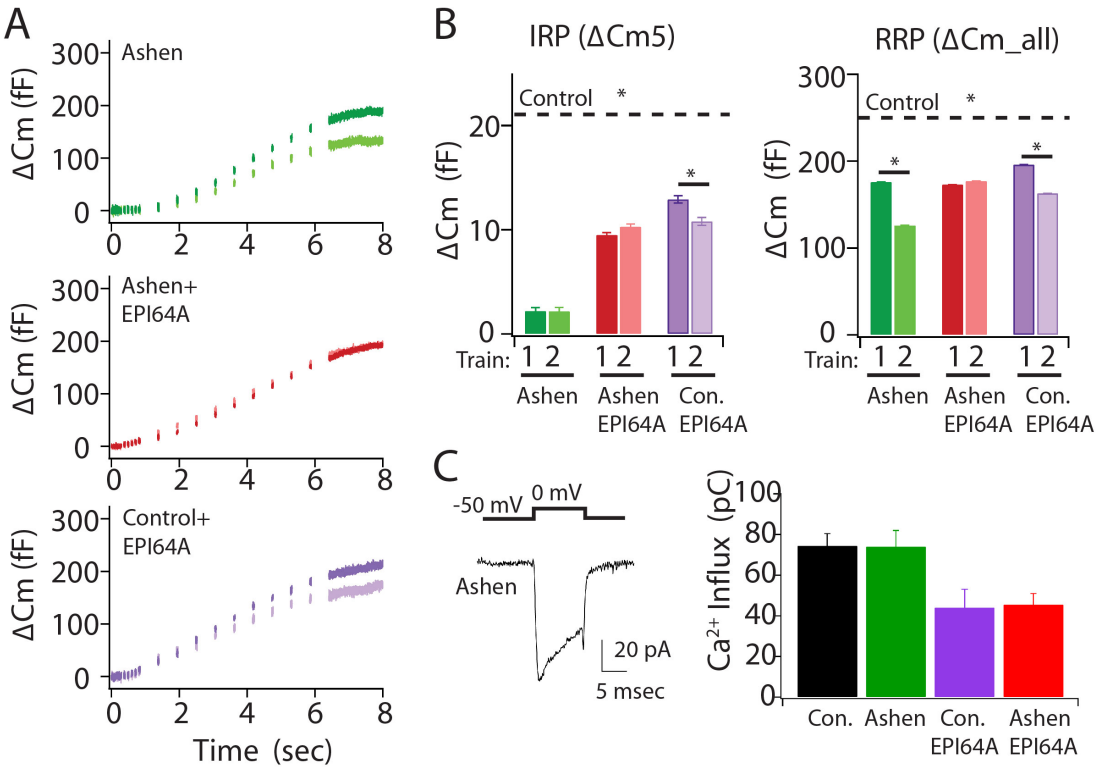
A
Ashen
Ashen+
EPI64A
Control+
EPI64A
ΔCm (fF)
Time (sec)
B
IRP (ΔCm5)
RRP (ΔCm_all)
Control
Train:
Ashen
Ashen
EPI64A
Con.
EPI64A
C
-50 mV
0 mV
Ashen
20 pA
5 msec
Ca2+ Influx (pC)
Con.
Ashen
Con.
EPI64A
Ashen
EPI64A

**Figure 2.6: Rab27A is essential to development of IRP and key to defining RRP size in β-cells.** A) Comparison of averaged ΔCm to sequentially applied pulse protocols (20-second interval) from pAdTrack EGFP-infected Ashen β-cells (upper, green, N = 22 cells, 4 animals), pAdTrack EPI64A/EGFP-infected Ashen β-cells (middle, red, N = 17 cells, 3 animals) and pAdTrack EPI64A/EGFP-infected wt β-cells (lower, violet, N = 11 cells, 3 animals). ΔCm to first applied protocol shown in darker color. B) Averaged size of IRP (left) and RRP (right) for each condition to each applied pulse protocol. Dashed line indicates average size of IRP and RRP to first pulse protocol under control conditions (EGFP-infected wt β-cells, Figure 4). Asterisk on dashed line indicates significance from conditions below. C) Averaged voltage-gated Ca2+ current (holding potential −50 mV, step potential 0 mV) from β-cells used for each ΔCm analysis (left). Averaged time-integrated Ca2+ influx (pC) for each condition as measured from inward current evoked on step to 0 mV from −50 mV holding potential (right, N = control, 11; Ashen, 15; Ashen + EPI64A, 8; control + EPI64A, 3).

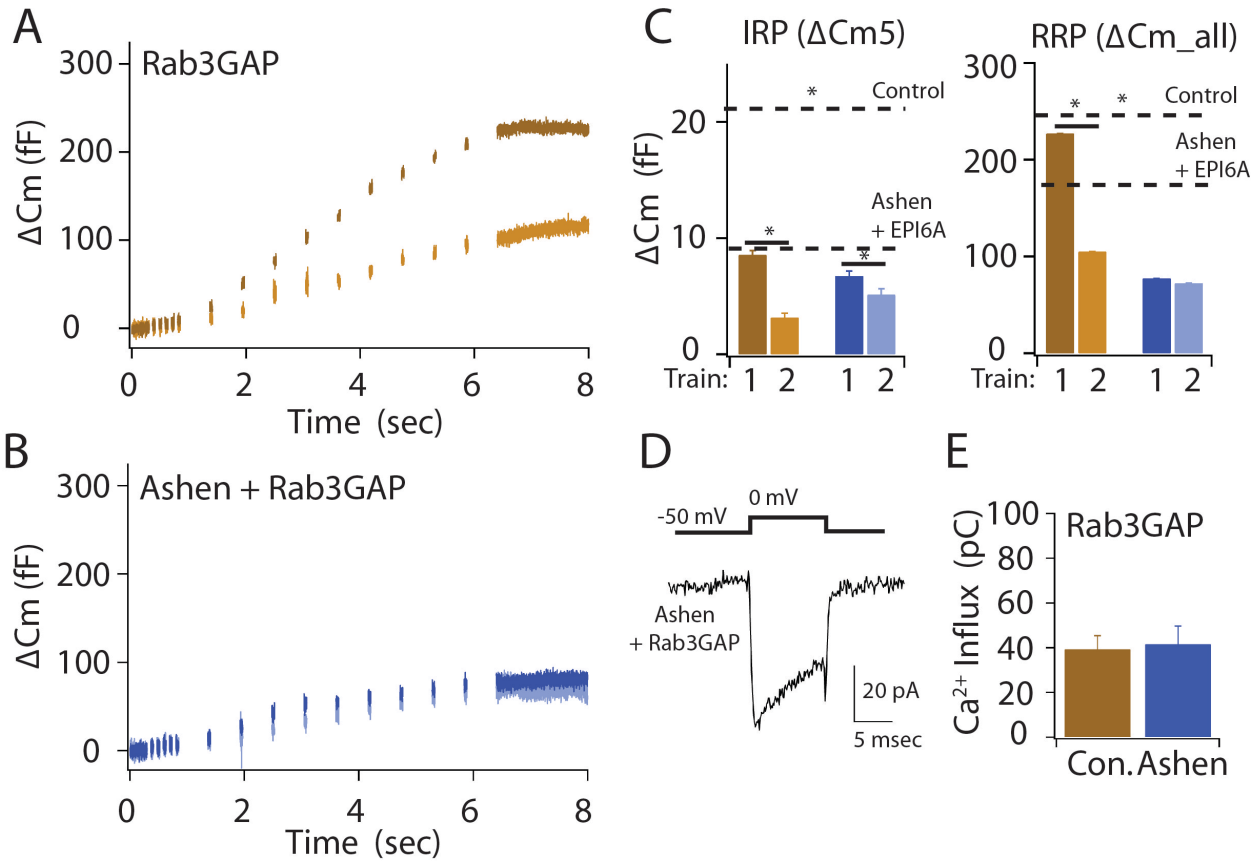
A
Rab3GAP
ΔCm (fF)
300
200
100
0
0
2
4
6
8
Time (sec)
B
Ashen + Rab3GAP
ΔCm (fF)
300
200
100
0
0
2
4
6
8
Time (sec)
C
IRP (ΔCm5)
ΔCm (fF)
20
10
0
Control
Ashen
+ EPI6A
Train: 1 2 1 2
RRP (ΔCm_all)
300
200
100
0
Control
Ashen
+ EPI6A
Train: 1 2 1 2
D
-50 mV
0 mV
Ashen
+ Rab3GAP
20 pA
5 msec
E
Rab3GAP
Ca2+ Influx (pC)
100
80
60
40
20
0
Con.
Ashen

**Figure 2.7: Rab3 exerts a central role in rapid refilling of RRP in β-cells.** A) Comparison of averaged ΔCm to sequentially applied pulse protocols (20-second interval) from pAdTrack Rab3GAP/EGFP-infected wt β-cells (brown, N = 15 cells, 4 animals), with darker color showing data from first pulse protocol. B) Averaged ΔCm responses from pAdTrack Rab3GAP/EGFP-infected Ashen β-cells (blue, N = 15 cells, 3 animals). Darker color shows data from first pulse protocol. C) Averaged size of IRP (left) and RRP (right) for each condition determined from each applied pulse protocol. Dashed lines indicate average size of IRP and RRP to first pulse protocol under control conditions (EGFP-infected wt β cells) and in Ashen cells. D) Averaged Ca2+ current from Ashen β-cells infected with pAdTrack Rab3GAP/EGFP used for ΔCm analysis. E) Averaged Ca2+ influx (pC) for β-cells from wt (control) and Ashen mice infected with pAdTrack Rab3GAP/EGFP (N = control + Rab3GAP, 5; Ashen + Rab3GAP, 9).

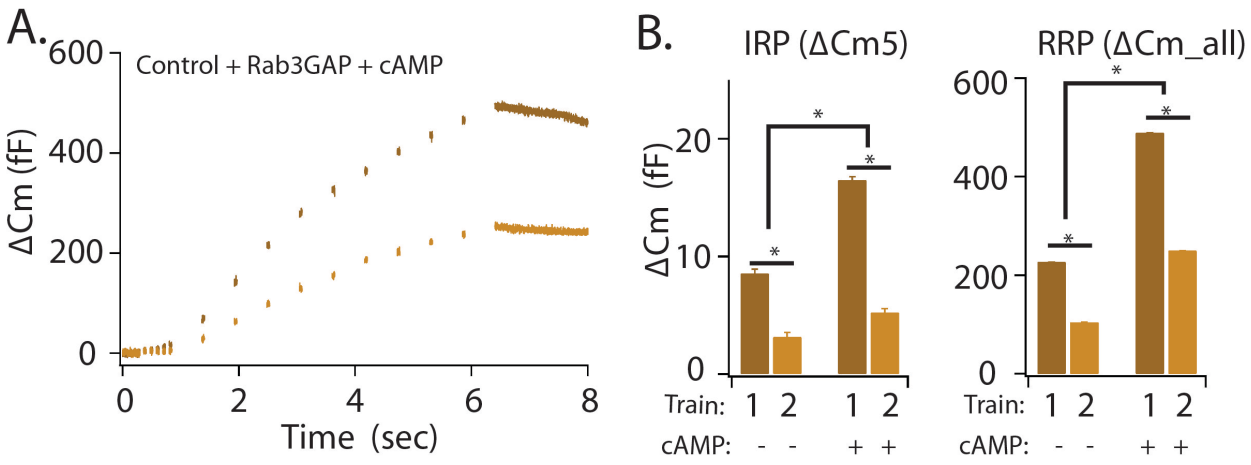
A.
Control + Rab3GAP + cAMP
ΔCm (fF)
600
400
200
0
0
2
4
6
8
Time (sec)
B.
IRP (ΔCm5)
RRP (ΔCm_all)
ΔCm (fF)
20
10
0
600
400
200
0
*
Train: 1 2 1 2
cAMP: - - + +

**Figure 2.8: Rab3 actions on rapid refilling of RRP are downstream of cAMP enhancement of IRP and RRP size.** A) Averaged ΔCm to sequentially applied pulse protocols from pAdTrack Rab3GAP/EGFP-infected wt β-cells (brown, N = 9 cells, 3 animals) in which the patch pipette solution contained 100 μM cAMP, with darker color showing data from first pulse protocol. B) Averaged size of IRP (left) and RRP (right) for the cAMP recorded pAdTrack Rab3GAP/EGFP-infected wt β-cells. Average results from the non-cAMP Rab3GAP condition (Figure 7) are shown for comparison.

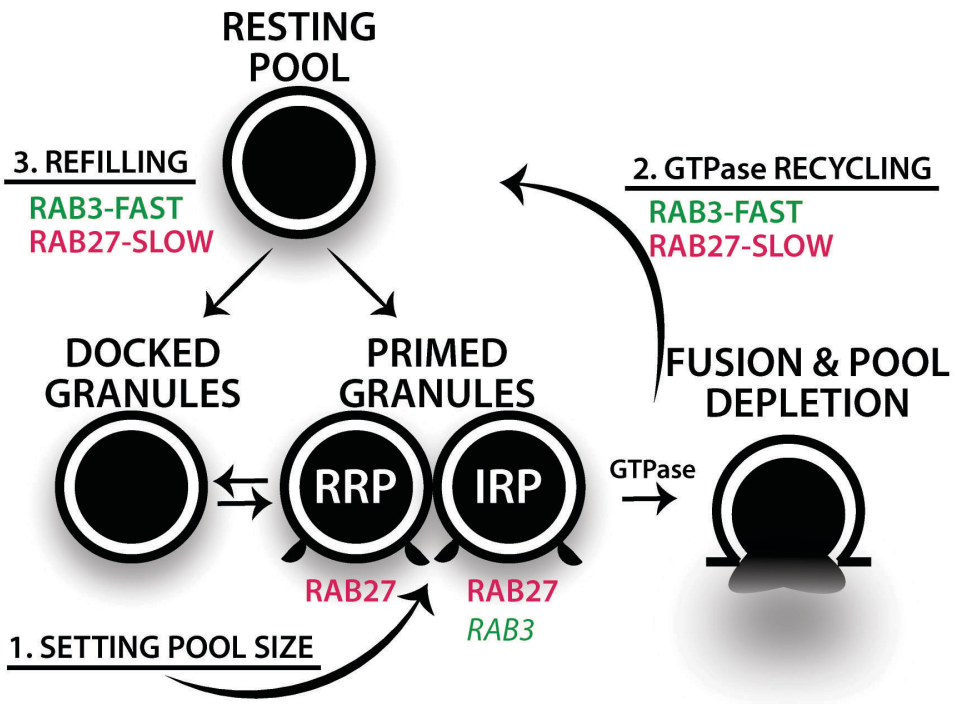
RESTING
POOL
3. REFILLING
RAB3-FAST
RAB27-SLOW
2. GTPase RECYCLING
RAB3-FAST
RAB27-SLOW
DOCKED
GRANULES
PRIMED
GRANULES
FUSION & POOL
DEPLETION
RRP
IRP
GTPase
RAB27
RAB27
RAB3
1. SETTING POOL SIZE

**Figure 2.9: Summary of Chapter 2 findings.** Rab GTPases associated with insulin-containing secretory granules (SGs) are key in targeting, docking and assembly of molecular complexes governing pancreatic β-cell exocytosis. Four Rab3 isoforms along with Rab27A are associated with insulin granules, yet elucidation of the distinct roles of these Rab families on exocytosis remains unclear. To define specific actions of these Rab families we employ Rab3GAP and/or EPI64A GTPase-activating protein overexpression in β-cells from wild-type or Ashen mice to selectively transit the entire Rab3 family or Rab27A to a GDP-bound state. Ashen mice carry a spontaneous mutation that eliminates Rab27A expression. Using membrane capacitance measurements we find that GTP/GDP nucleotide cycling of Rab27A is essential for generation of the functionally defined immediately releasable pool (IRP) and central to regulating the size of the readily releasable pool (RRP). By comparison, nucleotide cycling of Rab3 GTPases, but not of Rab27A, is essential for a kinetically rapid filling of the RRP with SGs. Aside from these distinct functions, Rab3 and Rab27A GTPases demonstrate considerable functional overlap in building the readily releasable granule pool. Hence, while Rab3 and Rab27A cooperate to generate release-ready SGs in β-cells, they also direct unique kinetic and functional properties of the exocytotic pathway.

## 2.6 References


1. Porte D, Kahn SE. beta-cell dysfunction and failure in type 2 diabetes: potential mechanisms. Diabetes 2001;50 Suppl 1:S160–3.
2. Ashcroft FM, Rorsman P. KATP channels and islet hormone secretion: new insights and controversies. Nat Rev Endocrinol 2013;9:660–669.
3. Henquin JC. Triggering and amplifying pathways of regulation of insulin secretion by glucose. Diabetes 2000;49:1751–1760.
4. Straub SG, Sharp GWG. Glucose-stimulated signaling pathways in biphasic insulin secretion. Diabetes Metab Res Rev 2002;18:451–463.
5. Rutter GA. Visualising insulin secretion. The Minkowski Lecture 2004. Diabetologia. 2004;47:1861–1872.
6. MacDonald PE, Joseph JW, Rorsman P. Glucose-sensing mechanisms in pancreatic beta-cells. Philos Trans R Soc Lond, B, Biol Sci 2005;360:2211–2225.
7. Sadoul K, Lang J, Montecucco C, Weller U, Regazzi R, Catsicas S, Wollheim CB, Halban PA. SNAP-25 is expressed in islets of Langerhans and is involved in insulin release. J Cell Biol 1995;128:1019–1028.
8. Nagamatsu S, Fujiwara T, Nakamichi Y, Watanabe T, Katahira H, Sawa H, Akagawa K. Expression and functional role of syntaxin 1/HPC-1 in pancreatic beta cells. Syntaxin 1A, but not 1B, plays a negative role in regulatory insulin release pathway. J Biol Chem 1996;271:1160–1165.
9. Gaisano HY, Ostenson C-G, Sheu L, Wheeler MB, Efendic S. Abnormal expression of pancreatic islet exocytotic soluble N-ethylmaleimide-sensitive factor attachment protein receptors in Goto-Kakizaki rats is partially restored by phlorizin treatment and accentuated by high glucose treatment. Endocrinology 2002;143:4218–4226.
10. Zerial M, McBride H. Rab proteins as membrane organizers. Nat Rev Mol Cell Biol 2001;2:107–117.
11. Hutagalung AH, Novick PJ. Role of Rab GTPases in membrane traffic and cell physiology. Physiol Rev 2011;91:119–149.

12. Regazzi R, Vallar L, Ullrich S, Ravazzola M, Kikuchi A, Takai Y, Wollheim CB. Characterization of small-molecular-mass guanine-nucleotide-binding regulatory proteins in insulin-secreting cells and PC12 cells. Eur J Biochem 1992;208:729–737.
13. Merrins MJ, Stuenkel EL. Kinetics of Rab27a-dependent actions on vesicle docking and priming in pancreatic beta-cells. J Physiol (Lond) 2008;586:5367–5381.
14. Schlüter OM, Schmitz F, Jahn R, Rosenmund C, Südhof TC. A complete genetic analysis of neuronal Rab3 function. J Neurosci 2004;24:6629–6637.
15. Regazzi R, Ravazzola M, Iezzi M, Lang J, Zahraoui A, Andereggen E, Morel P, Takai Y, Wollheim CB. Expression, localization and functional role of small GTPases of the Rab3 family in insulin-secreting cells. Journal of Cell Science 1996;109 ( Pt 9):2265–2273.
16. Coppola T, Perret-Menoud V, Lüthi S, Farnsworth CC, Glomset JA, Regazzi R. Disruption of Rab3-calmodulin interaction, but not other effector interactions, prevents Rab3 inhibition of exocytosis. EMBO J 1999;18:5885–5891.
17. Chung SH, Joberty G, Gelino EA, Macara IG, Holz RW. Comparison of the effects on secretion in chromaffin and PC12 cells of Rab3 family members and mutants. Evidence that inhibitory effects are independent of direct interaction with Rabphilin3. J Biol Chem 1999;274:18113–18120.
18. Fukuda M. Assay and functional interactions of Rim2 with Rab3. Meth Enzymol 2005;403:457–468.
19. Yasuda T, Shibasaki T, Minami K, Takahashi H, Mizoguchi A, Uriu Y, Numata T, Mori Y, Miyazaki J-I, Miki T, Seino S. Rim2a Determines Docking and Priming States in Insulin Granule Exocytosis. Cell Metab 2010;12:117–129.
20. Zhao S, Torii S, Yokota-Hashimoto H, Takeuchi T, Izumi T. Involvement of Rab27b in the regulated secretion of pituitary hormones. Endocrinology 2002;143:1817–1824.
21. Waselle L, Coppola T, Fukuda M, Iezzi M, El-Amraoui A, Petit C, Regazzi R. Involvement of the Rab27 binding protein Slac2c/MyRIP in insulin exocytosis. Mol Biol Cell 2003;14:4103–4113.
22. Lam AD, Ismail S, Wu R, Yizhar O, Passmore DR, Ernst SA, Stuenkel EL. Mapping dynamic protein interactions to insulin secretory granule behavior with TIRF-FRET. Biophys J 2010;99:1311–1320.

23. Haddad EK, Wu X, Hammer JA, Henkart PA. Defective granule exocytosis in Rab27a-deficient lymphocytes from Ashen mice. J Cell Biol 2001;152:835–842.
24. Kasai K, Ohara-Imaizumi M, Takahashi N, Mizutani S, Zhao S, Kikuta T, Kasai H, Nagamatsu S, Gomi H, Izumi T. Rab27a mediates the tight docking of insulin granules onto the plasma membrane during glucose stimulation. J Clin Invest 2005;115:388–396.
25. Yi Z, Yokota H, Torii S, Aoki T, Hosaka M, Zhao S, Takata K, Takeuchi T, Izumi T. The Rab27a/granuphilin complex regulates the exocytosis of insulin-containing dense-core granules. Mol Cell Biol 2002;22:1858–1867.
26. Pavlos NJ, Jahn R. Distinct yet overlapping roles of Rab GTPases on synaptic vesicles. Small GTPases 2011;2:77–81.
27. Iezzi M, Escher G, Meda P, Charollais A, Baldini G, Darchen F, Wollheim CB, Regazzi R. Subcellular distribution and function of Rab3A, B, C, and D isoforms in insulin-secreting cells. Mol Endocrinol 1999;13:202–212.
28. Barr F, Lambright DG. Rab GEFs and GAPs. Curr Opin Cell Biol 2010;22:461–470.
29. Figueiredo AC, Wasmeier C, Tarafder AK, Ramalho JS, Baron RA, Seabra MC. Rab3GEP is the non-redundant guanine nucleotide exchange factor for Rab27a in melanocytes. J Biol Chem 2008;283:23209–23216.
30. Tanaka M, Miyoshi J, Ishizaki H, Togawa A, Ohnishi K, Endo K, Matsubara K, Mizoguchi A, Nagano T, Sato M, Sasaki T, Takai Y. Role of Rab3 GDP/GTP exchange protein in synaptic vesicle trafficking at the mouse neuromuscular junction. Mol Biol Cell 2001;12:1421–1430.
31. Itoh T, Fukuda M. Identification of EPI64 as a GTPase-activating protein specific for Rab27A. J Biol Chem 2006;281:31823–31831.
32. Handley MTW, Haynes LP, Burgoyne RD. Differential dynamics of Rab3A and Rab27A on secretory granules. Journal of Cell Science 2007;120:973–984.
33. Pavlos NJ, Grønborg M, Riedel D, Chua JJE, Boyken J, Kloepper TH, Urlaub H, Rizzoli SO, Jahn R. Quantitative analysis of synaptic vesicle Rabs uncovers distinct yet overlapping roles for Rab3a and Rab27b in Ca2+-triggered exocytosis. J Neurosci 2010;30:13441–13453.

34. Kimura T, Kaneko Y, Yamada S, Ishihara H, Senda T, Iwamatsu A, Niki I. The GDP-dependent Rab27a effector coronin 3 controls endocytosis of secretory membrane in insulin-secreting cell lines. Journal of Cell Science 2008;121:3092–3098.
35. Fukuda M. Slp4-a/granuphilin-a inhibits dense-core vesicle exocytosis through interaction with the GDP-bound form of Rab27A in PC12 cells. J Biol Chem 2003;278:15390–15396.
36. Kondo H, Shirakawa R, Higashi T, Kawato M, Fukuda M, Kita T, Horiuchi H. Constitutive GDP/GTP exchange and secretion-dependent GTP hydrolysis activity for Rab27 in platelets. J Biol Chem 2006;281:28657–28665.
37. Fukuda M. Rab27 and its effectors in secretory granule exocytosis: a novel docking machinery composed of a Rab27.effector complex. Biochem Soc Trans 2006;34:691–695.
38. Fukuda M. Distinct Rab binding specificity of Rim1, Rim2, rabphilin, and Noc2. Identification of a critical determinant of Rab3A/Rab27A recognition by Rim2. J Biol Chem 2003;278:15373–15380.
39. Cheviet S, Waselle L, Regazzi R. Noc-king out exocrine and endocrine secretion. Trends Cell Biol 2004;14:525–528.
40. Shirakawa R. Munc13-4 Is a GTP-Rab27-binding Protein Regulating Dense Core Granule Secretion in Platelets. Journal of Biological Chemistry 2003;279:10730–10737.
41. Handley MTW, Burgoyne RD. The Rab27 effector Rabphilin, unlike Granuphilin and Noc2, rapidly exchanges between secretory granules and cytosol in PC12 cells. Biochemical and Biophysical Research Communications 2008;373:275–281.
42. Göpel S, Kanno T, Barg S, Galvanovskis J, Rorsman P. Voltage-gated and resting membrane currents recorded from B-cells in intact mouse pancreatic islets. J Physiol (Lond) 1999;521 Pt 3:717–728.
43. Huang Y-C, Rupnik M, Gaisano HY. Unperturbed islet α-cell function examined in mouse pancreas tissue slices. J Physiol (Lond) 2011;589:395–408.
44. Fukui K, Sasaki T, Imazumi K, Matsuura Y, Nakanishi H, Takai Y. Isolation and characterization of a GTPase activating protein specific for the Rab3 subfamily of small G proteins. J Biol Chem 1997;272:4655–4658.

45. Grosshans BL, Andreeva A, Gangar A, Niessen S, Yates JR, Brennwald P, Novick P. The yeast lgl family member Sro7p is an effector of the secretory Rab GTPase Sec4p. J Cell Biol 2006;172:55–66.
46. Tsuboi T, Fukuda M. Rab3A and Rab27A cooperatively regulate the docking step of dense-core vesicle exocytosis in PC12 cells. Journal of Cell Science 2006;119:2196–2203.
47. Stevens DR, Schirra C, Becherer U, Rettig J. Vesicle pools: lessons from adrenal chromaffin cells. Front Syn Neurosci 2011;3:2.
48. Feng W, Liang T, Yu J, Zhou W, Zhang Y, Wu Z, Xu T. RAB-27 and its effector RBF-1 regulate the tethering and docking steps of DCV exocytosis in C. elegans. Sci China Life Sci 2012;55:228–235.
49. Leenders AG, Lopes da Silva FH, Ghijsen WE, Verhage M. Rab3a is involved in transport of synaptic vesicles to the active zone in mouse brain nerve terminals. Mol Biol Cell 2001;12:3095–3102.
50. Coleman WL, Bill CA, Bykhovskaia M. Rab3a deletion reduces vesicle docking and transmitter release at the mouse diaphragm synapse. Neuroscience 2007;148:1–6.
51. Gomi H, Mori K, Itohara S, Izumi T. Rab27b is expressed in a wide range of exocytic cells and involved in the delivery of secretory granules near the plasma membrane. Mol Biol Cell 2007;18:4377–4386.
52. Johnson JL, Brzezinska AA, Tolmachova T, Munafo DB, Ellis BA, Seabra MC, Hong H, Catz SD. Rab27a and Rab27b Regulate Neutrophil Azurophilic Granule Exocytosis and NADPH oxidase Activity by Independent Mechanisms. Traffic 2010;11:533–547.
53. Burke NV, Han W, Li D, Takimoto K, Watkins SC, Levitan ES. Neuronal peptide release is limited by secretory granule mobility. Neuron 1997;19:1095–1102.
54. Oheim M, Loerke D, Stühmer W, Chow RH. The last few milliseconds in the life of a secretory granule. Docking, dynamics and fusion visualized by total internal reflection fluorescence microscopy (TIRFM). Eur Biophys J 1998;27:83–98.
55. J A Steyer WA. Tracking single secretory granules in live chromaffin cells by evanescent-field fluorescence microscopy. Biophys J 1999;76:2262.
56. Johns LM. Restriction of Secretory Granule Motion Near the Plasma Membrane of Chromaffin Cells. J Cell Biol 2001;153:177–190.

57. Degtyar VE, Allersma MW, Axelrod D, Holz RW. Increased motion and travel, rather than stable docking, characterize the last moments before secretory granule fusion. Proceedings of the National Academy of Sciences 2007;104:15929–15934.
58. Straub SG, Shanmugam G, Sharp GWG. Stimulation of insulin release by glucose is associated with an increase in the number of docked granules in the beta-cells of rat pancreatic islets. Diabetes 2004;53:3179–3183.
59. Barg S, Eliasson L, Renström E, Rorsman P. A subset of 50 secretory granules in close contact with L-type Ca2+ channels accounts for first-phase insulin secretion in mouse beta-cells. Diabetes 2002;51 Suppl 1:S74–82.
60. Olofsson CS, Göpel SO, Barg S, Galvanovskis J, Ma X, Salehi A, Rorsman P, Eliasson L. Fast insulin secretion reflects exocytosis of docked granules in mouse pancreatic B-cells. Pflugers Arch 2002;444:43–51.
61. Ge Q, Dong Y-M, Hu Z-T, Wu Z-X, Xu T. Characteristics of Ca2+-exocytosis coupling in isolated mouse pancreatic beta cells. Acta Pharmacol Sin 2006;27:933–938.
62. Yang Y, Gillis KD. A highly Ca2+-sensitive pool of granules is regulated by glucose and protein kinases in insulin-secreting INS-1 cells. J Gen Physiol 2004;124:641–651.
63. Regazzi R, Kikuchi A, Takai Y, Wollheim CB. The small GTP-binding proteins in the cytosol of insulin-secreting cells are complexed to GDP dissociation inhibitor proteins. J Biol Chem 1992;267:17512–17519.
64. Iezzi M, Escher G, Meda P, Charollais A, Baldini G, Darchen F, Wollheim CB, Regazzi R. Subcellular distribution and function of Rab3A, B, C, and D isoforms in insulin-secreting cells. Molecular Endocrinology 1999;13:202–212.
65. Reczek D. Identification of EPI64, a TBC/rabGAP Domain-containing Microvillar Protein That Binds to the First PDZ Domain of EBP50 and E3KARP. J Cell Biol 2001;153:191–206.
66. Malaisse WJ, Malaisse-Lagae F, Mayhew D. A possible role for the adenylcyclase system in insulin secretion. J Clin Invest 1967;46:1724–1734.
67. Montague W, Howell SL. The mode of action of adenosine 3“:5-”cyclic monophosphate in mammalian islets of Langerhans. Preparation and properties of islet-cell protein phosphokinase. Biochem J 1972;129:551–560.

68. Pipeleers DG, in't Veld PA, Van de Winkel M, Maes E, Schuit FC, Gepts W. A new in vitro model for the study of pancreatic A and B cells. Endocrinology 1985;117:806–816.
69. Kashima Y, Miki T, Shibasaki T, Ozaki N, Miyazaki M, Yano H, Seino S. Critical role of cAMP-GEFII--Rim2 complex in incretin-potentiated insulin secretion. J Biol Chem 2001;276:46046–46053.
70. Shibasaki T, Sunaga Y, Fujimoto K, Kashima Y, Seino S. Interaction of ATP sensor, cAMP sensor, Ca2+ sensor, and voltage-dependent Ca2+ channel in insulin granule exocytosis. J Biol Chem 2004;279:7956–7961.
71. Sakane A, Manabe S, Ishizaki H, Tanaka-Okamoto M, Kiyokage E, Toida K, Yoshida T, Miyoshi J, Kamiya H, Takai Y, Sasaki T. Rab3 GTPase-activating protein regulates synaptic transmission and plasticity through the inactivation of Rab3. Proc Natl Acad Sci U S A 2006;103:10029–10034.
72. Müller M, Liu KSY, Sigrist SJ, Davis GW. RIM Controls Homeostatic Plasticity through Modulation of the Readily-Releasable Vesicle Pool. J Neurosci 2012;32:16574–16585.
73. Weiss N, Sandoval A, Kyonaka S, Felix R, Mori Y, de Waard M. Rim1 modulates direct G-protein regulation of Ca(v)2.2 channels. Pflugers Arch - Eur J Physiol 2011;461:447–459.
74. Han Y, Kaeser PS, Südhof TC, Schneggenburger R. RIM determines $Ca^2$+ channel density and vesicle docking at the presynaptic active zone. Neuron 2011;69:304–316.
75. Kaeser PS, Deng L, Wang Y, Dulubova I, Liu X, Rizo J, Südhof TC. RIM proteins tether Ca2+ channels to presynaptic active zones via a direct PDZ-domain interaction. Cell 2011;144:282–295.
76. Bustos MA, Lucchesi O, Ruete MC, Mayorga LS, Tomes CN. Rab27 and Rab3 sequentially regulate human sperm dense-core granule exocytosis. Proceedings of the National Academy of Sciences 2012;109:E2057–66.
77. Tsuboi T, Fukuda M. The Slp4-a linker domain controls exocytosis through interaction with Munc18-1.syntaxin-1a complex. Mol Biol Cell 2006;17:2101–2112.
78. Südhof TC. Function of Rab3 GDP-GTP exchange. Neuron 1997;18:519–522.
79. Fischer von Mollard G, Südhof TC, Jahn R. A small GTP-binding protein dissociates from synaptic vesicles during exocytosis. Nature 1991;349:79–81.

80. Coppola T, Perret-Menoud V, Gattesco S, Magnin S, Pombo I, Blank U, Regazzi R. The death domain of Rab3 guanine nucleotide exchange protein in GDP/GTP exchange activity in living cells. Biochem J 2002;362:273–279.
81. Maycox PR, Link E, Reetz A, Morris SA, Jahn R. Clathrin-coated vesicles in nervous tissue are involved primarily in synaptic vesicle recycling. J Cell Biol 1992;118:1379–1388.
82. Graham ME, Handley MTW, Barclay JW, Ciufo LF, Barrow SL, Morgan A, Burgoyne RD. A gain-of-function mutant of Munc18-1 stimulates secretory granule recruitment and exocytosis and reveals a direct interaction of Munc18-1 with Rab3. Biochem J 2008;409:407–416.
83. Dulubova I, Lou X, Lu J, Huryeva I, Alam A, Schneggenburger R, Südhof TC, Rizo J. A Munc13/RIM/Rab3 tripartite complex: from priming to plasticity? EMBO J 2005;24:2839–2850.
84. Iezzi M, Regazzi R, Wollheim CB. The Rab3-interacting molecule RIM is expressed in pancreatic beta-cells and is implicated in insulin exocytosis. FEBS Lett 2000;474:66–70.
85. Shibasaki T, Sunaga Y, Seino S. Integration of ATP, cAMP, and Ca2+ signals in insulin granule exocytosis. Diabetes 2004;53 Suppl 3:S59–62.
86. Staunton J, Ganetzky B, Nonet ML. Rabphilin potentiates soluble N-ethylmaleimide sensitive factor attachment protein receptor function independently of rab3. J Neurosci 2001;21:9255–9264.
87. Johannes L, Doussau F, Clabecq A, Henry JP, Darchen F, Poulain B. Evidence for a functional link between Rab3 and the SNARE complex. Journal of Cell Science 1996;109 ( Pt 12):2875–2884.
88. Henry JP, Johannes L, Dousseau F, Poulain B, Darchen F. Role of Rab3a in neurotransmitter and hormone release: a discussion of recent data. Biochem Soc Trans 1996;24:657–661.
89. Ohya T, Miaczynska M, Coskun U, Lommer B, Runge A, Drechsel D, Kalaidzidis Y, Zerial M. Reconstitution of Rab- and SNARE-dependent membrane fusion by synthetic endosomes. Nature 2009;459:1091–1097.
90. Ohara-Imaizumi M, Nagamatsu S. Insulin exocytotic mechanism by imaging technique. J Biochem 2006;140:1–5.

91. Ohara-Imaizumi M, Fujiwara T, Nakamichi Y, Okamura T, Akimoto Y, Kawai J, Matsushima S, Kawakami H, Watanabe T, Akagawa K, Nagamatsu S. Imaging analysis reveals mechanistic differences between first- and second-phase insulin exocytosis. J Cell Biol 2007;177:695–705.
92. Straub SG, Sharp GWG. Evolving insights regarding mechanisms for the inhibition of insulin release by norepinephrine and heterotrimeric G proteins. AJP: Cell Physiology 2012;302:C1687–C1698.
93. Ohara-Imaizumi M, Nakamichi Y, Tanaka T, Ishida H, Nagamatsu S. Imaging exocytosis of single insulin secretory granules with evanescent wave microscopy: distinct behavior of granule motion in biphasic insulin release. J Biol Chem 2002;277:3805–3808.
94. Ohara-Imaizumi M, Nishiwaki C, Kikuta T, Kumakura K, Nakamichi Y, Nagamatsu S. Site of docking and fusion of insulin secretory granules in live MIN6 beta cells analyzed by TAT-conjugated anti-syntaxin 1 antibody and total internal reflection fluorescence microscopy. J Biol Chem 2004;279:8403–8408.
95. Michael DJ, Xiong W, Geng X, Drain P, Chow RH. Human insulin vesicle dynamics during pulsatile secretion. Diabetes 2007;56:1277–1288.
96. Shibasaki T, Takahashi H, Miki T, Sunaga Y, Matsumura K, Yamanaka M, Zhang C, Tamamoto A, Satoh T, Miyazaki J-I, Seino S. Essential role of Epac2/Rap1 signaling in regulation of insulin granule dynamics by cAMP. Proceedings of the National Academy of Sciences 2007;104:19333–19338.
97. Lin C-C, Huang C-C, Lin K-H, Cheng K-H, Yang D-M, Tsai Y-S, Ong R-Y, Huang Y-N, Kao L-S. Visualization of Rab3A dissociation during exocytosis: a study by total internal reflection microscopy. J Cell Physiol 2007;211:316–326.
98. Larijani B, Hume AN, Tarafder AK, Seabra MC. Multiple factors contribute to inefficient prenylation of Rab27a in Rab prenylation diseases. J Biol Chem 2003;278:46798–46804.
99. Tiwari S, Italiano JE, Barral DC, Mules EH, Novak EK, Swank RT, Seabra MC, Shivdasani RA. A role for Rab27b in NF-E2-dependent pathways of platelet formation. Blood 2003;102:3970–3979.

100. Coppola T, Frantz C, Perret-Menoud V, Gattesco S, Hirling H, Regazzi R. Pancreatic beta-cell protein granuphilin binds Rab3 and Munc-18 and controls exocytosis. Mol Biol Cell 2002;13:1906–1915.

101. Gomi H, Mizutani S, Kasai K, Itohara S, Izumi T. Granuphilin molecularly docks insulin granules to the fusion machinery. J Cell Biol 2005;171:99–109.

102. Fukuda M. Versatile Role of Rab27 in Membrane Trafficking: Focus on the Rab27 Effector Families. J Biochem 2005;137:9–16.

103. Kimura T, Niki I. Rab27a, actin and beta-cell endocytosis. Endocr J 2011;58:1–6.

104. Kimura T, Taniguchi S, Niki I. Actin assembly controlled by GDP-Rab27a is essential for endocytosis of the insulin secretory membrane. Archives of Biochemistry and Biophysics 2010;496:33–37.

105. Göpel S, Zhang Q, Eliasson L, Ma X-S, Galvanovskis J, Kanno T, Salehi A, Rorsman P. Capacitance measurements of exocytosis in mouse pancreatic alpha-, beta- and delta-cells within intact islets of Langerhans. J Physiol (Lond) 2004;556:711–726.

106. Allersma MW, Bittner MA, Axelrod D, Holz RW. Motion matters: secretory granule motion adjacent to the plasma membrane and exocytosis. Mol Biol Cell 2006;17:2424–2438.

## Chapter III

## Dynamic partitioning of synaptic vesicle pool by the SNARE protein Tomosyn

### 3.1 Abstract

Neural networks often engage in high-frequency activity that relies on highly regulated vesicle fusion from distinct functional synaptic vesicle (SV) pools. In this study we investigated the role that the soluble SNARE Tomosyn1 (Tomo1) may exert on presynaptic SV pools at hippocampal synapses. By controlling Tomosyn1 expression at hippocampal synapses together with use of V-Glut1-pHluorin (vGpH) as a direct reporter of presynaptic vesicle fusion and dynamics we find that Tomo1 acts as a central regulator on transition of SVs between the Total Recycling Pool (TRP) and Resting Pool (ResP), as well as on the Readily-Releasable Pool (RRP). Tomo1's regulation of the fractional distribution of SVs between the TRP and ResP is sensitive to neural activity and requires Cdk5. We further demonstrate that Tomo1 is a direct substrate of Cdk5 phosphorylation and correlate changes in its level of phosphorylation to alterations in neural activity. While mechanistic details by which Tomo1 participates in reallocation of SVs between TRP and ResP at presynaptic terminals remain to be elaborated, we provide initial evidence that Tomo1 specifically interacts with GTP bound Rab3A, and through this interaction with Synapsin1 proteins. The latter interaction is notable as Synapsin proteins have been well established

to restrict vesicle release via interaction with the presynaptic actin cytoskeleton and, interestingly, also recently reported to be associated with Cdk5 modulation of the TRP. In addition, our results show that Tomo1 regulatory control over the TRP occurred independent of its C-terminal SNARE domain, demonstrating that Tomo1 actions on neurotransmission extend well beyond inhibition of SV priming into the RRP. We conclude that Tomo1 is a critical modulator of SV distribution among functionally defined pools, with its actions being sensitive to neural activity indicating it may be a key mediator in use dependent changes in presynaptic release probability.

**3.2 Introduction:**

The passage of information fundamental to neural circuitry within the mammalian central nervous system occurs primarily at chemical synapses, which are comprised of structurally and functionally polarized and highly dynamic pre- and post-synaptic elements. With regard to presynaptic compartments, transmitter release closely follows action potential invasion, activation of voltage-gated $Ca^{2+}$ channels and SNARE protein mediated synaptic vesicle (SV) fusion. The regulation of neurotransmitter containing synaptic vesicles (SVs) is essential to the functional dynamics of synapses since SVs immediately competent for release are highly restricted to a small set of SVs within a readily releasable pool (RRP) at the presynaptic active zone (AZ). The limited capacity of the RRP suggests that under physiological conditions, such as during bursts of action potentials in spiking neurons, sustained release requires the recruitment of SVs into the RRP from other functionally distinct pool(s) of SVs within the presynaptic bouton. The importance of this recruitment and cycling of presynaptic SVs to neurotransmission is

evidenced by the relationship of specific forms of short-term synaptic plasticity to speed of vesicle recruitment, development of release competency and/or depletion of the RRP [1]. In addition, synchronous and asynchronous release evoked by action potentials has been suggested to result from different sets of SVs and/or SVs differing in calcium sensitivity and release probability [2,3]. Defining the regulatory controls on transition of SVs between functionally distinct SV pools is, therefore, of key importance to understanding use-dependent changes in the probability of vesicle release (Pr), as well as changes in the efficacy of presynaptic release that accompanies synaptic plasticity.

Within mammalian hippocampal neurons SVs have been found to occupy three functionally distinct pools that include a RRP, comprised of only a few SVs (5-8 vesicles) docked at the AZ and fully primed for immediate release, a substantively larger Recycling Pool (RP; ~20 to 60% of SVs) that undergoes continuous exocytotic/endocytotic cycling and a Resting Pool (ResP), which often represent a significant population (up to 40-80%) that mostly appear recalcitrant to activity driven exocytotic/endocytotic cycling [4,5]. The RRP together with the RP form the total recycling pool (TRP) of SVs. Reallocation of vesicles among these functionally defined pools may serve to modify activity-dependent changes in synaptic strength, which is defined as the product of individual vesicle fusion probability and the number of release ready vesicles (or the RRP). Indeed, the RRP has been shown to scale with the size of the RP during high-frequency AP firing [6], and recruitment of ResP vesicles into the RP has been reported to impact the expression of Hebbian as well as homeostatic forms of synaptic plasticity at cortical and hippocampal synapses [7-10]. In addition, release reluctant vesicles have been suggested to participate in SV recycling by serving as a protein sink [11]; facilitate vesicle interchange between

boutons of a given neuron [12,13]; serve as a depot pool for immature synapses [8,14]; or a SV pool for spontaneous fusion events [15,16], although this latter view remains contested [17-19]. Thus SV recruitment from the ResP appears to be dynamic and important for synapse function. Yet, the molecular mechanisms that clamps or promotes the transition of SVs from the inactive non-cycling ResP to active and cycling TRP are not well understood. Recently, in hippocampal synapses, cyclin-dependent kinase 5 (Cdk5) has been recognized as a signal for inducing changes in TRP/ResP partitioning since pharmacological or genetic ablation led to the unfettering of a significant portion of ResP SVs into the mobile and release active TRP[9]. Moreover, while some studies have shown that Synapsin1 and actin can arrest SVs in a non-releasable state, others have shown that pool partitioning occurs independent of actin dynamics suggesting that additional molecular mechanisms may exist [20-22]. Taken together, these findings suggest that distribution of SVs among functional pools may be sensitive to phosphorylation state of particular effectors, although the specific effectors involved and the signaling cascades have not been defined.

In this study we investigated the role of the inhibitory protein Tomosyn1 (Tomo1) in defining SV distribution among presynaptic SV pools at hippocampal synapses. Tomo1 proteins contain a C-terminal SNARE domain that is homologous to the vesicle SNARE synaptobrevin/ VAMP-2. Thus, it competes with VAMP and Munc18 for interaction with reactive Syntaxin and SNAP25 to form to non-fusogenic SNARE complexes [23-26]. As a result, Tomo1 acts a potent inhibitor of evoked release from the RRP [27,28] and alterations in Tomosyn expression result in behavioral defects in mice [29], Drosophila [30] and C. elegans [31]. However, Tomo1 may exert effects on SVs outside of priming into the RRP as suggested from membrane capacitance monitoring of exocytotic activity in

bovine chromaffin cells to sustained elevated calcium. Under these stimulus conditions, Tomo1 overexpression led to a 50% reduction in the RRP size and an accompanying decrease in Pr, but importantly, also impaired maturation of vesicles into the RRP [27]. Similarly, at *Drosophila* and *C. elegans* neuromuscular junctions (NMJ) a loss of function mutation of Tomosyn or targeted knockdown of its expression led to enhanced neurotransmitter release from a pool of vesicles that supplies delayed release and is less calcium sensitive[30,32]. In addition, the Tomosyn homologs in yeast, Sro7p and Sro77p, interact with the vesicle GTPase Sec4 and when overexpressed results in the accumulation of non-fusiogenic vesicle clusters [33-35]. Thus it appears that Tomosyn proteins may play a more central role in regulating release from multiple pools to impact synaptic strength.

The purpose of these investigations were to determine it Tomo1 exerts distinct mechanistic functions on distribution of SVs among functional pools, beyond that characterized for the RRP Our results uncover a novel site and mechanism for Tomo1 inhibition of SV release. We find that in addition to inhibiting priming of SVs into the RRP, Tomo1 clamps SVs in the ResP preventing transition into the TRP independently of its R-SNARE motif. Moreover, our results suggest that Tomo1 is an activity-dependent phosphorylation substrate of Cdk5 and that it requires its catalytic activity to exert regulatory control over the TRP/ResP partitions. The clamping of SVs in the ResP by Tomo1 appears to occur via an identified novel interaction between Tomo1 and SV-associated Rab3A, which together form a complex with Synapsin1 proteins. Finally, we show that Tomo1 phosphorylation and thus regulatory actions are activity-dependent and that Tomo1 is necessary for compensatory enhancements in SV release induced by chronic silencing of neuronal activity.

**3.3 Results**:

*Tomosyn1 inhibits evoked but not basal synaptic transmission*

To determine the specific function of Tomo1 on presynaptic physiology and to define its sites of action on each of functionally defined SV pool at excitatory central synapses experiments were conducted on cultures of rat hippocampal neurons. The studies focused on Tomo1 since it is predominantly expressed at excitatory synapses and is presynaptically enriched relative to Tomosyn2, which is mainly postsynaptic [36]. Our results also demonstrate localization of endogenous Tomo1 at presynaptic sites within cultured hippocampal neurons as shown by colocalization analysis relating Tomo1 immunofluorescence to that of the SV integral membrane protein Synaptophysin (Syp) (Figure 1A). Moreover, fluorescence intensity profile of a straightened axon fragment shows that Tomo1 immunofluorescence intensity spiked coincidently with that of Syp (Figure 1A, A2). To examine Tomo1 regulatory effects on electrically evoked and basal neurotransmission we applied treatment to specifically alter Tomo1 expression levels. Relative to control (infection with shRNA-scramble lentivirus or GFP alone) lentiviral infection of Tomo1 led to significant protein overexpression (OE) (YFP-mTomo1, mean (μ) = 10.6 fold increase, SEM = ±3.12), while shRNA-mediated Tomosyn knock-down (KD) strongly reduced its expression (μ = 84.7% KD, SEM = ±0.02) (Figure 1B). The shRNA constructs used to KD Tomo1 were specific as the level of 4 other synaptic proteins measured was unaffected (Figure 1—Supplement). To assess the effects these treatments exerted on release probability (Pr), paired-pulse ratios (PPR) were determined from excitatory post-synaptic current (EPSC) measurements recorded under whole-cell voltage

clamp[1,37]. As shown in Figure 1C-E, OE of Tomo1 resulted in synaptic facilitation (EPSC2>EPSC1) over inter-stimulus intervals (ISI) ranging from 50 to 250 ms that was significantly greater than of control (50 ms PPR μ = 1.96 ±0.18 vs. μ = 1.11 ±0.05). Conversely, PPR from Tomo1 KD neurons demonstrated synaptic depression relative to control for the 50 ms ISI (μ = 0.79 ±0.13 vs. μ = 1.11 ±0.05). As Tomo1 OE increased facilitation while Tomo1 KD depressed facilitation relative to control the results confirm that Tomo1 likely serves as a strong negative regulator of release probability (Pr) at hippocampal synapses. Neuroendocrine cell secretion studies, as well as measurement of spontaneous miniature synaptic events at the *C. elegans* and *Drosophila* neuromuscular junction, have reported that alterations in Tomo1 expression selectively affects stimulated, but not basal, secretion. To test for Tomo1 effects on spontaneous release at hippocampal synapses, we recorded miniature EPSCs (mEPSC) under Tomo1 OE and KD conditions as compared to control. The recordings were conducted in the presence of the voltage-gated sodium channel blocker tetrodotoxin (TTX) in order to prevent AP firing and network activation. Consistent with the prior reports [30,32,38], our data demonstrated no significant changes in frequency or amplitude of mEPSCs among the conditions tested (Figure 1F) . Taken together, the electrophysiological assessments indicate that Tomo1 inhibition of neurotransmission in hippocampal synapses is restricted to evoked release.

*Tomosyn inhibits multiple vesicle pools*

To specifically determine if Tomo1 participates in active partitioning of SVs between the RRP, TRP and RestP we employed a direct optical reporter of presynaptic vesicle cycling, VGLUT1-pHluorin (vGpH) or VGLUT1-pHluorin-mCherry (vGpH-mCH). Field

stimulation protocols applied to elicit AP firing [4,39] were used to drive release of the RRP (20 Hz, 40 AP) [40-43] and TRP (20 Hz, 900 AP) [9,39,44], with a subsequent alkalinization by application of ammonium chloride to measure remaining vGpH that is associated with non-releasable RestP vesicles [45] . All experiments were carried out in the presence of the V-type ATPase inhibitor bafilomycin-A1 to prevent reacidifcation of vesicles and restrict measurements to net exocytosis [45]. Initially, the role of Tomo1 was evaluated in neurons transfected with shRNA-meditated Tomo1 KD or recombinant mCh-m-Tomo1 OE together with the vGpH reporter. Relative to control (vGpH + empty vector), Tomo1 KD resulted in a significant enhancement in the estimated size of the RRP, while Tomo1 OE resulted in a significant decrease in the RRP size (Figure 2A). These data are consistent with the PPR results which indicated that Tomosyn KD and OE alter Pr (Figure 1C-E) and also line with membrane capacitance (Cm) measurements from adrenal chromaffin cells where OE of Tomo1 reduced the RRP component of release by 87% [27]. We next tested whether Tomo1 affects the distribution of SVs among functionally defined pools beyond the RRP. Remarkably, as shown in Figure 2B-D Tomo1 KD results in an overall greater TRP at the expense of the ResP using two distinct shRNA sequences, ($\mu$ =0.678 ±0.044 & 0.744 ±0.036) compared to Tomo1 OE and control ($\mu$ =0.367 ±0.043; 0.516 ±0.036). Regulation by Tomo1 on the fraction of TRP vesicles was distributed across the entire population of synaptic boutons as evidenced by cumulative frequency distributions of TRP size (Figure 1D). Notably, Tomo-1 KD demonstrated a significant right-shift toward greater TRP fractions (Median = 0.67 & 0.72) and mCH-Tom1 a left-shift, toward smaller TRP fractions (Median = 0.41) relative to control (Median = 0.54). No statistically significant differences were observed between conditions in TRP depletion kinetics (t, con $\mu$ =18.2 ±3.15; KD $\mu$ =18.12

±4.96; OE μ =17.36 ±6.05); or total SV pool size ($f_{NH4Cl} - f_0$, con μ =7007 ±1325; KD μ =6622 ±2278; OE μ =12191 ±1813). These data demonstrate a previously unknown site of inhibitory action for Tomo1 within the SV cycle at central excitatory synapses. That is, Tomo1 is not limited to inhibiting priming of SVs into the RRP pool; but is also involved in a molecular mechanism that acts to clamp vesicles into the release-recalcitrant ResP (Figure 2 B-D).

Tomosyn was discovered as Syntaxin1A-binding protein [23] that is capable of forming a ternary complex with Syntaxin and SNAP25 that mitigates VAMP on secretory vesicles from forming into SNARE complexes [24,25,46]. Therefore, we next tested if the VAMP-like SNARE domain was required for Tomosyn's inhibtory action on TRP. For these experiments we expressed a C-terminally truncated m-Tomo1 (Tomo1-ΔCT; m-Tomo1 (1-1069)) deficient in the SNARE motif and assessed changes in the fraction of SVs in the TRP and ResP. Immunoprecipitations (IPs) from PC12 cell lysates expressing Tomo1-ΔCT vs. wt Tomo1 confirm that Tomo1-ΔCT fails to interact with SNARE proteins Syntaxin1A and SNAP25 (Figure 2F). Expression of the Tomo1-ΔCT in neurons significantly inhibited the TRP relative to control (Figure 2E,F) to a similar degree as wt Tomo1. Taken together the data demonstrate that Tomo1 regulates fractional changes in the TRP and ResP in hippocampal neurons independent of its VAMP-like SNARE motif. The ability of Tomo1 to allocate vesicles to a non-releasable ResP may reflect an evolutionary conserved function with its yeast homolog Sro7, which when overexpressed results in non-fusiogenic vesicle clusters independent of the cognate SNARE sec9 [34].

*Activity-dependent Cdk5 regulation and Tomosyn phosphorylation*

The partitioning of vesicles at nerve terminals between the TRP and the ResP may be dynamically regulated in response to neuronal activity. For example, in cultured hippocampal neurons NMDA-receptor dependent potentiation of neurotransmitter release drives an increase in the fraction of recycling vesicles [7]. In addition, engagement of homeostatic plasticity in response to strong elevations or decreases in global network activity has demonstrated compensatory shifts in SVs to and from the ResP, respectively, in both acute hippocampal slices and hippocampal and neocortical neuron cultures[8-10]. While numerous pre and post-synaptic mediators of homeostatic plasticity have been identified, the specific presynaptic signaling pathways that direct changes in the SV pool distribution during plasticity remain poorly defined. Among those exerting established effects on the TRP is Cdk5, which has been demonstrated via pharmacological blockade with roscovitine (rosco) to drive populational increase in the TRP concomitant with a decrease in the ResP in hippocampal brain slices and cultured hippocampal neurons [9,21]. Cdk5 is a proline-directed Ser/Thr kinase whose activators (p35, p25 and p39) are mainly brain specific[47-49]. Cdk5 has been ascribed functions primarily as a neural-specific kinase critical to neurite development and synaptogenesis, synaptic function and plasticity, and dysregulation of its activity has been linked to the pathology of neurodegenerative diseases such as Alzheimer's, Parkinson's and Huntington's [50-53]. Important to the current investigations, the reported extent to which Cdk5 modulates TRP size closely mirrored the distributional changes we observed upon alterations of Tomo1 expression. Therefore, we next evaluated if the state of Cdk5 activation is sensitive to synaptic activity and if Tomo1 serves as a Cdk5 substrate.

Unlike other cyclin dependent kinases, Cdk5 is not activated by cyclins but rather by necessary interaction with non-cyclin regulatory partners (p35/p25, p39) [53]. In addition, although T-Loop phosphorylation of Cdk5 is not required for full catalytic activation, its phosphorylation at Ser159 elicits a marked increase in Cdk5 activity [54,55]. Therefore, to initially test if neuronal activity modulates the activation state of Cdk5 we used anti-phospho-Cdk5-Ser159 antibody in immunocytochemistry of hippocampal cultures. Figure 3A shows that relative to immunofluorescence intensity of controls, treatment of cultures (30 min) with rosco (100 μM) demonstrated lower averaged immunofluorescence intensity (μ =0.75 ±0.021), while cyclosporine A (CSA) treatment, an inhibitor of the presynaptic serine/threonine phosphatase calcineurin that opposes the functional effects of Cdk5 on SV pools[9], showed higher averaged intensity (μ =1.234 ±0.148). Together these data indicate that anti-phospho-Cdk5-Ser159 immunofluorescence reports the relative activation of Cdk5. To assess the role of neural activity on Cdk5 activation in hippocampal cultures the immunostaining studies were repeated, comparing TTX treatment (1 μM , 24 hours) to block global AP firing to vehicle-treated controls. The results showed that blocking neuronal spiking with TTX led to strong reductions in phosphorylated Cdk5 immunofluorescence intensity (μ =0.7 ±0.004) relative to control (Figure 3B). Thus, the data strongly suggest that Cdk5 activation is sensitive to neuronal.

To determine if Tomo1 is a Cdk5 phosphorylation substrate we first tested for intermolecular interaction by co-IP from hippocampal neuron culture lysate. The results established that Cdk5 co-IPs with Tomo1, and that the co-precipitation was independent of whether Cdk5 or Tomo1 was the primary IP protein (Figure 3C). Next, we investigated whether Tomo1 is a phosphorylation target of Cdk5, as Tomo1 contains several consensus

sequences for Cdk5 phosphorylation. For this, *in vitro* phosphorylation reactions were conducted using active p25/Cdk5 in the presence of γ-[$^{32}$P]-ATP, together with biotin-tagged m-Tomo1 protein that was affinity purified from transfected HEK-293 cells for proper folding. Analysis of the reactions by Western blotting showed direct correlation between $^{32}$P-radiolabeling and Tomo1 immunoreactivity (Figure 3D). $^{32}$P-phosphorylation of Tomo1 was mediated by Cdk5 as radiolabeling was not observed in the empty-vector control samples or in Tomo1 p25/Cdk5 samples containing rosco (1mM) (Figure 3D). An *in silico* analysis of the Tomo1 protein sequence for Cdk5 phosphorylation motifs ([S/T]PX[K/H/R]) yielded a total of 11 predicted sites using the Group-based prediction system 3.0 with a high-threshold allowing only a 2% false positive rate [56]. The *in silico* studies were then followed up by mass-spectrometry analysis of in vitro Cdk5 phosphorylated mTomo1 protein, which confirmed phosphorylation of 3 sites from the prediction list (S269, S867, T1004). Altogether results from these biochemical studies further strengthen the hypothesis that Tomo1 is a Cdk5 phosphorylation substrate.

*Tomosyn and Cdk5 share a common pathway in regulating SV pools*

To determine if Tomo1 actions on the TRP were under specific regulation by Cdk5 we evoked presynaptic release in control and Tomo1KD neurons under conditions were Cdk5 was pharmacologically inhibited As shown in Figure 4, inhibition of Cdk5 with rosco (100 μm, 30 m) enhanced the fraction of recycling vesicles relative to that observed in carrier-treated (0.1% DMSO) controls (Figure 4A, black trace left vs. right;). These findings are similar to those previously reported [9]. Importantly, however, the effect of Cdk5 inhibition was specific to the presence of Tomo1, as a further enhancement in the TRP

proportion was absent in the Tomo1 KD condition (Figure 4A, blue trace, right vs. black trace, right). Note also that Tomo1 KD alone led to an enhancement in the fraction of recycling vesicles (Figure 4A, blue trace, left), similar to that observed with Cdk5 inhibition (Figure 4A, black trace, right).

As a complement to these studies, we next compared the effects in control vs. Tomo1 KD neurons when Cdk5 activity was genetically depressed by expression of the catalytically inactive, dominant-negative Cdk5 mutant (Cdk5(D144N)). Notably, we observed an enhancement in the TRP fraction on Cdk5-D144N expression that was comparable to that observed upon treatment with rosco (Figure 4A, magenta trace, left). Moreover, application of rosco in the Cdk5-D144N expression condition did not significantly increase the TRP size (Figure 4A, magenta trace, right), confirming that the effects of rosco on the TRP are specific to Cdk5. These results confirm previous data demonstrating that Cdk5's catalytic activity inhibits the size of the TRP. More importantly, the results demonstrate that: 1) Tomo1 KD or ablation of Cdk5 catalytic activity lead to significant increase in fraction of SVs in the TRP, and 2) down-regulation of Tomo1 expression or Cdk5 activity occludes the increases in the TRP that are normally mediated by the other (Figure 4B). Finally, analysis of cumulative frequency distributions of TRP size from bouton ensembles across cells show that, genetic or pharmacological inhibition of Cdk5, KD of Tomo1, or downregulation of both proteins result in a comparable right-shift (towards greater TRPs) relative to non-treated control cells (Figure 4C). Together, these results strongly support Tomo1 and Cdk5 as acting within the same signal-transduction pathway that regulates the fraction of SVs in the ResP.

*Identification of a novel Tomo1 effector complex regulated by kinase activity*

We next examined how Tomo1 may participate, independent of its SNARE motif, in the regulation of vesicle availability for release. In the rat brain, Tomosyn is localized to the cytosol, plasma membrane and SVs [23,32,57]. As a non-integral membrane protein Tomosyn's association with the plasma membrane has been well documented to be via interaction with Syntaxin1A [58], yet the mechanism by which Tomosyn associates with SVs is unknown. However, the yeast homologs of Tomosyn (Sro7p/77p) interact with Rab GTPases, which are vesicle-associated proteins important in tethering and docking of vesicles at sites of fusion. At central synapses, the primary exocytotic Rab GTPases are of the Rab3 family, comprised of four Rab3 isoforms A-D that compensate for one another functionally [59]. Based on a potential for evolutionary conservation of effector interactions we tested if Tomo1 interacts with Rab GTPases by conducting co-IP assays using cultured hippocampal neuron lysates. As shown in the representative Western blot in Figure 5A, Rab3A was observed to co-precipitate with endogenous Tomo1, as well as with YFP-Tomo1 resulting from lentiviral OE. Moreover, as confirmation of the specificity of the interaction, we did not observe co-IP of other synaptic (RIM1/2, actin) or integral SV (Synaptophysin) proteins with Tomo1 (Figure 5A). Interestingly, while Rab3A normally binds and co-precipitates with RIM proteins our results suggest that it may not do so when bound to Tomo1, since it was not apparent in co-precipitates containing Rab3A. As GTPases, Rab3 proteins cycle between an active effector interacting GTP state and an inactive GDP bound state; being present on SVs only when GTP bound [60]. To test whether the nucleotide state of Rab3A affected Tomo1 binding we conducted IP assays from hippocampal lysates where Rab3A was freed of nucleotide binding and then locked into a

GTP or GDP bound state with non-hydrolysable nucleotide analogs. We observed that Tomo1 bound preferentially to Rab3A-GTP compared to GDP or nucleotide free (Figure 5B-C).

To complement the IP results, we next tested for detection of Tomo1/Rab3A interaction within a cell context using a proximity ligation assay (PLA). For these experiments cells were submitted to immunocytochemistry using rabbit polyclonal anti-Tomo1 and mouse monoclonal anti-Rab3A antibodies prior to treatment with species-specific PLA secondary antibodies that contain unique short DNA strands. Should the DNA strands from the PLA secondary antibodies be in close proximity (<40nm) they possess the ability to be ligated, amplified and fluorescently labeled to yield high intensity fluorescent puncta at sites of putative protein-protein interactions. Insulin secreting Min6 cells were used as they possess large (~270 nm diameter) secretory granules, utilize exocytotic machinery similar to that of neurons and present a well resolved cell periphery that promotes quantitative analysis of the PLA fluorescent puncta. Robust PLA signals between Rab3A and Tomo1 were observed (Figure 5D,E; $\mu$ =0.378 ±0.02 puncta/μm) that appear localized with secretory granules (Figure 5F). Analysis shows that the density of PLA fluorescent puncta was not significantly different from that of Rab3A and RIM2 ($\mu$ =0.437 ±0.015 puncta/μm), for which an interaction is well established within presynaptic compartments [61,62]. As PLA assay controls (Figure 5E), negligible PLA signals were observed between Rab3A and the SV membrane protein Syp ($\mu$ =0.077 ±0.008 puncta/μm) or when cells were probed for Rab3A alone ($\mu$ =0.07 ±0.007 puncta/μm). PLA experiments in cultured hippocampal cells also show robust signals between Tomo1 and Rab3A, Rim1/2 and Rab3A but not Synaptophysin and Rab3A (Figure 5G). The interaction between Tomo1

and Rab3A-GTP in hippocampal neurons provides a mechanism supporting vesicle localization of Tomo1, and reflects an evolutionary conservation to the yeast homolog Sro7 interaction with Sec4-GTP. In addition, this may serve as a candidate molecular mechanism for clamping vesicles in the ResP, as studies in yeast show that Sro7 induced accumulation of non-fusiongenic vesicles depends on Sec4-GTP [34], while mammalian studies on exocytosis have revealed that Rab3A-GTP can also clamp SV release [63-65].

*Kinase activity modulates the formation of a Tomo1/Rab3A/Synapsin complex*

Rab GTPases and Synapsin phosphoproteins are the major regulatory proteins for tethering and docking SVs at the AZ. While the association of Rab3 to SVs is mediated via its GTPase activity, Synapsin proteins transit on/off vesicles depending on their phosphorylation state [66]. Phosphorylation of Synapsin by PKA, CaMKs, Erk, or Cdk1 decreases binding to SVs and conversely phosphorylation by Src enhances SV binding [67-70]. Importantly, because Rab3A-GTP also binds to Synapsins [71]; we next determined if Synapsin1 was present in Tomo1 IPs from hippocampal lysates, since such an interaction may be central to Tomo1 exerting regulatory actions on the TRP. As shown in the representative Western blot (Figure 6A), Synapsin1 proteins were present in Tomo1 IPs. As a control assessment for the specificity of co-precipitation, use of a rabbit IgG isotype-control yielded no detectable IP of Tomo1, Rab3A or Synapsin1 proteins (Figure 6B). Next, to determine if the Tomo1 and Synapsin1 interaction was direct or if it occurred as a function of Rab3A binding we conducted Tomo1 IPs from neuronal lysates that were previously cleared by IP with a Rab3A antibody. Figure 6C shows that in the absence of Rab3A, Synapsin1 proteins no longer Co-IP with Tomo1. These results imply that Tomo1

forms a complex with Synapsin1 proteins via its interaction with Rab3A in hippocampal neurons.

To determine if differences in Cdk5 kinase activity, as occur to changes in neural activity, result in corresponding changes in Tomo1/Rab3A/Synapsin1 interactions we compared the relative levels of Rab3A and Synapsin1 Co-IP with Tomo1 following treatment (30 minutes) of hippocampal neurons with rosco, CSA, or vehicle (Figure 6D,E). Notably, a significant increase in Tomo1/Rab3A/Synapsin1 interaction was observed with CSA treatment relative to control; a condition expected to result in enhanced levels of Cdk5 phosphorylation. By comparison, no significant change in co-IP was observed with rosco treatment relative to control. The lack of a discernable decrease in Tomo1/Rab3/Synapsin1 interaction likely results from immunoblot sensitivity, as the low level of Rab3A in complex with Tomo1 (<1%) under control conditions may hinder accurate detection of small decreases. By comparison, a strengthening of the interaction is measurable as a result of substantially greater range for increase. Altogether, the data strongly suggest that the interaction of Tomo1 with Rab3A and Synapsin1 is sensitive to Cdk5 catalytic activity, though we cannot rule out that the formation of this complex is directed by other kinases given that calcineurin serves as a general phosphatase in neurons. Nonetheless, the discovery of this molecular complex is a strong potential molecular mechanism modulating the availability of SVs for evoked release.

*Tomo1 phosphorylation state is sensitive to neuronal activity and is important for synaptic scaling*

Importantly, in a final series of investigations we tested if neuronal activity leads to changes in Tomo1 phosphorylation by Cdk5 and if Tomo1 exerts a central role in homeostatic presynaptic changes in neurotransmitter release arising from alterations in neural activity. First, we assessed if Tomo1 is phosphorylated in neurons by conducting IP assays from hippocampal cultures in which cytosolic ATP was labeled by $^{32}P$ orthophosphate. As shown in Figure 7A-B, we find that Tomo1 is phosphorylated *in situ* and that treatment with rosco (100mM), to inhibit Cdk5, leads to a ~50% reduction in basal phosphorylation levels. Critically, our results also show that chronic elevation in neural activity induced by treatment with the $GABA_A$ receptor antagonist, picrotoxin (Ptx, 50 mM, 4 hrs), and an elevation in extracellular calcium (4mM) increased the amount of phosphorylated Tomo1 relative to control. Inhibiting Cdk5 by application of rosco (100mM) 30 minutes prior to, and throughout the pharmacologically-induced elevations in neural activity did not completely abrogate the increase in Tomo1 phosphorylation; however, it did result in a modest decrease compared to chronic activity alone. This suggests that, while Cdk5 is an activity-dependent kinase for Tomo1 other kinases also phosphorylate Tomo1 during elevations in neuronal spiking. Notably, Tomo1 is a known substrate for PKA, thus potentially implicating it in activity-dependent regulation [28]. We next assessed if Tomo1 was necessary for compensatory elevations in SV release that are reported to appear as a homeostatic presynaptic plasticity response following chronic silencing of neural activity[72,73]. As shown in Figure 7C-D chronic silencing of network activity in the hippocampal cultures by the competitive antagonists of AMPA/kainate

glutamate receptors (CNQX, 40 mM) for 24 hrs resulted in greater vGpH responses to a 100P/10Hz stimulus relative to vehicle-treated controls. . Importantly, Tomo1 KD neurons lacked the ability to undergo these compensatory enhancements in neurotransmitter release relative to vehicle-treated shTomo1 neurons. . While, KD of Tomo1 alone leads to a significant enhancement in SV release (Figure 2); the results indicate that the ability of synapses to upregulate SV release within the context of prolonged activity blockade requires Tomo1.. Considered together, the data indicated that the phosphorylation state of Tomo1 is sensitive to neural activity and that Tomo1 has a pivotal role in activity-dependent compensatory synaptic scaling.

**3.4 Discussion**

The partition of SVs at small central synapses into distinct functional pools has been well established and in some cases, morphological and molecular correlates have been defined [4,5,74]. The fractional distribution of SVs among pools (RRP, RP and ResP) has been shown to strongly impact presynaptic performance (namely, Pr) and the expression of Hebbian as well as homeostatic forms of synaptic plasticity [7-9,20,75]. Moreover, between individual presynaptic boutons of any given neuron, the fractional distribution of SVs among releasable (TRP) vs. non-releasable (ResP) pools may be highly heterogeneous, raising the possibility for local regulation by signaling molecules and effector proteins in response to local activity [7,12,16,76-79]. Here we establish that Tomo1, a non-integral membrane R-SNARE protein, is a central molecular mediator of SV distribution within functionally defined presynaptic SV pools. We find that Tomo1 inhibits not only priming of SVs into the RRP but, importantly, also defines the distribution of vesicles between the TRP and ResP, an effect independent of its C-terminal localized SNARE domain. Moreover, our

results link previously reported effects of Cdk5 on dynamic changes in the TRP to Tomo1, which we demonstrate is an activity-dependent phosphorylation substrate of Cdk5. Furthermore, we identify a novel protein interaction between Tomo1 and Rab3A GTPases. We find that Tomo1 interacts with SV localized Rab3A-GTP, more strongly than GDP and promotes formation of a complex along with Synapsin1 proteins; thus, providing a potential mechanism by which SVs may be appropriated into a release-recalcitrant ResP.

The molecular signaling pathways sensitive to neural activity, which confer precise yet dynamic structural and functional partitioning of SVs between the TRP and ResP remain poorly established. This information is of considerable physiological importance as small central synapses such as those of hippocampal neurons contain few total SVs (~200) [41,78,80], thus sequestering of SVs into a ResP can strongly limit synaptic performance during sustained activity. Most measurements of the TRP size from dissociated hippocampal neurons or in hippocampal brain slice show that on average it accounts for 50% of the total SV population [7,12,77,78], though some report smaller percent recycling [21,81]; and one recent study has reported that in organotypic brain slices all SVs are able to participate in exocytotic activity [8]. In contrast, different structural and functional dynamics of SV partitioning, particularly with regard to the ResP may be found in presynaptic terminals that contain a substantially greater number of SVs and/or multiple AZs, such as frog, *Drosophila, C. elegans* NMJs or the Calyx of Held(see review by [5]). In terms of the morphological organization of the SV pools at small central synapses, structural analysis of hippocampal boutons from CA3 Schaffer collateral fibers in brain slices revealed that TRP vesicles are spatially positioned closer to the AZ relative to ResP vesicles, and that ResP SVs do not appear to be part of the SV superpool of vesicles that

dynamically exchanges between boutons [13,21]. Moreover, the total number of SVs in a bouton does not correlate with the fraction that is in the TRP or with Pr; however, the TRP size is positively correlated with number of docked SVs in the AZ [21,82]. Thus, it would appear that TRP SVs are more likely to be closer to the release site than ResP SVs, though spatial positioning does not strictly define them. Nonetheless, this implies the possibility that structural dynamics like remodeling of the actin cytoskeleton may contribute to defining spatial clustering of pools. Indeed, in cultured hippocampal neurons pharmacological stabilization of actin dynamics mitigated TRP clustering near the AZ, but did not alter SV pool sizes[21]. In addition, the use of compounds that disrupt actin dynamics has been reported to leave SV clusters at synapses unaffected [83] and fluorescence imaging of eGFP-tagged, as well as EM analysis of immunogold-labeled actin have revealed that it predominantly surrounds only the distal edges of SV clusters, further supporting a role for actin in spatial clustering but not pool partitioning [66,84]. Therefore, while actin may participate in positioning of SVs within functionally defined pools, distinct signaling pathways likely mediate the partitioning of SVs between the ResP and TRP. One such signaling pathway is mediated by Cdk5, which has been established as a regulator of the ResP size [9]. It has been shown that Cdk5 phosphorylates Synapsin1 promoting its association with F-actin resulting in a sequestration of vesicles to perisynaptic sites in a non-releasable state [20]. These studies account for how SVs may be silenced by morphological clustering at perisynaptic sites and how Synapsins can function as regulatory elements for controlling lateral vesicle sharing between synapses [22], yet they do not fully account for how SVs are partitioned independent of actin dynamics and within the SV cluster into distinct pools. Here we show that Tomo1 is an activity-dependent

phosphorylation substrate of Cdk5 able to define the TRP/ResP partition. Moreover, we determined that Tomo1 bound to Rab3A is able to form into complex with Synapsin1 proteins. Notably, this molecular complex is sensitive to S/T kinase activity, thus adding a novel, potent and activity regulated signaling system for reallocation of SVs among functional pools. Indeed, the diverse molecular actions of an SV-associated complex containing Synapsin1, Rab3A and Tomo1 may be more important for restricting the release capability of SVs within the AZ cluster, as each of these proteins has been found capable of independently limiting SV release. This would represent a multifaceted inhibitory complex for restricting SV transition from ResP to TRP since clamping could occur at distinct stages of the SV cycle. For example, ResP SVs could be defined by tethering functions of Synapsin1 dimers [85-87], Rab3A binding to docking/priming factors like RIM and Munc18 [88-90] or Tomo1 interactions with Q-SNAREs [24,25,91] all which localize SVs to the AZ but can exert a regulatory brake on release-competence. In accordance, in this study we find that while Tomo1 is able to inhibit the size of TRP, it had no effects on TRP release kinetics. By comparison, phosphorylation of Synapsin1 proteins delays depletion kinetics of the TRP. Thus, specific components of this complex in theory could confer distinct ResP dynamics as they clamp at different stages of the SV cycle.

Tomosyn proteins have been well characterized as potent inhibitors of evoked transmitter release in neuroendocrine cells [24,27,58,92], rat superior cervical ganglion [28], hippocampal dentate gyrus mossy fibers [29], C. elegans [32,93] and Drosophila [30]NMJs. The predominant mechanistic model of Tomosyn action is that it exerts inhibitory effects via its C-terminal R-SNARE domain, which competes with VAMP and Munc18 for interaction with reactive syntaxin1A. The interaction with syntaxin1A and

SNAP25 leads to non-fusogenic SNARE complexes that have been proposed to limit vesicle priming [24,25,91]. Remarkably, in spite of their key importance, there have been few evaluations of Tomosyn effects on SV cycling at small central synapses. Our results present a completely novel site and mechanism for Tomo1 inhibition of SV release that provides a remarkable shift in the conventional view of Tomo1, as we observe that it not only regulates priming into the RRP (i.e. RP→RRP) but also transitions from the ResP to the TRP. These findings help explain previous data from mouse chromaffin cells and NMJs (C elegans and Drosophila) that indicate inhibitory actions of Tomosyn beyond the RRP pool. In addition, our data indicate that the large N-terminal WD-40 repeat domain of Tomo1, as opposed to the C-terminal VAMP2 homologous SNARE domain, comprises the region specific for its effects on SV ResP to TRP transitions. Little has been previously established concerning functional roles the N-terminus of Tomosyn plays in SV release, although Tomo1 based on a structural homology model closely aligns with the yeast Tomosyn homologue, Sro7 [38].

Here we show that Tomo1 is also a binding partner of Rab3-GTP, a discovery that implicates evolutionary conservation with an interaction occurring in the budding yeast where the secretory Rab, Sec4-GTP and the Tomo1 homolog, Sro7p act to coordinate the tethering of vesicles to fusion sites and priming for release [33-35,94]. In fact, overexpression of Sro7p in yeast results in a pronounced growth defect and the formation of a large cluster of 'ResP-like' non-releasable post-Golgi vesicles within the cell, in a manner dependent on Sec4-GTP[35]. Consistent with this, in mammals overexpression of a GTP-locked point mutant of Rab3A (Q81L) impairs the size of the recycling pool [65]; and as shown here expression of Tomo1 leads to an increase in the ResP. Moreover, structural

analysis of the *C. elegans* NMJ show that a loss of function mutation of Tomosyn leads to an increase in the number of SVs contacting the plasma membrane [95]. Altogether these results suggest that the Tomo1, Rab3-GTP interaction may form the central components of an SV clamping mechanism.

One of the most prominently observed ResP functions has been as a functional locus for presynaptic scaling of neurotransmission in response to chronic changes in synaptic activity. ResP pools size dynamically shrinks or expands leading to changes in presynaptic strength that counter strong or chronic changes in synaptic activity [8,9,20,75]. Neural networks commonly encounter strong variations in synaptic activity during sleep [96]; stroke and trauma[97]; and in early formation of neural circuits when massive numbers of synapses are added or pruned [98-100]. Cdk5 was one of the first identified critical presynaptic substrates that can regulate the fraction of ResP SVs in hippocampal cultures for synaptic scaling. Its effects on synaptic scaling in response to chronic silencing have been evidenced by findings showing that long term, TTX-induced silencing of the activity of hippocampal neurons in culture or of excitatory hippocampal CA3 recurrent synapses in brain slice lead to a compensatory upregulation of neurotransmitter that depends on Cdk5 [9,101]. Interestingly, Kim and Ryan (2010) note in their study that chronic silencing of neurons with TTX results in a 50% reduction of Cdk5 protein levels [9]. While other presynaptic proteins were largely unaffected, the next greatest change was a 15% reduction of Tomosyn proteins. Here we discover that Tomo1 proteins are subjected to Cdk5 phosphorylation in an activity-dependent manner and moreover, that compensatory enhancements in release after chronic dampening of network activity require Tomo1 proteins. This provides a coherent conceptual model for how neuronal activity is linked to

fractional changes in the ResP. This is further supported by findings in *C. elegans* where synaptic scaling was shown to occur by coordination of presynaptic SV release and post-synaptic receptor activity [102,103]. Specifically, scaling was mediated by a trans-synaptic signaling mechanism in which the cell-adhesion molecules Neurexin and Neuriligin mediate a retrograde signal to shunt neurotransmitter release. This signal was engaged by the inactivation of a muscle microRNA (*mir-1*) and results in a specific inhibition of less-calcium sensitive (i.e. EGTA-sensitive) SVs. Importantly, the presynaptic effects of the retrograde signal (i.e. inhibition of SV release) depended on the actions of Tomosyn and correlated to increases in the protein levels of both Tomosyn and Rab3 [102,103]. In accordance, increases in neurotransmitter release associated with synaptic scaling at the Drosophila NMJ require the function of Rab3-GAP presumably because it releases Rab3 from a synaptic repressor by promoting GTP to GDP cycling [104], a finding consistent with a model positing Tomo1 as the repressor. Thus, several reports have coalesced to implicate Cdk5, Rab3 and Tomosyn as conserved regulators of presynaptic scaling in distinct model systems further strengthening observations that TRP/ResP partitioning is a primary mechanism for altering presynaptic efficacy in response to neural circuit activity.

The data presented here together with previous reports detailing the function of Tomosyn proteins demonstrates that they play a significant role in regulating the efficacy of evoked synaptic transmission. However, in addition, and perhaps related to their cellular function, Tomosyn proteins are important for learning and implicated in disease pathology. Two recent studies stress this importance: (1) a homozygous mutation in the Tomo1 gene explains an infantile-onset neurodegenerative disorder characterized by sensorimotor axonal neuropathy, optic atrophy and cognitive deficit[105]. (2) The Tomosyn gene was

identified as a novel disease locus found to be commonly deleted in a cohort of families with at least one child with autism who also had facial dysmorphology, limb, digit or ocular abnormalities[106]. While the specific mechanisms underlying Tomosyn's participation in these diseases remains unknown, recent evidence has demonstrated that Tomo1-overexpression in dentate gyrus neurons of the mouse hippocampus results in modest impairments in spatial learning and memory retention [29]. In addition, the labile component of cAMP-dependent associative memory in *Drosophila* requires Tomosyn and Synapsin proteins[30,107,108]. Further, outside the CNS, Tomosyn function appears to be critical, for example, it was recognized as an important susceptibility gene for type-2 diabetes due to its integral role in regulating insulin secretion and insulin-dependent GLUT4 exocytosis[109,110]. In the cardiovascular system, Tomosyn was shown to be required for normal platelet secretion and hemostasis[111]. Thus, there appears to be a certain degree of intolerance to perturbations in Tomosyn function and/or protein levels in several physiological systems. In agreement with this, it is known that the mRNA levels of Tomosyn are developmentally regulated, as is the expression of many Tomosyn1 & 2 protein isoforms [38,112]. Moreover, in the 3xTgAD mouse model of Alzheimer's disease Tomosyn protein levels are enriched [113]. Taken together, these studies suggest that future investigations aimed at discovering the links between Tomosyn function and learning and memory or disease pathology have the potential to be a worthwhile challenge as it concomitantly provides the opportunity to answer fundamental questions of how regulation of SVs and the efficacy of synaptic transmission feeds into greater behavioral phenomena and neuropathology. Moreover, while developmental processes have not been addressed in these studies, it is important to consider that Tomosyn has a role in neurite

development likely by using it SNARE-binding capabilities to localize to sites of extension as its counterpart Sro7 does during yeast growth [33,114]. Thus, it is possible, since partitioning of the ResP was shown to be developmentally refined, that SV pool partitioning dynamics could play integral roles in defining or at least safeguarding activity-dependent wiring of neural circuits during early synapse development [8,14]. Especially when considering that the catalytic activity of Cdk5 [51-53] and the GTPase activity of Rab3 [115-117] have also been linked to strong neurodevelopmental deficits. Clearly, further work will be needed to detail the molecular mechanisms and triggers for SV partitioning and future studies should consider the developmental and pathophysiological implications.

### 3.5 Materials and methods

*Antibodies*

The following primary antibodies were used: anti-Synapsin1 (SYSY, Göettingen ,Germany; rabbit, #106011, 1:1000), anti-Tomo1 (SYSY, rabbit, #183103, WB 1:1000, ICC 1:400; BD Biosciences, mouse, #611296, WB 1:400), anti-Rab3A (SYSY, mouse, #107011, WB 1:1000; SYSY, rabbit, #107003, ICC 1:1000), anti-Cdk5 (Santa Cruz, Dallas, TX; rabbit, #SC173, WB 1:200; mouse, #SC6247, WB 1: 200; anti-phospho-specific Cdk5, (Santa Cruz, rabbit, #SC12919, ICC 1:100), anti-synaptophysin (Sigma-Aldrich, St. Louis, MO, mouse, #S5768, ICC, WB 1:250 ), anti-RIM (SYSY, rabbit, #140003, WB, ICC 1:500), Proximity ligation assay (Sigma-Aldrich, DUO92102), anti-actin (Sigma-Aldrich, mouse, #A2228#, WB 1:5000), IRDye800CW and IRDye680LT (LI-COR, Lincoln, NE 1:5000) and Alexa488 and Alexa594 (Life Technologies, Grand Island, NY), Vectashield with DAPI (Vector Laboratories, Burlingame, CA, #H-1200).

*cDNA constructs and lentiviral vectors*

The pCAGGS super ecliptic vGLUT1-pHluorin construct was obtained from Robert Edwards (UCSF) [44]. mCherry was subcloned in frame to the C terminus of vGLUT1-pHluorin to create vGLUT1-pHluorin-mCh with mCh exposed to the cytoplasmic region on expression. Recombinant constructs were used in expression studies included: pLP-mCherry vector (CMV promoter); pLP vector (CMV promoter) containing mCherry fused to N-terminus of mouse m-Tomo1 ; pDNR (CMV promoter) containing a deletion (residues 1067-1131) of the C-Terminal SNARE domain of m-Tomo1 (MTomo1 DCT)[38]; pCDNA CAPTEV-CT Gateway vector containing rat m-Tomo1 ; and pLentih (Synapsin promoter) containing YFP fused to the N-terminus of m-Tomo1 [29]. Lentiviral vectors encoding a short hairpin RNAi for targeted knockdown of all Tomo1 isoforms or a non-targeted scrambled RNAi were obtained from Origene (Rockville, MD). The RNAi sequences: KD1 ACTGCTTCAGCCAGTGATTGTGTCTCCAA, KD2-CCGTATGCTGTGGTTGTTCTCCTGGAGAA, or a scrambled control Scr- CAGGAACGCATAGACGCATGA were expressed by a U6 promoter in either pGFP-C-shLenti or pRFP-CB-shLenti. Cdk5 (D144N) [118]. Lentiviral plasmids were submitted to the University of Michigan Vector Core for the production of high-titer lentiviruses. Briefly, HEK293T cells were transfected by Lipofectamine (Invitrogen) with vectors encoding REV, MDL, pvSVG and a lentiviral plasmid containing expression construct. Forty-two hours post-transduction, the medium containing the viruses was collected, filtered through a 0.45 mm filter to remove cell debris, then ultracentrifuged at 42,152xG at 4 °C for 2 h. The supernatant was discarded and virus pellet gently resuspended in 10 mL of Nb4Activ. Aliquots containing 500 ml of NB4Activ with viruses were quickly frozen and stored at -80 °C.

*Primary neuronal culture and transfections/infections*

Neuronal cultures were prepared from postnatal day 1-2 rat hippocampi of either sex as previously reported [119]. Briefly, the hippocampi were dispersed into a single cell suspension via enzymatic treatment with papain (Sigma, 2mg/ml) in HBSS without $Ca^{2+}$ or $Mg^{2+}$ (Life Technologies) with L-cysteine added (1 mM) followed by mechanical trituration. Hippocampal neurons were plated on poly-D-lysine coated, 22mm diameter, #1.5 thickness coverglass (Neuvitro, Vancouver, WA) or on 14 mm microwell glass bottom 35 mm culture dishes (MatTek, Ashland, MA) at a density of 400 cells/$mm^2$. Neurons were cultured in NBActiv4 (Brain Bits, Springfield, IL). Cells were maintained in a 37°C, 95% $O_2$/5% $CO_2$ humidified incubator and half the media was exchanged every 3-4 days with fresh NBActiv4 media.

Neuronal cultures were transfected at 10-14 days *in vitro* (DIV). Transfection was achieved using Lipofectamine 2000 (Life Technologies) according to the manufacturers recommendations, except that culture media was exchanged with fresh NBActiv4 media; 0.8-1µg of selected plasmid DNA was mixed with 1µL of Lipofectamine in 200µL of NBActiv4 media per dish and allowed to stand for 30 minutes prior to being dripped onto the cell cultures. Cultures were incubated for 1hr with the Lipofectamine/DNA mix after which media was exchanged with fresh NBActiv4 media. For lentiviral infections the stock virus (~1x$10^7$MOI/ml) stored at -80 was thawed and diluted 1:10 in NBActiv4 culture media and added to neuronal cultures (5-9 DIV). 12 hours later, additional NBActiv4 media was added diluting the virus 1:2. After 2 days the culture media was exchanged with fresh NBActiv4 and neurons were used for experimentation between 7-14 days post-infection.

*vGpH imaging and analysis*

vGpH imaging was performed on individual neurons 3-10 days post-transfection and 14-24 DIV. Glass coverslips containing the neuronal cultures were mounted into a chamber outfitted for field stimulation (RC-49MFS, Warner Instruments) and perfused (0.5 ml/min) for rapid solution exchange (chamber volume, 100 ml) with temperature controlled (37$^{o}$C; TC-324B, Warner Instruments) physiological saline containing (in mM): NaCl 136, KCl 2.5, Hepes 10, Glucose 10, $CaCl_2$ 2, $MgCl_2$ 1.3, AP5 0.05 (TOCRIS, Minneapolis, MN), CNQX 0.01 (TOCRIS), that was adjusted to pH 7.4. Action potentials were evoked by field stimulation with 2 msec current pulses applied through platinum-iridium electrodes spatially placed within the chamber to achieve 10 V/cm fields. The frequency and period of stimulus application was controlled by a Winston Electronics A65 Timer that was gated by and synchronized to Metamorph image acquisition software (Molecular Devices, Sunnyvale, CA). Transfected neurons were spatially localized on coverslips by mCherry fluorescence of vGpH-mCh expression [9]. The effectiveness of each applied stimulus within a train to evoke action potentials was confirmed on initial sets of Fluo4 treated neuronal cultures by measurement of time-synchronized alterations in intracellular calcium. vGpH responses to field-stimulation were always conducted in the presence of 1μM Bafilomycin-A1 (BafA1, LC Laboratories, Woburn, MA) to isolate exocytosis from endocytosis. Acquired vGpH fluorescent signals preceding and during stimulation were normalized to maximal vGpH fluorescence ($F_{MAX}$). This was done by brief application of a bath solution containing (in mM): $NH_4Cl$ 50, NaCl 86, KCl 2.5, Hepes 10, Glucose 10, $CaCl_2$ 2, $MgCl_2$ 1.3, adjusted to set pH at 7.4 and osmolarity of 290-300, which leads to alkalization of the total vesicle pool [45]. Fluorescence imaging was carried out on an Olympus IX81

microscope with Plan-Apochromat 100x 1.4 NA or ApoN 60X 1.49 oil immersion objectives (Olympus America, Center Valley, PA). Illumination was provided by a Lambda LS 300 Watt Xenon arc lamp (Sutter Instruments, Novato CA) coupled to an electronically shuttered liquid light guide for controlled transmission of light to the microscope optics. Images were acquired using an ImagEM EM-CCD Hamamatsu ( Hamamatsu City, Japan) camera. Optical filter-sets designed for mCherry and eGFP respectively: Ex, 472/30; 416/25 and Em, 520/35; 464/23 we used. vGpH time-series images were acquired at 5 Hz, using a 40ms integration time, not binned (512x512), with gain settings set to achieve the full dynamic 16-bit depth. A single image in the mCherry channel was acquired at the beginning and end of the time series. Microscope, camera, and stimulus gating were controlled using the MetaMorph software (Molecular Devices, Sunnyvale CA).

Analysis of spatial and temporal changes in fluorescence intensity within acquired vGpH time series image stacks was carried out using FIJI [120], an open source distribution of ImageJ (http://imagej.nih.gov/ij/) focused on life sciences. Regions of interest (ROI) were defined as puncta of fluorescent intensity localized along neuronal processes in images during $NH_4Cl$ treatment. Binary ROI masks were created by manual thresholding of a $\mathbf{\Delta}F_{NH4Cl}$ image. The $\mathbf{\Delta}F_{NH4Cl}$ image was calculated as $F_{NH4Cl} - F_{pre}$, where $F_{NH4Cl}$ is defined as an average of 10 frames during $NH_4CL$ application and $F_{pre}$ is defined as an average of 10 frames prior to application of any electrical stimulus in normal physiological saline. The resulting $\mathbf{\Delta}F_{NH4Cl}$ image was then subjected to a watershed protocol to create distinct ROIs for closely adjoining puncta. The resulting ROIs were then applied to each image within the time series and the average fluorescent intensity within each ROI per image was determined using a custom-built plugin [121]. The resulting time series of averaged

intensity for each ROI was imported into Igor Pro (Wavemetrics) and corrected for photobleach decay using a double exponential fit procedure [122]. The baseline intensity of each ROI was then subtracted ($F_{pre}$) and the data of each ROI normalized to its max intensity ($F_{NH4Cl}$). Time-series data for ROIs in each cell were averaged per time point to identify fractional TRP and ResP sizes. ROI time-series data were also grouped into ensembles for each treatment to generate cumulative frequency distributions of fractional TRP size. Data were plotted and statistical analysis performed using Prism 6 (Graphpad,).

*Immunoprecipitation*

Neuronal cultures (14-26 DIV) on glass bottom dishes were washed twice with phosphate-buffered saline (PBS, Life Technologies). Cells were then lysed using a cell scraper and 70µl IP lysis buffer per culture dish at 4°C. Lysis buffer contained (in mM): Tris-HCl 25, NaCl 50, $MgCl_2$ 2, $CaCl_2$ 1, 0.5% NP-40 adjusted to pH 7.4. Protease and phosphatase inhibitors were added immediately prior to lysis (Cell Signaling, Danvers MA). The lysates were pre-cleared via centrifugation at 2,000xG for 3 minutes. For IP, magnetic Protein A beads (Life Technologies #10002D) prebound to 0.5 – 1 µg of antibody was incubated with cell lysate and rotated at 4°C for 1 hour. Beads were then collected and rinsed 3X with ice cold PBS using a magnetic system (Invitrogen). IP pellet, supernatant and final wash samples were fractionated by SDS-PAGE and Western blotted onto a nitrocellulose membrane. Immunoreactivity against the primary IP protein and co-precipitated proteins was assessed (1 hour, RT) by labeling the bound primary antibodies with infrared-tagged species-specific secondary antibodies (45 min, RT) with imaging using an Odyssey CLx (Li-Cor Biosciences). Fluorescence density was determined on ROI of

images using the Gel Analyzer plugin in Fiji. For IP experiments that evaluated binding efficiency of Tomo1 to specific nucleotide-bound states of Rab3A, the cells were lysed in IP lysis buffer containing 4.0 μM EDTA to release endogenous nucleotide binding. Pre-cleared lysates were then incubated at 37°C fro 10 minutes with a saturating concentration of non-hydrolysable GTP (GTP-g-S, 200mM, Sigma-Aldrich) or GDP (GDP-b-S, 200mM, Sigma-Aldrich) added to the supernatant, and $MgCl_2$ to a final concentration of 20 mM.

*In Vitro phosphorylation of Tomo1*

A NativePure streptavidin-agarose affinity purification procedure was used to purify biotin epitope tagged m-Tomo1 protein from HEK293 cells transfected with pCDNA capTEV-m-Tomo1 according to the manufacturer's protocol (Invitrogen, Life Technologies). As a control, HEK293 cells were transfected with the empty pCDNA capTEV vector and subjected to an identical purification procedure. In brief, five dishes (10 cm) of HEK293 cells at 70% confluency were transfected with 12μg of DNA/dish using Lipofectamine 2000 (Life Technologies). At 48 hours post-transfection cells were collected in NativePure lysis buffer, subjected to 3 liquid nitrogen freeze/thaw cycles and then centrifuged at 10,000 x g for 10 min at 4C. Streptavidin beads were added to the post-nuclear supernatant and rotated for 3 hours at 4 C. Beads were then collected (1000xg for 2 min), rinsed and the purified tomosyn protein stored in lysis buffer with 0.1mM sodium azide. SDS-PAGE gel electrophoresis followed by commassie staining was used to assess protein purification. For *in vitro* Cdk5/p25 phosphorylation reactions 11.5 μg of m-Tomo1 on streptavidin beads was rinsed in phosphorylation buffer containing (in mM) 25 MOPS pH 7.2, 12.5 β-glycerol phosphate, 25 $MgCl_2$, 5 EGTA, 2 EDTA, 0.25 DTT and 250μg of active

Cdk5/p25 kinase (Signal Chem, Richmond, BC, Canada). Reactions were initiated by adding 50μM γ-[$^{32}$P]ATP (Perkin Elmer, Waltham, MA) with incubation at 30°C and intermittent mixing for 15 min. Reactions were terminated by centrifugation at 1,000 x g for 1 min, followed by 3 washes of bead pellet in cold kinase buffer (4$^{o}$C) lacking Cdk5/p25 and γ-[$^{32}$P]ATP. Bead pellet samples were then fractionated by SDS-PAGE, blotted and the $^{32}$P labeled tomosyn detected using a Molecular Imager FX (BioRad, Hercules, CA). Tomosyn on the nitrocellulose membrane was subsequently immunolocalized by Western Blotting. Controls included reactions with purified Tomosyn protein containing 1 mM Rosco, purified Tomosyn with no Cdk5/p25 kinase added, and streptavidin beads used in empty vector purification.

*Mass Spectrometry*

Mass spectrometry analysis of Cdk5 phosphorylated Tomo1 affinity purified protein was conducted by the University of Michigan Proteomics Resource Facility (PRF). Samples were submitted after in vitro phosphorylation reactions were separated on a poly-acrylamide gel, and proteins were visualized with colloidal Coomassie stain. The PRF conducted in-gel digestion followed by identification of phosphorylation site mapping as described previously [123]. Briefly, on trypsin digestion, peptides were resolved on a nano-capillary reverse phase column and subjected to a high-resolution, linear ion-trap mass spectrometer (LTQ Orbitrap XL; Thermo Fisher Scientific). The full mass spectrometry (MS) scan was collected in Orbitrap (resolution 30,000 at 400 m/z), and data-dependent MS/MS spectra on the nine most intense ions from each full MS scan were acquired. Proteins and peptides were identified by searching the data against Swissprot human

protein database, appended with decoy (reverse) sequences, using X!Tandem/Trans-Proteomic Pipeline (TPP) software suite. All proteins identified with a ProteinProphet probability of >0.9 (fdr < 1%) were accepted. Spectral matches to phosphorylated peptides were manually verified.

*In situ Tomosyn Phosphorylation*

Neuronal cultures plated on 14 mm microwell glass bottom dishes were rinsed 3X in warmed phosphate deficient DMEM with high glucose (#11971-025, Life Technologies). Cultures were then incubated in 50 µl of DMEM containing 500mCi/ml of $^{32}P$ orthophosphate for 4 hours in a 37°C, 95% $O_2$/5% $CO_2$ humidified incubator to achieve $^{32}P$ labeling of cytosolic ATP. Treatments included ± rosco (100 µM, 4.5 hr) with ± picrotoxin (50 µM, 4 hr). Picrotoxin was applied 30 min following treatment ± the Cdk5 inhibitor rosco. Cultures were then rinsed 3X with ice cold Tris-buffered saline (TBS) containing (in mM; Tris-HCl 50, NaCl 100, $Na_2HPO_4$ 20 with pH adjusted to 8.0) and lysed in IP lysis buffer. Tomosyn was immunoprecipitated, subjected to SDS-PAGE fractionation and blotted onto nitrocellulose. To detect and quantify $^{32}P$ incorporation the Tomosyn blots were imaged using a Molecular Imager FX (BioRad) and subsequently immunoblotted for Tomosyn.

*Electrophysiology*

Whole-cell patch clamp recordings were performed with a HEKA 10 amplifier and Patchmaster Software (HEKA Elektronik, Dr. Schulze GmbH) from 17 to 24 DIV cultured hippocampal pyramidal-like neurons. The extracellular bath solution for recording

miniature excitatory postsynaptic currents (mEPSCs) contained (in mM): NaCl 119, KCl 5, $CaCl_2$ 2, $MgCl_2$ 2, glucose 30, and HEPES, 10 that was adjusted to pH to 7.4 with NaOH. Tetrodotoxin (TTX, 1 μM) and the $GABA_A$ receptor antagonist bicuculine (10 μM) were added just prior to use. The extracellular solution for recording evoked excitatory postsynaptic currents (EPSCs) was similar, with the exceptions that $CaCl_2$ was reduced to 0.5 mM, $MgCl_2$ increased to 3.5 mM and TTX and bicuculine were omitted. The internal pipette solution contained (in mM): Cs-gluconate 105, $MgCl_2$ 5, EGTA 0.2, ATP 2, GTP 0.3, and HEPES 40 adjusted to pH to 7.2 with CsOH. Pipette resistance ranged from 2 to 5 MΩ. Neurons were voltage clamped to -70 mV. Evoked EPSCs were produced by positioning 25 mm diameter bipolar stimulating electrode close to the neuron (100 – 200 mm) and applying 0.4 msec current pulses of constant amplitude (WPI A360 Stimulus Isolater). Measurement of amplitude and frequency of mEPSC and amplitudes of evoked EPSC was performed offline using Patcher's Power tools (Dr. Francisco Mendez and Frank Würriehausen, Max-Planck-Institute, Göttingen, Germany) and Taro Tools (Taro Ishikawa, Jikei University School of Medicine, Tokyo, Japan) plugins for Igor Pro (Wavemetrics, Lake Oswego, OR).

*Immunocytochemistry, Proximity Ligation Assay and Image analysis*

Immunocytochemistry (ICC) was conducted following a published protocol[124]. Briefly, cells were washed 2X with ice-cold PBS and fixed with 4% PFA/Sucrose in PBS for 10 minutes. Fixation was quenched by replacing 4% PFA/Sucrose with 0.1M glycine in PBS (Sigma-Aldrich). Next, cells were permeabilized with 0.25% Triton-X100 (Fisher-Scientific) for 10 minutes followed by 1 hour blocking with 10% bovine serum albumin (BSA, Sigma-

Aldrich). The selected primary antibodies were added at the desired dilution in 3% BSA for one hour followed by washes (3% BSA in PBS, 5X, 5 minutes) and addition of secondary antibodies (diluted in PBS) for 45 minutes followed by five 5 min washes in PBS. The cells treated for ICC were maintained in the fluorescence antifade reagent Vectashield + DAPI (Vector Laboratories) until microscopic analysis. PLA reactions were carried out identical to ICC procedures through the addition of primary antibodies. In place of secondary antibodies, PLA+ and PLA- probes (Sigma-Aldrich) were added for 45 min at 37°C followed by three 5min washes (0.2% BSA, 0.1% Triton-X100 in PBS). Next, ligation and amplification solutions (Sigma-Aldrich) were sequentially added for 30 min and 100 min, respectively, with two washes after each.

Where indicated, colocalization analysis was carried using the JACoP plugin for FIJI [125]. The Pearson *R* correlation coefficient and Mander's overlap coefficient is generated for pairs of images using fluorescent intensities of spatially matched pixels. The pixels included in the analysis are determined by the Coste's automatic thresholding method [126]. For PLA density analysis, images were manually segmented using a bright-field channel to create an ROI that demarcates MIN6 cell boundaries. Next, the particle analysis plugin in FIJI was used to automatically count the number of fluorescent puncta contained within the ROI that were at least 3 x 3 pixels in size. For comparisons of pCdk5 immunofluorescence intensity, ROIs were created around puncta positive for Synapsin1-Alexa488 immunolabeling from images that were background subtracted with a 50-pixel rolling-ball radius, thresholded and converted into binary masks. ROIs were then applied to the alternate channel of the same image field containing pCdk5-Alexa594 to extract

individual fluorescence intensity per ROI. Straightened axon images were generated using the Straighten plugin for FIJI.

*Statistical analyses*

All statistical analysis was done using GraphPad Prism. Where indicated, one-way analysis of variance (ANOVA) tests were used for comparisons of population means with significance set to a $p < 0.05$. *Post hoc t*-tests with Dunnett's correction were used for multiple comparisons between specific groups.

## 3.6 Acknowledgements

This work was supported by NIH grant RO1 NIDDK-DK077050 to E. L. S. We thank Christian Althaus and Cynthia Carruthers for technical support and reagents.

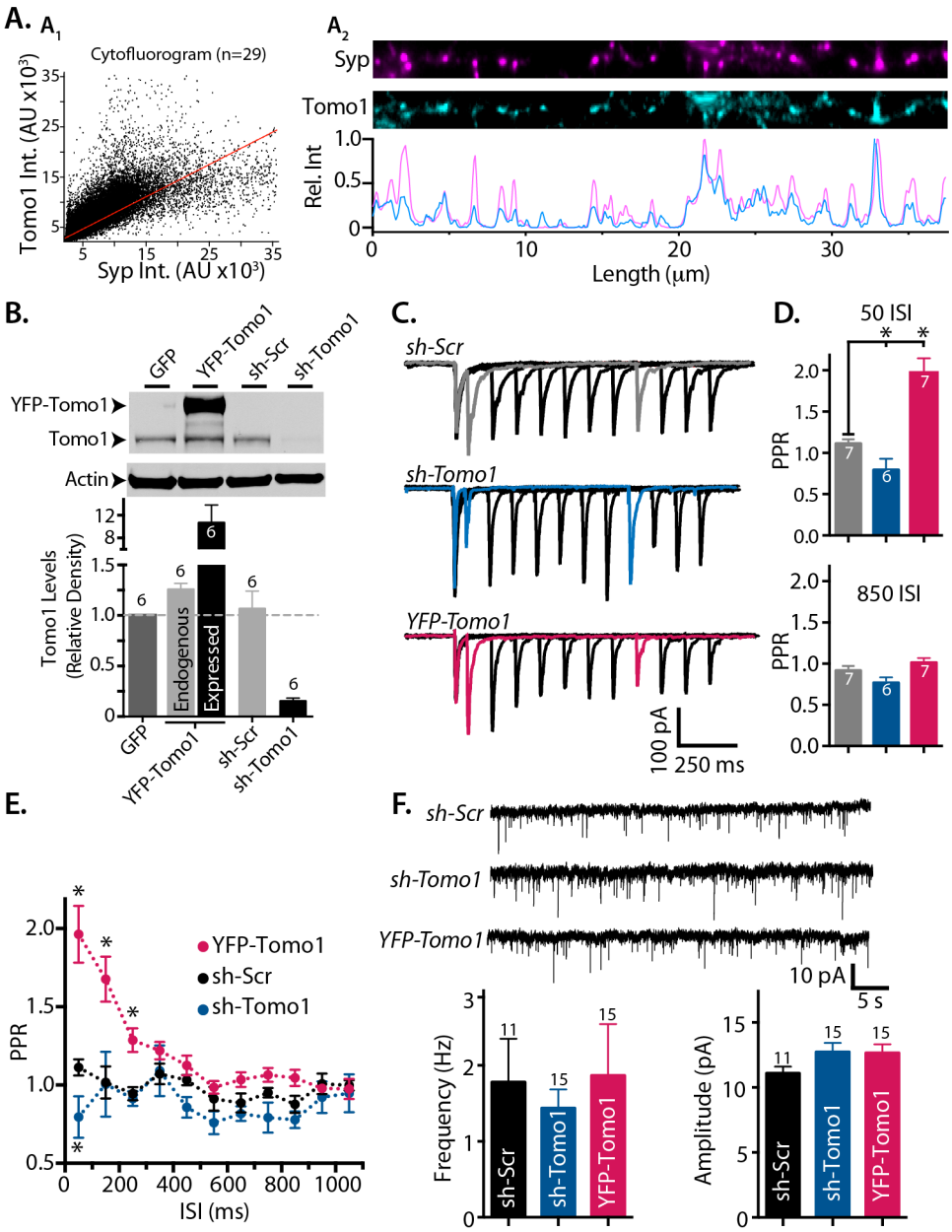
A.
A1
Cytofluorogram (n=29)
Tomo1 Int. (AU x10³)
Syp Int. (AU x10³)
A2
Syp
Tomo1
Rel. Int
Length (μm)
B.
GFP
YFP-Tomo1
sh-Scr
sh-Tomo1
YFP-Tomo1
Tomo1
Actin
Tomo1 Levels (Relative Density)
Endogenous
Expressed
C.
sh-Scr
sh-Tomo1
YFP-Tomo1
100 pA
250 ms
D.
50 ISI
850 ISI
PPR
E.
YFP-Tomo1
sh-Scr
sh-Tomo1
PPR
ISI (ms)
F.
sh-Scr
sh-Tomo1
YFP-Tomo1
10 pA
5 s
Frequency (Hz)
Amplitude (pA)

**Figure 3.1: Tomo1 localizes to presynaptic boutons and inhibits evoked neurotransmitter release in cultured hippocampal neurons.** (A) Cytofluorogram comparing spatially matched Tomo1 and Syp fluorescence (Pearson R= 0.73, Mander's M1= 0.8, M2= 0.85 n=29 ($A_1$) and representative immunofluorescence image of straightened axon segment demonstrates colocalization between endogenous Tomo1 (Tomo1, cyan) and presynaptic vesicular protein Synaptophysin (Syp, magenta) ($A_2$). Intensity line-scan analysis ($A_2$, lower) of axon segment shows coincident immunofluorescent spikes between Tomo1 and Synaptophysin.). (B) Western blot comparing Tomo1 immunoreactivity (anti-Tomo1) from lysates of lentivirus infected hippocampal neurons expressing GFP, YFP-Tomo1 (YFP-Tomo1), shRNA-Scramble (sh-Scr) or shRNA-Tomo1 (sh-Tomo1, upper). Lower, Tomo1 expression quantified using immunoreactive band density, normalized to loading control (actin) and graphed relative to control GFP-expressing cells (n=6). (C-E) Effects of Tomo1 expression and shRNA-mediated knock-down relative to sh-Scramble control on Paired-Pulse Ratio (PPR). (C) Representative EPSC responses with responses to the 50 ms and 850 ms inter-stimulus interval (ISI) highlighted in alternate color (corresponding averaged PPR plotted in (D)). (E) Averaged PPR for all ISI values. Tomo1 expression (n=11) led to significantly greater facilitation of PPR for the 50, 150, 250 ms ISI compared to shRNA-Scamble control (n=8), while shRNA-Tomo1 resulted in depression of PPR (n=5) at the 50ms ISI. (F) Representative mEPSC records (upper), and quantification (lower) show that the shRNA-mediated knock-down (n=15) or Tomo1 overexpression (n=15) does not significantly alter the frequency or amplitude of spontaneous mEPSC relative to control (n=11). For this and all subsequent figures, graphs show mean ± SEM, asterisks denote statistical significance compared to experimental control ($p < 0.05$).

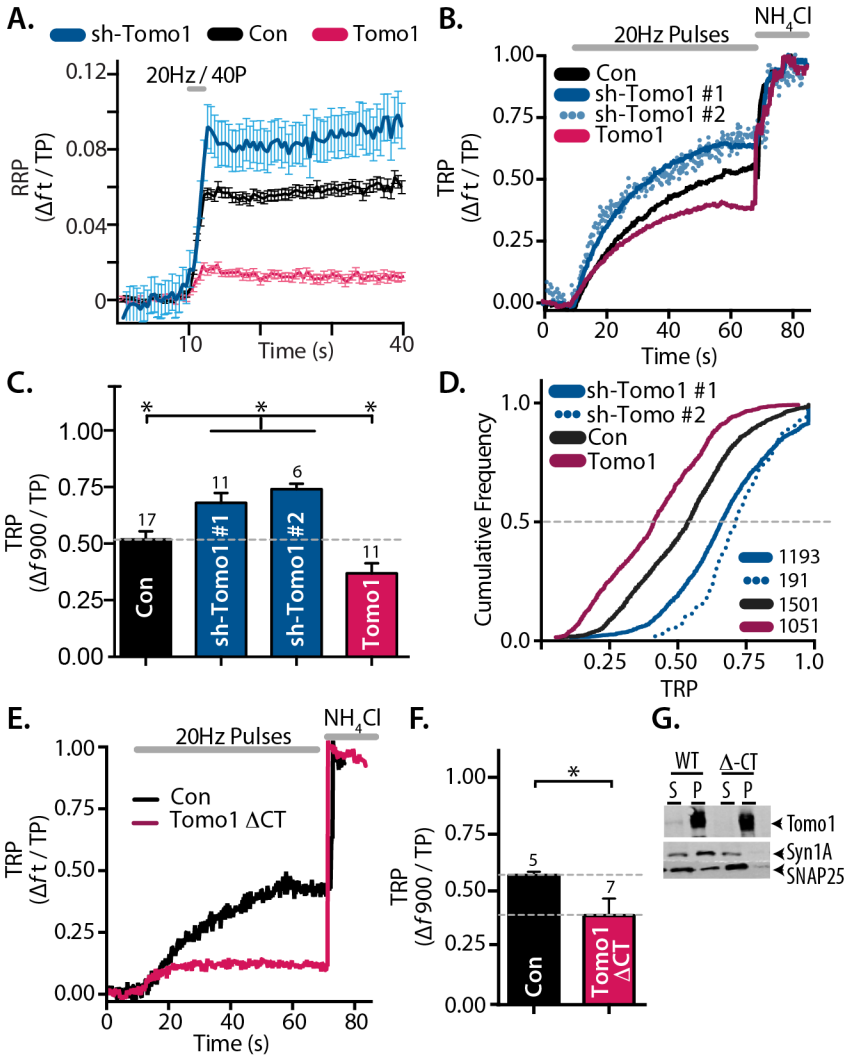
A.
sh-Tomo1
Con
Tomo1
20Hz / 40P
RRP (Δf t / TP)
Time (s)
B.
20Hz Pulses
NH4Cl
Con
sh-Tomo1 #1
sh-Tomo1 #2
Tomo1
TRP (Δf t / TP)
Time (s)
C.
TRP (Δf900 / TP)
17
11
6
11
Con
sh-Tomo1 #1
sh-Tomo1 #2
Tomo1
D.
sh-Tomo1 #1
sh-Tomo #2
Con
Tomo1
Cumulative Frequency
1193
191
1501
1051
TRP
E.
20Hz Pulses
NH4Cl
Con
Tomo1 ΔCT
TRP (Δf t / TP)
Time (s)
F.
TRP (Δf900 / TP)
5
7
Con
Tomo1 ΔCT
G.
WT
Δ-CT
S P S P
Tomo1
Syn1A
SNAP25

**Fig. 3.2: Effects of Tomo1 expression on distribution of SVs among functionally defined presynaptic SV pools.** (A) Comparison of Tomo1 overexpression (magenta, n=15) and sh-Tomo1 knockdown (sh-blue, n=9) to control (empty vector, black, n=10) on RRP size defined as mean vGpH responses following 40 electrical pulses delivered at 20Hz. Each vGpH measurement is normalized to vGpH maximum fluorescence to $NH_4CL$ application (total vesicle pool, TP). (B) Representative measurements of normalized vGpH response ($Df_t$ / TP) in single neurons to a 20Hz pool-depleting stimulus of 900 pulses. Total releasable pool (TRP) is defined as $Df_{900}$/TP. (C) Comparison of mean TRP among given treatments (n= cell number, number of boutons given in D). (D) Cumulative frequency distributions comparing shift in TRP for bouton ensembles of each condition (n = boutons; dashed gray line indicates distribution median). (E) Comparison of representative $Df_t$/TP (20Hz/900 stimuli) in neuron overexpressing Tomo1 lacking the SNARE domain (Tomo1 DCT ) with control neuron (empty vector). (F) Averaged TRP for control (black) and Tomo1 DCT conditions. Note, that expression of Tomo1-wt (lower dashed gray line, data from C) and Tomo1 DCT result in comparable decrease in TRP. (G) IP of overexpressed Tomo1 WT or Tomo1 D-CT in PC-12 cells shows co-precipitation of Syntaxin1A and SNAP25 SNARE proteins only with Tomo1 WT. These data indicate necessity of Tomosyn's SNARE domain for Q-SNARE complex formation. For this figure and all subsequent Western blot images, lanes: supernatant (S), last wash (W), IP pellet (P).

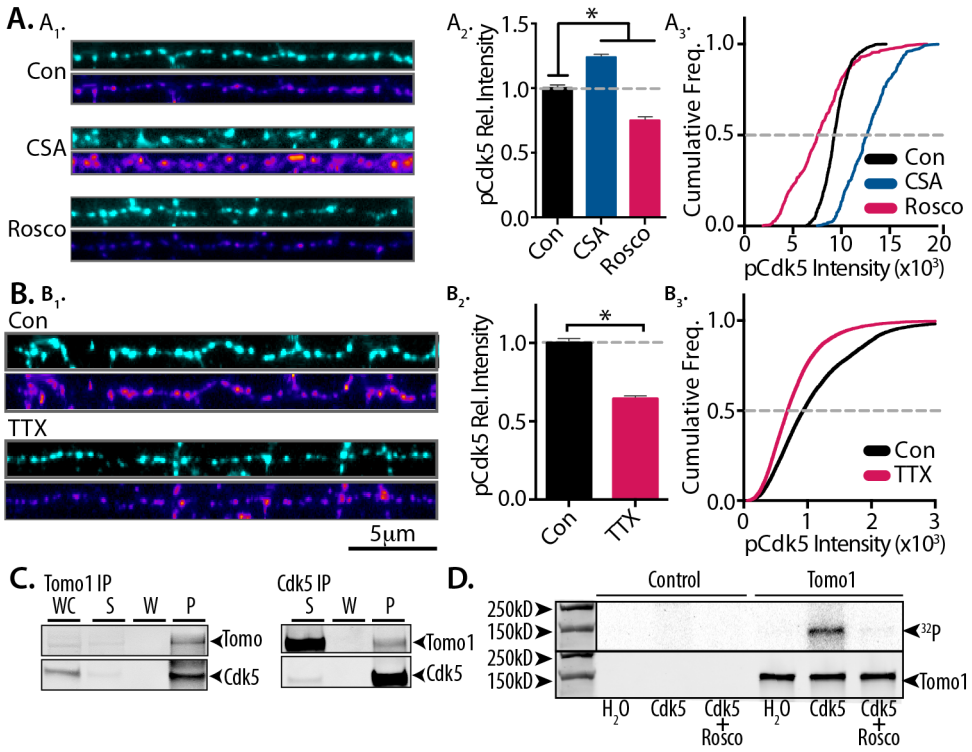
A. A1.
Con
CSA
Rosco
A2.
pCdk5 Rel. Intensity
1.5
1.0
0.5
0.0
*
Con
CSA
Rosco
A3.
Cumulative Freq.
1.0
0.5
0.0
0
5
10
15
20
pCdk5 Intensity (x10³)
Con
CSA
Rosco
B. B1.
Con
TTX
5μm
B2.
pCdk5 Rel. Intensity
1.0
0.5
0.0
*
Con
TTX
B3.
Cumulative Freq.
1.0
0.5
0.0
0
1
2
3
pCdk5 Intensity (x10³)
Con
TTX
C. Tomo1 IP
WC
S
W
P
Tomo
Cdk5
Cdk5 IP
S
W
P
Tomo1
Cdk5
D.
Control
Tomo1
250kD
150kD
250kD
150kD
32P
Tomo1
H2O
Cdk5
Cdk5 + Rosco
H2O
Cdk5
Cdk5 + Rosco

**Figure 3.3: Tomo1 serves as Cdk5 interacting partner and catalytic substrate with Cdk5 activation sensitive to neural activity.** (A) Representative immunofluorescent images of straightened axon segments from neuronal cultures (A1) treated with CSA (50 mM), rosco (100 mM) or vehicle-control (DMSO, 0.5%) for 30 minutes and subsequently subjected to immunocytochemical analysis of endogenous Synapsin1 (cyan, upper, for bouton localization) and phosphorylated Cdk5 (pCdk5, lower, heat scale). (A2) Quantification of mean pCdk5 immunofluorescence intensity relative to vehicle-control, and (A3) cumulative frequency of pCdk5 intensity across boutons show that inhibition of Cdk5 by rosco significantly reduces pCdk5 immunoreactivity, while treatment with CSA enhances pCdk5 relative to control. (B1-B3) pCdk5 immunofluorescence images comparing chronic silencing of neural activity by TTX (24 hrs, 1mM) and control. (B2) Averaged pCdk5 intensity and (B3) cumulative frequency of pCdk5 intensity demonstrate that chronic dampening of neural activity significantly reduces Cdk5 activation. In (A) and (B) immunocytochemical analysis was performed on 45 images per neuron preparation for each condition, and was repeated in 3 neuronal preparations. (C) Immunoblots showing co-precipitation of Tomo1 and Cdk5 from cultured hippocampal neuron lysates regardless of primary target of IP (Tomo1 or Cdk5) reaction. In-vitro phosphorylation of affinity purified Tomo1 by Cdk5/p25 as measured by $^{32}$P-labeling. Upper, $^{32}$P-radioactive signal on blot corresponding to conditions indicated. Lower, anti-Tomo1 immunoreactivity for identical portion of blot. Conditions include: absence of Cdk5/p25 kinase ($H_2O$), Cdk5/p25 kinase (Cdk5) and Cdk5/p25 + rosco (Cdk5 + rosco; 1 mM).

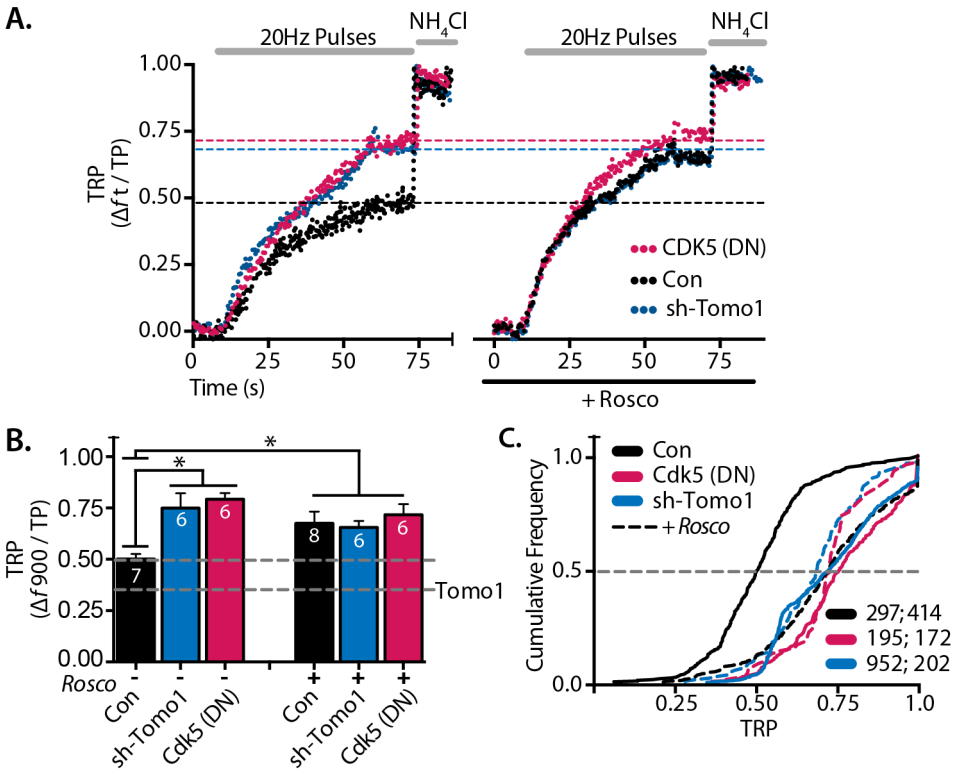
A.
20Hz Pulses
NH4Cl
20Hz Pulses
NH4Cl
TRP (Δf t / TP)
1.00
0.75
0.50
0.25
0.00
0
25
50
75
Time (s)
+ Rosco
CDK5 (DN)
Con
sh-Tomo1
B.
TRP (Δf 900 / TP)
Tomo1
Rosco
Con
sh-Tomo1
Cdk5 (DN)
C.
Cumulative Frequency
Con
Cdk5 (DN)
sh-Tomo1
+ Rosco
297; 414
195; 172
952; 202
TRP

**Figure 3.4: Tomosyn and Cdk5 share common signaling pathway regulating the TRP.** (A) Comparison of representative vGpH responses ($Df_t$/TP) averaged from boutons of single control (black), sh-Tomo1 expressing (blue) or dominant-negative Cdk5 expressing (Cdk5 (DN), magenta) neurons during stimulation (20 Hz, 900 stimuli) in the presence (left) and absence (right) of rosco (100 mM, 30 min pretreatment). (B) Comparison of mean TRP among expression conditions ± rosco. Lower dashed line illustrates mean TRP to Tomo1 overexpression (Fig 2C). (C) Cumulative frequency distributions comparing TRP for bouton ensembles of each condition. Dashed distributions represent treatments (color matched) with rosco. Notably, sh-Tomo1 and Cdk5 DN expression resulted in significant enhancement in the TRP compared to control, which was not further increased with rosco treatment. B, n= # cells; C, n= # boutons.

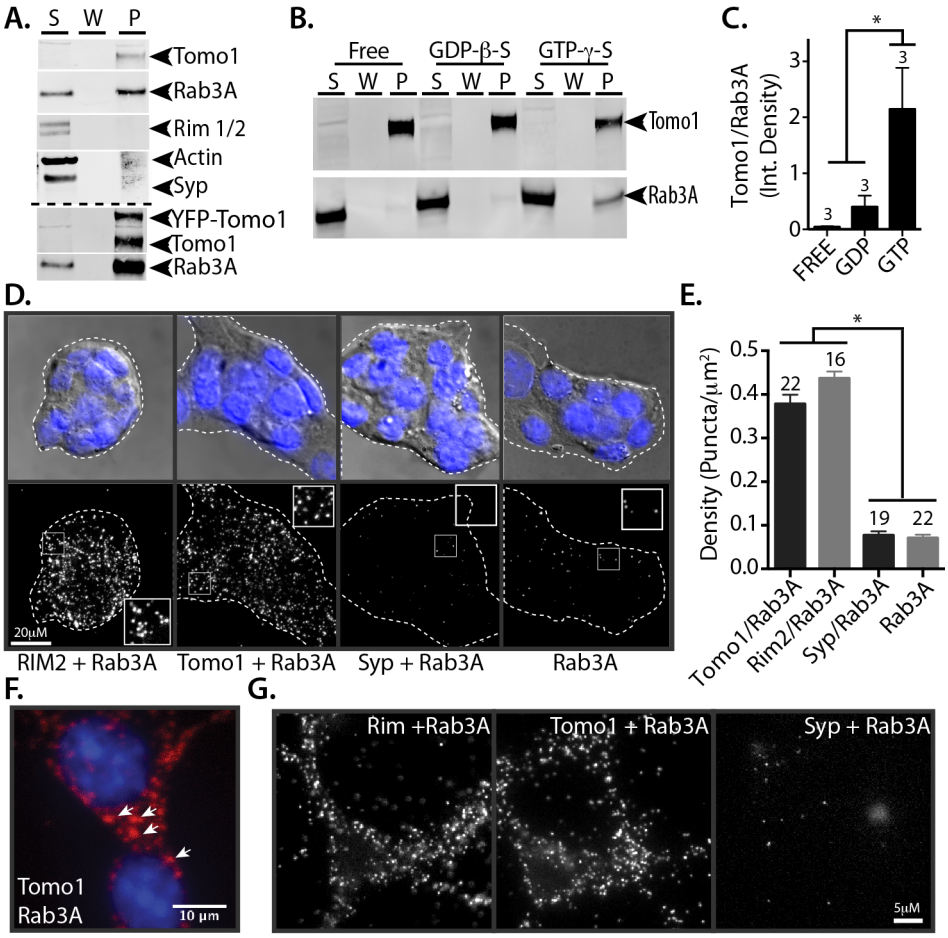
A.
S W P
Tomo1
Rab3A
Rim 1/2
Actin
Syp
YFP-Tomo1
Tomo1
Rab3A
B.
Free
GDP-β-S
GTP-γ-S
S W P S W P S W P
Tomo1
Rab3A
C.
Tomo1/Rab3A (Int. Density)
FREE
GDP
GTP
D.
20μM
RIM2 + Rab3A
Tomo1 + Rab3A
Syp + Rab3A
Rab3A
E.
Density (Puncta/μm²)
Tomo1/Rab3A
Rim2/Rab3A
Syp/Rab3A
Rab3A
F.
Tomo1
Rab3A
10 μm
G.
Rim +Rab3A
Tomo1 + Rab3A
Syp + Rab3A
5μM

**Figure 3.5: Tomo1 interacts with Rab3A-GTP.** (A) Western blot showing that IP of Tomo1 from non-transfected as well as YFP-Tomo1 transfected cultured hippocampal neuronal lysates results in co-precipitation of Rab3A, but not Rim1/2, actin or synaptophysin (Syp). (B) Western blot comparing Tomo1 co-precipitation of Rab3A for neuronal lysates initially treated to drive GTPases into a GTP-loaded (GTP Ɣ-S), GDP-loaded (GDP β-S), or nucleotide-free state (n= 3 experiment from separate neuronal preparations). (C) Averaged Rab3A co-precipitation normalized to the level of Tomo1 IP for indicated nucleotide-loaded conditions. (D) Representative images of cultured MIN6 cells subjected to PLA to assess in-cell interaction of Tomo1 and Rab3A compared to putative interacting protein partners. Interactions tested by PLA as indicated. Upper row, DAPI staining overlaid on DIC brightfield to define cell cluster and plasma membrane periphery. Lower row, PLA fluorescent puncta for each interaction set. Insets, enlarged spatial region of cytosol. (E) Comparisons of mean PLA signal density for indicated protein interaction sets (n= number of cell clusters). (F) PLA signal for Tomo1 + Rab3A interaction in Min6 cell shown at high magnification demonstrate clusters of fluorescent puncta likely localized to dense core secretory granules. (G) Images of PLA fluorescent puncta resulting from assay of indicated protein interactions on hippocampal neurons.

# Figure 6

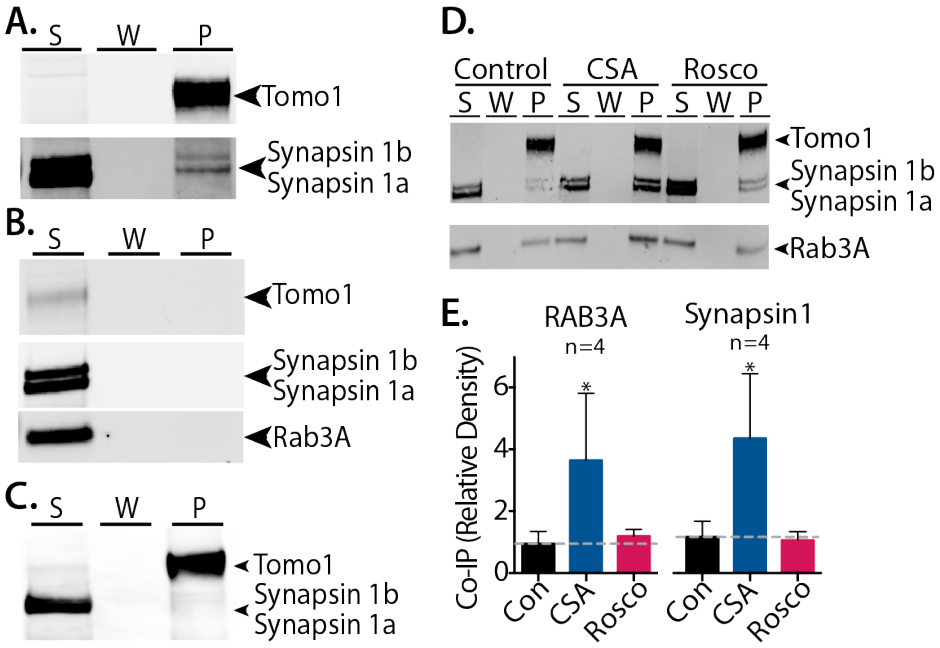
A.
S
W
P
Tomo1
Synapsin 1b
Synapsin 1a
B.
S
W
P
Tomo1
Synapsin 1b
Synapsin 1a
Rab3A
C.
S
W
P
Tomo1
Synapsin 1b
Synapsin 1a
D.
Control
CSA
Rosco
S W P S W P S W P
Tomo1
Synapsin 1b
Synapsin 1a
Rab3A
E.
RAB3A
n=4
Synapsin1
n=4
Co-IP (Relative Density)
0
2
4
6
Con
CSA
Rosco
Con
CSA
Rosco

**Figure 3.6: Tomo1 interaction with Rab3A and Synapsin1 is regulated by Cdk5.** (A) Western blot showing that IP of Tomo1 from hippocampal neuronal lysates results in co-precipitation of Synapsin1 (a and b isoforms). (B) IP with isotype-control Rabbit IGG does not pull-down Tomo1, Rab3A or Synapsin1 verifying the specificity co-precipitation with anti-Tomo1 antibody. (C) Neuronal lysate pre-cleared by anti-Rab3A IP and subsequently with anti-Tomo1 IP eliminates co-precipitation of Synapsin1, indicating Tomo1 interaction with Synapsin1 is via Rab3A. (D) Western blot comparing the effect of CSA (50 μM) and rosco (100 μM) pretreatment (30 m) to vehicle control on Tomo1 co-precipitation of Rab3A and Synapsin1 from neuronal lysates. (E) Averaged Rab3A and Synapsin1 co-precipitation normalized to Tomo1 IP for each condition.

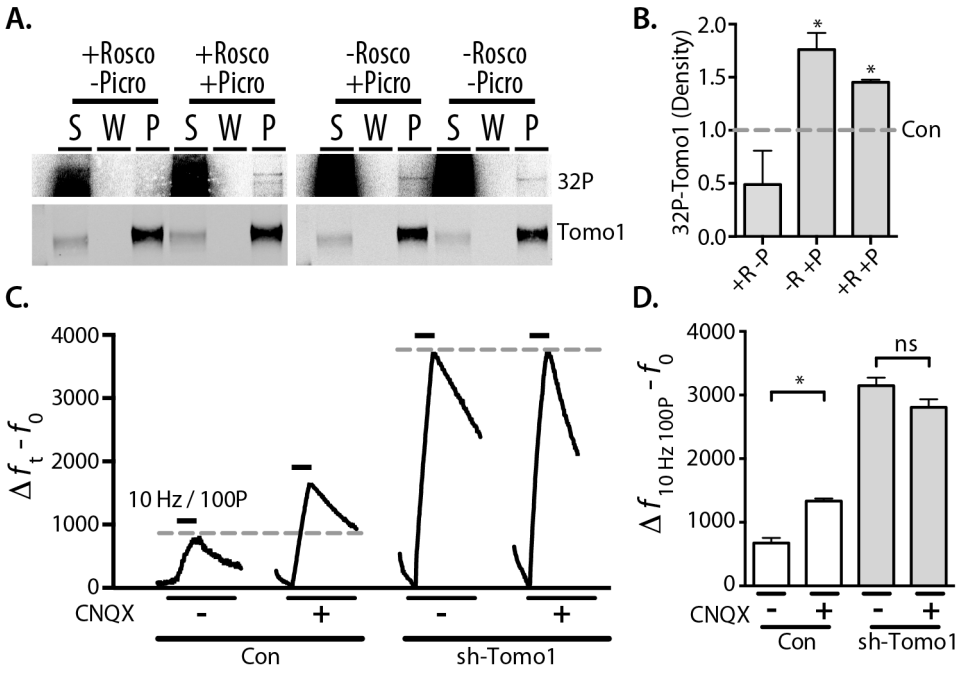
A.
+Rosco
-Picro
+Rosco
+Picro
-Rosco
+Picro
-Rosco
-Picro
S W P S W P S W P S W P
32P
Tomo1
B.
32P-Tomo1 (Density)
2.0
1.5
1.0
0.5
0.0
Con
*
*
+R-P
-R+P
+R+P
C.
$\Delta f_t - f_0$
4000
3000
2000
1000
0
10 Hz / 100P
CNQX
-
+
-
+
Con
sh-Tomo1
D.
$\Delta f_{10\,Hz\,100P} - f_0$
4000
3000
2000
1000
0
*
ns
CNQX
-
+
-
+
Con
sh-Tomo1

**Figure 3.7: Activity dependent phosphorylation of Tomo1 and its role in synaptic scaling.** (A) *In situ* phosphorylation assay of Tomo1 in hippocampal neurons as measured by endogenous $^{32}$P-labeling (upper) of Tomo1 by IP shown in western blot for ± rosco (100 μM, 4.5 hrs) and ± picrotoxin (PTX, 50 μM) with 4mM $Ca^{2+}$ (4 hours). (B) Graph showing relative levels of Tomo1 *in situ* phosphorylation quantified as the $^{32}$P-band density from region corresponding to Tomo1 for each condition on immunoblot and shown relative to vehicle-treated control (0.5% DMSO, n = 3 experiments from separate neuronal preparations). (C) Sh-Tomo1 and control (empty vector) vGpH responses ($Df_t$/TP) averaged from boutons in response to a 10 Hz / 100 pulses stimulus used for comparing changes in presynaptic release in response to chronic silencing of neuronal activity (CNQX, 40 mM, 24 hours) to vehicle-treated controls (equal volume $H_2O$). (D) Plot shown mean Df – $f_0$ for all boutons of specified condition (n numbers: con = 121, con + CNQX = 134, sh-Tomo1 = 750, sh-Tomo1 + CNQX = 409).

## 3.8 Bibliography


1. Zucker RS, Regehr WG. Short-term synaptic plasticity. Annu Rev Physiol 2002;64:355–405.

2. Pang ZP, Südhof TC. Cell biology of Ca2+-triggered exocytosis. Curr Opin Cell Biol 2010;22:496–505.

3. Chapman ER. How does synaptotagmin trigger neurotransmitter release? Annu Rev Biochem 2008;77:615–641.

4. Alabi AA, Alabi AA, Tsien RW, Tsien RW. Synaptic vesicle pools and dynamics. Cold Spring Harbor Perspectives in Biology 2012;4:a013680.

5. Rizzoli SO, Betz WJ. Synaptic vesicle pools. Nat Rev Neurosci 2005;6:57–69.

6. Jack Waters SJS. Vesicle pool partitioning influences presynaptic diversity and weighting in rat hippocampal synapses. J Physiol (Lond) 2002;541:811–823.

7. Ratnayaka A, Marra V, Bush D, Burden JJ, Branco T, Staras K. Recruitment of resting vesicles into recycling pools supports NMDA receptor-dependent synaptic potentiation in cultured hippocampal neurons. J Physiol (Lond) 2012;590:1585–1597.

8. Rose T, Schoenenberger P, Jezek K, Oertner TG. Developmental refinement of vesicle cycling at schaffer collateral synapses. Neuron 2013;77:1109–1121.

9. Kim SH, Ryan TA. CDK5 serves as a major control point in neurotransmitter release. Neuron 2010;67:797–809.

10. Virmani T, Atasoy D, Kavalali ET. Synaptic vesicle recycling adapts to chronic changes in activity. J Neurosci 2006;26:2197–2206.

11. Denker A, Kröhnert K, Bückers J, Neher E, Rizzoli SO. The reserve pool of synaptic vesicles acts as a buffer for proteins involved in synaptic vesicle recycling. Proceedings of the National Academy of Sciences 2011;108:17183–17188.

12. Fernández-Alfonso T, Ryan TA. A heterogeneous “resting” pool of synaptic vesicles that is dynamically interchanged across boutons in mammalian CNS synapses. Brain Cell Bio 2008;36:87–100.

13. Staras K, Branco T, Burden JJ, Pozo K, Darcy K, Marra V, Ratnayaka A, Goda Y. A Vesicle Superpool Spans Multiple Presynaptic Terminals in Hippocampal Neurons. Neuron 2010;66:37–44.

14. Mozhayeva MG, Sara Y, Liu X, Kavalali ET. Development of vesicle pools during maturation of hippocampal synapses. J Neurosci 2002;22:654–665.

15. Sara Y, Virmani T, Deák F, Liu X, Kavalali ET. An Isolated Pool of Vesicles Recycles at Rest and Drives Spontaneous Neurotransmission. Neuron 2005;45:563–573.

16. Fredj NB, Burrone J. A resting pool of vesicles is responsible for spontaneous vesicle fusion at the synapse. Nature Publishing Group 2009;12:751–758.

17. Groemer TW, Klingauf J. Synaptic vesicles recycling spontaneously and during activity belong to the same vesicle pool. Nat Neurosci 2007;10:145–147.

18. Hua Y, Sinha R, Martineau M, Kahms M, Klingauf J. A common origin of synaptic vesicles undergoing evoked and spontaneous fusion. Nat Neurosci 2010;13:1451–1453.

19. Wilhelm BG, Groemer TW, Rizzoli SO. The same synaptic vesicles drive active and spontaneous release. Nat Neurosci 2010;13:1454–1456.

20. Verstegen AMJ, Tagliatti E, Lignani G, Marte A, Stolero T, Atias M, Corradi A, Valtorta F, Gitler D, Onofri F, Fassio A, Benfenati F. Phosphorylation of Synapsin I by Cyclin-Dependent Kinase-5 Sets the Ratio between the Resting and Recycling Pools of Synaptic Vesicles at Hippocampal Synapses. J Neurosci 2014;34:7266–7280.

21. Marra V, Burden JJ, Thorpe JR, Smith IT, Smith SL, Häusser M, Branco T, Staras K. A Preferentially Segregated Recycling Vesicle Pool of Limited Size Supports Neurotransmission in Native Central Synapses. Neuron 2012;76:579–589.

22. Orenbuch A, Shalev L, Marra V, Sinai I, Lavy Y, Kahn J, Burden JJ, Staras K, Gitler D. Synapsin selectively controls the mobility of resting pool vesicles at hippocampal terminals. J Neurosci [Internet] 2012;32:3969–3980. Available from: http://www.jneurosci.org/content/32/12/3969.full

23. Fujita Y, Shirataki H, Sakisaka T, Asakura T, Ohya T, Kotani H, Yokoyama S, Nishioka H, Matsuura Y, Mizoguchi A, Scheller RH, Takai Y. Tomosyn: a syntaxin-1-binding protein that forms a novel complex in the neurotransmitter release process. Neuron 1998;20:905–915.

24. Hatsuzawa K, Lang T, Fasshauer D, Bruns D, Jahn R. The R-SNARE motif of tomosyn forms SNARE core complexes with syntaxin 1 and SNAP-25 and down-regulates exocytosis. J Biol Chem 2003;278:31159–31166.

25. Pobbati AV, Razeto A, Böddener M, Becker S, Fasshauer D. Structural basis for the inhibitory role of tomosyn in exocytosis. J Biol Chem [Internet] 2004;279:47192–47200. Available from: http://www.jbc.org/content/279/45/47192.full

26. D'Andrea-Merrins M, Chang L, Lam AD, Ernst SA, Stuenkel EL. Munc18c interaction with syntaxin 4 monomers and SNARE complex intermediates in GLUT4 vesicle trafficking. J Biol Chem 2007;282:16553–16566.

27. Yizhar O, Matti U, Melamed R, Hagalili Y, Bruns D, Rettig J, Ashery U. Tomosyn inhibits priming of large dense-core vesicles in a calcium-dependent manner. Proc Natl Acad Sci U S A 2004;101:2578–2583.

28. Baba T, Sakisaka T, Mochida S, Takai Y. PKA-catalyzed phosphorylation of tomosyn and its implication in Ca2+-dependent exocytosis of neurotransmitter. J Cell Biol 2005;170:1113–1125.

29. Barak B, Okun E, Ben-Simon Y, Lavi A, Shapira R, Madar R, Wang Y, Norman E, Sheinin A, Pita MA, Yizhar O, Mughal MR, Stuenkel E, van Praag H, Mattson MP, Ashery U. Neuron-specific expression of tomosyn1 in the mouse hippocampal dentate gyrus impairs spatial learning and memory. Neuromolecular medicine 2013;15:351–363.

30. Chen K, Richlitzki A, Featherstone DE, Schwärzel M, Richmond JE. Tomosyn-dependent regulation of synaptic transmission is required for a late phase of associative odor memory. Proceedings of the National Academy of Sciences 2011;108:18482–18487.

31. Gracheva EO, Burdina AO, Touroutine D, Berthelot-Grosjean M, Parekh H, Richmond JE. Tomosyn negatively regulates CAPS-dependent peptide release at Caenorhabditis elegans synapses. J Neurosci 2007;27:10176–10184.

32. McEwen JM, Madison JM, Dybbs M, Kaplan JM. Antagonistic regulation of synaptic vesicle priming by Tomosyn and UNC-13. Neuron 2006;51:303–315.

33. Lehman K, Rossi G, Adamo JE, Brennwald P. Yeast homologues of tomosyn and lethal giant larvae function in exocytosis and are associated with the plasma membrane SNARE, Sec9. J Cell Biol 1999;146:125–140.

34. Rossi G, Brennwald P. Yeast homologues of lethal giant larvae and type V myosin cooperate in the regulation of Rab-dependent vesicle clustering and polarized exocytosis. Mol Biol Cell 2011;22:842–857.

35. Rossi G, Watson K, Demonch M, Temple B, Brennwald P. In vitro reconstitution of Rab GTPase-dependent vesicle clustering by the yeast lethal giant larvae/tomosyn homolog, Sro7. Journal of Biological Chemistry 2015;290:612–624.

36. Barak B, Williams A, Bielopolski N, Gottfried I, Okun E, Brown MA, Matti U, Rettig J, Stuenkel EL, Ashery U. Tomosyn Expression Pattern in the Mouse Hippocampus Suggests Both Presynaptic and Postsynaptic Functions. Front Neuroanat 2010;4.

37. Dobrunz LE, Stevens CF. Heterogeneity of release probability, facilitation, and depletion at central synapses. Neuron 1997;18:995–1008.

38. Williams AL, Bielopolski N, Meroz D, Lam AD, Passmore DR, Ben-Tal N, Ernst SA, Ashery U, Stuenkel EL. Structural and functional analysis of tomosyn identifies

domains important in exocytotic regulation. Journal of Biological Chemistry 2011;

39. Burrone J, Li Z, Murthy VN. Studying vesicle cycling in presynaptic terminals using the genetically encoded probe synaptopHluorin. Nat Protoc 2006;1:2970–2978.

40. Rosenmund C, Stevens CF. Definition of the readily releasable pool of vesicles at hippocampal synapses. Neuron 1996;16:1197–1207.

41. Schikorski T, Stevens CF. Morphological correlates of functionally defined synaptic vesicle populations. Nat Neurosci 2001;4:391–395.

42. Stevens CF, Williams JH. Discharge of the readily releasable pool with action potentials at hippocampal synapses. 2007;98:3221–3229. Available from: http://jn.physiology.org/cgi/doi/10.1152/jn.00857.2007

43. Schikorski T, Stevens CF. Quantitative ultrastructural analysis of hippocampal excitatory synapses. J Neurosci 1997;17:5858–5867.

44. Voglmaier SM, Kam K, Yang H, Fortin DL, Hua Z, Nicoll RA, Edwards RH. Distinct endocytic pathways control the rate and extent of synaptic vesicle protein recycling. Neuron 2006;51:71–84.

45. Sankaranarayanan S, De Angelis D, Rothman JE, Ryan TA. The Use of pHluorins for Optical Measurements of Presynaptic Activity. Biophys J 2000;79:2199–2208.

46. Bielopolski N, Lam AD, Bar-On D, Sauer M, Stuenkel EL, Ashery U. Differential interaction of tomosyn with syntaxin and SNAP25 depends on domains in the WD40 β-propeller core and determines its inhibitory activity. Journal of Biological Chemistry 2014;289:17087–17099.

47. Tang D, Yeung J, Lee KY, Matsushita M, Matsui H, Tomizawa K, Hatase O, Wang JH. An isoform of the neuronal cyclin-dependent kinase 5 (Cdk5) activator. J Biol Chem 1995;270:26897–26903.

48. Tsai L-H, Delalle I, Caviness VS, Chae T, Harlow E. p35 is a neural-specific regulatory subunit of cyclin-dependent kinase 5. , Published online: 29 September 1994; | doi:101038/371419a0 1994;371:419–423.

49. Xiong W, Pestell R, Rosner MR. Role of cyclins in neuronal differentiation of immortalized hippocampal cells. Mol Cell Biol 1997;17:6585–6597.

50. Su SC, Tsai L-H. Cyclin-dependent kinases in brain development and disease. Annu Rev Cell Dev Biol 2011;27:465–491.

51. Cheung ZH, Ip NY. Cdk5: a multifaceted kinase in neurodegenerative diseases. Trends Cell Biol 2012;22:169–175.

52. Lopes JP, Agostinho P. Cdk5: multitasking between physiological and pathological

conditions. Prog Neurobiol 2011;94:49–63.

53. Dhavan R, Tsai L-H. A Decade of CDK5. Nature 2001;2:749–759.

54. Czapski GA, Gąssowska M, Songin M, Radecka UD, Strosznajder JB. Alterations of cyclin dependent kinase 5 expression and phosphorylation in amyloid precursor protein (APP)-transfected PC12 cells. FEBS Lett 2011;585:1243–1248.

55. Sharma P, Sharma M, Amin ND, Albers RW, Pant HC. Regulation of cyclin-dependent kinase 5 catalytic activity by phosphorylation. Proc Natl Acad Sci U S A 1999;96:11156–11160.

56. Xue Y, Ren J, Gao X, Jin C, Wen L, Yao X. GPS 2.0, a tool to predict kinase-specific phosphorylation sites in hierarchy. - PubMed - NCBI. Molecular & Cellular Proteomics 2008;7:1598–1608.

57. Takamori S, Holt M, Stenius K, Lemke EA, Grønborg M, Riedel D, Urlaub H, Schenck S, Brügger B, Ringler P, Müller SA, Rammner B, Gräter F, Hub JS, De Groot BL, Mieskes G, Moriyama Y, Klingauf J, Grubmüller H, Heuser J, Wieland F, Jahn R. Molecular anatomy of a trafficking organelle. Cell 2006;127:831–846.

58. Gladycheva SE, Lam AD, Liu J, D'Andrea-Merrins M, Yizhar O, Lentz SI, Ashery U, Ernst SA, Stuenkel EL. Receptor-mediated regulation of tomosyn-syntaxin 1A interactions in bovine adrenal chromaffin cells. J Biol Chem 2007;282:22887–22899.

59. Schlüter OM, Schmitz F, Jahn R, Rosenmund C, Südhof TC. A complete genetic analysis of neuronal Rab3 function. J Neurosci 2004;24:6629–6637.

60. Südhof TC. Function of Rab3 GDP-GTP exchange. Neuron 1997;18:519–522.

61. Wang Y, Okamoto M, Schmitz F, Hofmann K, Südhof TC. Rim is a putative Rab3 effector in regulating synaptic-vesicle fusion. Nature 1997;388:593–598.

62. Dulubova I, Lou X, Lu J, Huryeva I, Alam A, Schneggenburger R, Südhof TC, Rizo J. A Munc13/RIM/Rab3 tripartite complex: from priming to plasticity? EMBO J 2005;24:2839–2850.

63. Holz RW, Brondyk WH, Senter RA, Kuizon L, Macara IG. Evidence for the involvement of Rab3A in Ca(2+)-dependent exocytosis from adrenal chromaffin cells. J Biol Chem 1994;269:10229–10234.

64. L Johannes PMLMRJDVJPHFD. The GTPase Rab3a negatively controls calcium-dependent exocytosis in neuroendocrine cells. EMBO J 1994;13:2029.

65. Star EN, Newton AJ, Murthy VN. Real-time imaging of Rab3a and Rab5a reveals differential roles in presynaptic function. J Physiol (Lond) 2005;569:103–117.

66. Shupliakov O, Haucke V, Pechstein A. How synapsin I may cluster synaptic vesicles. Seminars in Cell & Developmental Biology 2011;22:393–399.

67. Jovanovic JN, Benfenati F, Siow YL, Sihra TS, Sanghera JS, Pelech SL, Greengard P, Czernik AJ. Neurotrophins stimulate phosphorylation of synapsin I by MAP kinase and regulate synapsin I-actin interactions. Proc Natl Acad Sci U S A 1996;93:3679–3683.

68. Jovanovic JN, Sihra TS, Nairn AC, Hemmings HC, Greengard P, Czernik AJ. Opposing changes in phosphorylation of specific sites in synapsin I during Ca2+-dependent glutamate release in isolated nerve terminals. J Neurosci 2001;21:7944–7953.

69. Matsubara M, Kusubata M, Ishiguro K, Uchida T, Titani K, Taniguchi H. Site-specific phosphorylation of synapsin I by mitogen-activated protein kinase and Cdk5 and its effects on physiological functions. J Biol Chem 1996;271:21108–21113.

70. Onofri F, Giovedi S, Kao HT, Valtorta F, Bongiorno Borbone L, De Camilli P, Greengard P, Benfenati F. Specificity of the binding of synapsin I to Src homology 3 domains. J Biol Chem 2000;275:29857–29867.

71. Giovedi S, Vaccaro P, Valtorta F, Darchen F, Greengard P, Cesareni G, Benfenati F. Synapsin is a novel Rab3 effector protein on small synaptic vesicles. I. Identification and characterization of the synapsin I-Rab3 interactions in vitro and in intact nerve terminals. J Biol Chem 2004;279:43760–43768.

72. Henry FE, McCartney AJ, Neely R, Perez AS, Carruthers CJL, Stuenkel EL, Inoki K, Sutton MA. Retrograde Changes in Presynaptic Function Driven by Dendritic mTORC1. jneurosciorg [Internet] 2012;32:17128–17142. Available from: http://www.jneurosci.org/cgi/doi/10.1523/JNEUROSCI.2149-12.2012

73. Jakawich SK, Nasser HB, Strong MJ, McCartney AJ, Perez AS, Rakesh N, Carruthers CJL, Sutton MA. Local presynaptic activity gates homeostatic changes in presynaptic function driven by dendritic BDNF synthesis. Neuron 2010;68:1143–1158.

74. Denker A, Rizzoli SO. Synaptic vesicle pools: an update. Front Syn Neurosci 2010;2:135.

75. Murthy VN, Schikorski T, Stevens CF, Zhu Y. Inactivity produces increases in neurotransmitter release and synapse size. Neuron 2001;32:673–682.

76. Harata N, Ryan TA, Smith SJ, Buchanan J, Tsien RW. Visualizing recycling synaptic vesicles in hippocampal neurons by FM 1-43 photoconversion. Proc Natl Acad Sci U S A 2001;98:12748–12753.

77. Li Z, Burrone J, Tyler WJ, Hartman KN, Albeanu DF, Murthy VN. Synaptic vesicle recycling studied in transgenic mice expressing synaptopHluorin. Proc Natl Acad Sci U S A 2005;102:6131–6136.

78. Micheva KD, Smith SJ. Strong effects of subphysiological temperature on the function and plasticity of mammalian presynaptic terminals. J Neurosci 2005;25:7481–7488.

79. Welzel O, Henkel AW, Stroebel AM, Jung J, Tischbirek CH, Ebert K, Kornhuber J, Rizzoli SO, Groemer TW. Systematic Heterogeneity of Fractional Vesicle Pool Sizes and Release Rates of Hippocampal Synapses. Biophys J 2011;100:593–601.

80. Shepherd GM, Harris KM. Three-dimensional structure and composition of CA3-->CA1 axons in rat hippocampal slices: implications for presynaptic connectivity and compartmentalization. Journal of Neuroscience 1998;18:8300–8310.

81. Harata N, Pyle JL, Aravanis AM, Mozhayeva M, Kavalali ET, Tsien RW. Limited numbers of recycling vesicles in small CNS nerve terminals: implications for neural signaling and vesicular cycling. Trends in Neurosciences 2001;24:637–643.

82. Branco T, Marra V, Staras K. Examining size-strength relationships at hippocampal synapses using an ultrastructural measurement of synaptic release probability. J Struct Biol [Internet] 2010;172:203–210. Available from: http://linkinghub.elsevier.com/retrieve/pii/S1047847709003025

83. Shupliakov O, Bloom O, Gustafsson JS, Kjaerulff O, Low P, Tomilin N, Pieribone VA, Greengard P, Brodin L. Impaired recycling of synaptic vesicles after acute perturbation of the presynaptic actin cytoskeleton. Proc Natl Acad Sci U S A 2002;99:14476–14481.

84. Sankaranarayanan S, Atluri PP, Ryan TA. Actin has a molecular scaffolding, not propulsive, role in presynaptic function. Nat Neurosci 2003;6:127–135.

85. Gitler D, Takagishi Y, Feng J, Ren Y, Rodriguiz RM, Wetsel WC, Greengard P, Augustine GJ. Different presynaptic roles of synapsins at excitatory and inhibitory synapses. J Neurosci 2004;24:11368–11380.

86. Hosaka M, Südhof TC. Homo- and heterodimerization of synapsins. J Biol Chem 1999;274:16747–16753.

87. Benfenati F, Valtorta F, Rossi MC, Onofri F, Sihra T, Greengard P. Interactions of synapsin I with phospholipids: possible role in synaptic vesicle clustering and in the maintenance of bilayer structures. J Cell Biol 1993;123:1845–1855.

88. Graham ME, Handley MTW, Barclay JW, Ciufo LF, Barrow SL, Morgan A, Burgoyne RD. A gain-of-function mutant of Munc18-1 stimulates secretory granule recruitment and exocytosis and reveals a direct interaction of Munc18-1 with Rab3. Biochem J 2008;409:407–416.

89. Yasuda T, Shibasaki T, Minami K, Takahashi H, Mizoguchi A, Uriu Y, Numata T, Mori Y, Miyazaki J-I, Miki T, Seino S. Rim2a Determines Docking and Priming States in

Insulin Granule Exocytosis. Cell Metab 2010;12:117–129.

90. Sun L, Bittner MA, Holz RW. Rim and exocytosis: Rab3a-binding and secretion-enhancing domains are separate and function independently. Ann N Y Acad Sci 2002;971:244–247.

91. Yu H, Rathore SS, Gulbranson DR, Shen J. The N- and C-terminal domains of tomosyn play distinct roles in soluble N-ethylmaleimide-sensitive factor attachment protein receptor binding and fusion regulation. Journal of Biological Chemistry 2014;289:25571–25580.

92. Yizhar O, Lipstein N, Gladycheva SE, Matti U, Ernst SA, Rettig J, Stuenkel EL, Ashery U. Multiple functional domains are involved in tomosyn regulation of exocytosis. J Neurochem 2007;103:604–616.

93. Gracheva EO, Burdina AO, Touroutine D, Berthelot-Grosjean M, Parekh H, Richmond JE. Tomosyn negatively regulates both synaptic transmitter and neuropeptide release at the C. elegans neuromuscular junction. J Physiol (Lond) 2007;585:705–709.

94. Hattendorf DA, Andreeva A, Gangar A, Brennwald PJ, Weis WI. Structure of the yeast polarity protein Sro7 reveals a SNARE regulatory mechanism. Nature 2007;446:567–571.

95. Gracheva EO, Burdina AO, Holgado AM, Berthelot-Grosjean M, Ackley BD, Hadwiger G, Nonet ML, Weimer RM, Richmond JE. Tomosyn inhibits synaptic vesicle priming in Caenorhabditis elegans. PLoS Biol 2006;4:e261.

96. Bushey D, Tononi G, Cirelli C. Sleep and synaptic homeostasis: structural evidence in Drosophila. Science 2011;332:1576–1581.

97. Butz M, van Ooyen A, Wörgötter F. A Model for Cortical Rewiring Following Deafferentation and Focal Stroke. Frontiers in Computational Neuroscience 2009;3:10.

98. Kwon H-B, Sabatini BL. Glutamate induces de novo growth of functional spines in developing cortex. Nature 2011;474:100–104.

99. Turrigiano GG, Nelson SB. Homeostatic plasticity in the developing nervous system. Nat Rev Neurosci 2004;5:97–107.

100. Katz LC, Shatz CJ. Synaptic activity and the construction of cortical circuits. Science 1996;274:1133–1138.

101. Mitra A, Mitra SS, Tsien RW. Heterogeneous reallocation of presynaptic efficacy in recurrent excitatory circuits adapting to inactivity. Nat Neurosci 2012;15:250–257.

102. Choi Y-B, Li H-L, Kassabov SR, Jin I, Puthanveettil SV, Karl KA, Lu Y, Kim J-H, Bailey CH, Kandel ER. Neurexin-neuroligin transsynaptic interaction mediates learning-related synaptic remodeling and long-term facilitation in aplysia. Neuron 2011;70:468–481.

103. Simon DJ, Madison JM, Conery AL, Thompson-Peer KL, Soskis M, Ruvkun GB, Kaplan JM, Kim JK. The microRNA miR-1 regulates a MEF-2-dependent retrograde signal at neuromuscular junctions. Cell 2008;133:903–915.

104. Müller M, Pym ECG, Tong A, Davis GW. Rab3-GAP Controls the Progression of Synaptic Homeostasis at a Late Stage of Vesicle Release. Neuron 2011;69:749–762.

105. Kumar R, Corbett MA, Smith NJC, Jolly LA, Tan C, Keating DJ, Duffield MD, Utsumi T, Moriya K, Smith KR, Hoischen A, Abbott K, Harbord MG, Compton AG, Woenig JA, Arts P, Kwint M, Wieskamp N, Gijsen S, Veltman JA, Bahlo M, Gleeson JG, Haan E, Gecz J. Homozygous mutation of STXBP5L explains an autosomal recessive infantile-onset neurodegenerative disorder. Hum Mol Genet 2015;24:2000–2010.

106. Davis LK, Meyer KJ, Rudd DS, Librant AL, Epping EA, Sheffield VC, Wassink TH. Novel copy number variants in children with autism and additional developmental anomalies. J Neurodev Disord 2009;1:292–301.

107. Knapek S, Gerber B, Tanimoto H. Synapsin is selectively required for anesthesia-sensitive memory. - PubMed - NCBI. Learning & Memory 2010;17:76–79.

108. Michels B, Chen YC, Saumweber T, Mishra D, Tanimoto H, Schmid B, Engmann O, Gerber B. Cellular site and molecular mode of synapsin action in associative learning. - PubMed - NCBI. Learning & Memory 2011;18:332–344.

109. Bhatnagar S, Oler AT, Rabaglia ME, Stapleton DS, Schueler KL, Truchan NA, Worzella SL, Stoehr JP, Clee SM, Yandell BS, Keller MP, Thurmond DC, Attie AD. Positional cloning of a type 2 diabetes quantitative trait locus; tomosyn-2, a negative regulator of insulin secretion. PLoS Genet 2011;7:e1002323.

110. Nagano K, Takeuchi H, Gao J, Mori Y, Otani T, Wang D, Hirata M. Tomosyn is a novel Akt substrate mediating insulin-dependent GLUT4 exocytosis. International Journal of Biochemistry and Cell Biology 2015;62:62–71.

111. Ye S, Huang Y, Joshi S, Zhang J, Yang F, Zhang G, Smyth SS, Li Z, Takai Y, Whiteheart SW. Platelet secretion and hemostasis require syntaxin-binding protein STXBP5. J Clin Invest 2014;124:4517–4528.

112. Groffen AJA, Jacobsen L, Schut D, Verhage M. Two distinct genes drive expression of seven tomosyn isoforms in the mammalian brain, sharing a conserved structure with a unique variable domain. J Neurochem 2005;92:554–568.

113. Barak B, Shvarts-Serebro I, Modai S, Gilam A, Okun E, Michaelson DM, Mattson MP,

Shomron N, Ashery U. Opposing actions of environmental enrichment and Alzheimer's disease on the expression of hippocampal microRNAs in mouse models. Transl Psychiatry 2013;3:e304.

114. Sakisaka T, Baba T, Tanaka S, Izumi G, Yasumi M, Takai Y. Regulation of SNAREs by tomosyn and ROCK: implication in extension and retraction of neurites. J Cell Biol 2004;166:17–25.

115. Aligianis IA, Johnson CA, Gissen P, Chen D, Hampshire D, Hoffmann K, Maina EN, Morgan NV, Tee L, Morton J, Ainsworth JR, Horn D, Rosser E, Cole TRP, Stolte-Dijkstra I, Fieggen K, Clayton-Smith J, Mégarbané A, Shield JP, Newbury-Ecob R, Dobyns WB, Graham JM, Kjaer KW, Warburg M, Bond J, Trembath RC, Harris LW, Takai Y, Mundlos S, Tannahill D, Woods CG, Maher ER. Mutations of the catalytic subunit of RAB3GAP cause Warburg Micro syndrome. Nat Genet 2005;37:221–224.

116. Seabra MC, Mules EH, Hume AN. Rab GTPases, intracellular traffic and disease. Trends in Molecular Medicine 2002;8:23–30.

117. D'Adamo P, Menegon A, Nigro Lo C, Grasso M, Gulisano M, Tamanini F, Bienvenu T, Gedeon AK, Oostra B, Wu S-K, Tandon A, Valtorta F, Balch WE, Chelly J, Toniolo D. Mutations in GDI1 are responsible for X-linked non-specific mental retardation. - PubMed - NCBI. Nat Genet 1998;19:134–139.

118. Shuang R, Zhang L, Fletcher A, Groblewski GE, Pevsner J, Stuenkel EL. Regulation of Munc-18/syntaxin 1A interaction by cyclin-dependent kinase 5 in nerve endings. J Biol Chem 1998;273:4957–4966.

119. Jakawich SK, Neely RM, Djakovic SN, Patrick GN, Sutton MA. An essential postsynaptic role for the ubiquitin proteasome system in slow homeostatic synaptic plasticity in cultured hippocampal neurons. Neuroscience 2010;171:1016–1031.

120. Schindelin J, Arganda-Carreras I, Frise E, Kaynig V, Longair M, Pietzsch T, Preibisch S, Rueden C, Saalfeld S, Schmid B, Tinevez J-Y, White DJ, Hartenstein V, Eliceiri K, Tomancak P, Cardona A. Fiji: an open-source platform for biological-image analysis. Nat Methods 2012;9:676–682.

121. Balaji J, Ryan TA. Single-vesicle imaging reveals that synaptic vesicle exocytosis and endocytosis are coupled by a single stochastic mode. Proceedings of the National Academy of Sciences 2007;104:20576–20581.

122. Royle SJ, Granseth B, Odermatt B, Derevier A, Lagnado L. Imaging phluorin-based probes at hippocampal synapses. Methods Mol Biol 2008;457:293–303.

123. Ray D, Terao Y, Nimbalkar D, Hirai H, Osmundson EC, Zou X, Franks R, Christov K, Kiyokawa H. Hemizygous disruption of Cdc25A inhibits cellular transformation and mammary tumorigenesis in mice. Cancer Res 2007;67:6605–6611.

124. Glynn MW, McAllister AK. Immunocytochemistry and quantification of protein colocalization in cultured neurons. Nat Protoc 2006;1:1287–1296.

125. Bolte S, Cordelières FP. A guided tour into subcellular colocalization analysis in light microscopy. J Microsc 2006;224:213–232.

126. Costes SV, Daelemans D, Cho EH, Dobbin Z, Pavlakis G, Lockett S. Automatic and Quantitative Measurement of Protein-Protein Colocalization in Live Cells. Biophys J 2004;86:3993–4003.

## Chapter IV

## Discussion: Rab GTPases and SNARE proteins: The dynamic duo orchestrating vesicles to tune $Ca^{2+}$-mediated exocytosis

Initial studies of membrane fusion proposed that the pairing of cognate SNAREs provided the targeting specificity of membrane trafficking [1,2]. Indeed, the *in vitro* formation of SNARE-complexes by reconstitution of cognate SNAREs localized to distinct membrane compartments show that they can provide the specificity required for fusion, but that it is not sufficient to match the $Ca^{2+}$-mediated fusion rates seen in cells [3]. It appears that correct targeting and priming critically depends on other factors, including Rab proteins and their effectors [3,4]. Yet, the functional relationship between Rab GTPases and SNAREs has yet to be determined. Rab GTPases are critical in the recruitment of tethering, docking and priming factors in a manner that is governed by their GTPase cycle [5]. While, SNAREs located on distinct membranes can form stable complexes that enable overcoming the free energy barrier necessary to fuse a vesicle. The outstanding questions are, how do these two cycles coalesce? And importantly, how do they coordinate such that they coalesce in a spatially and temporally restricted manner?

The studies presented in this dissertation begin to address such questions. First we establish unique functional activities of Rab3 and Rab27 proteins on late stages of the exocytotic pathway (Chapter 2). Specifically, we find that Rab27A is critical in establishing

the size of the IRP and RRP (Figure 2.6), while Rab3A exerts a key and prominent role in rapidly refilling the RRP and modulatory role in building the size of the RRP (Figure 2.7). This finding is significant in that it enables the possibility that distinct Rab GTPases together with their effectors may cooperate to confer specificity to distinct modes of fusion. This specificity may be conferred through several possibilities including: (1) Via different effector interactions, although it is known that Rab3 and Rab27 share many effectors, it appears that they may have significantly different binding affinities [6-8]. (2) Specificity could be attained by distinct spatial localization as one study has found that Rab3 and Rab27 co-reside in only one portion of vesicles but are also present alone in distinct pools [9]. This study remains to be confirmed, but in addition, future studies should address if vesicles containing Rab3 alone, Rab27 alone or Rab3 and Rab27 differ in recruitment and priming kinetics. (3) Another alternative is that specificity of their actions is related to the dynamics of their GTPase activity. For example, Rab3 has been found to disassociate from vesicles rapidly upon stimulation and thus may be free to participate in rapid recruitment and refilling of vesicle pools [9-12]. Comparatively, Rab27 is not as readily available to re-enter the priming cycle as it remains with vesicle membranes longer, likely until the initiation of endocytosis [13-16].

Our second set of studies (Chapter 3), provide evidence that a cytosolic R-SNARE protein, Tomo1 regulates the partitioning of synaptic vesicle pools in hippocampal neurons (Figure 3.2). These findings are novel in that they indicate that a SNARE protein acts not

only in the late-stages of exocytosis but also upstream in regulating the fraction of SVs available to re-populate RRP vacancies. Critically, our results indicate that Tomo1 also inhibits the fraction of releasable vesicles via a mechanism independent of its SNARE motif (Figure 3.2). Thus, unlike most SNAREs, Tomo1 is a multifunctional protein able to regulate distinct steps of the vesicle cycle through multiple protein domains. In addition, we find that Tomo1 binds to Rab3A proteins and forms a complex with SynapsinI (Figure 3.5, 3.6). This interaction is particularly notable because it represents a mechanism by which the SNARE and Rab cycle may coordinate the release process. However significant questions remain to be defined, for example, does Tomo1 regulate Rab3? Or does Rab3 regulate Tomo1? And does this regulation occur at the plasma membrane where other SNAREs are localized or does it occur upstream during docking? Functional studies conducted in yeast seem to indicate that Sro7, a Tomosyn homolog, coordinates the transition from docking (mediated by Rabs) to priming (mediated by SNAREs) [17,18]. These studies show that overexpression of Sro7p leads to an accumulation and clustering of non-releasable vesicles that eventually leads to cell-lethality [17]. This clustering phenotype is dependent on the actions of the Rab Sec4-GTP [17]; however the severity of vesicle clustering can be ameliorated by the interaction of the N-terminal of Sro7p with the Qbc-motif of the Q-SNARE Sec9p [18]. Thus, from the studies in yeast one may conclude that Sro7p bridges the targeting/docking process with priming and as such may act as a regulatory gate switching between priming-permissive and intolerant states. Analogous to these findings are results

from our studies showing that: (1) Tomo1 leads to an increase in the fraction of vesicles that are release recalcitrant; (2) that it interacts with Rab3-GTP; and from previous studies, (3) that it is able to switch off its inhibitory mode based on the conformation of its interaction with the Q-SNARE Syntaxin [19,20]. Thus, in keeping with the Sro7 yeast model, it is possible that Tomo1 may function as a regulatory gate that determines the fraction of vesicles amenable for recruitment and further priming. For this to be established, future investigations must determine functional reliance of Tomo1 on the actions of Rab3-GTP in controlling the transition of vesicles from ResP to TRP and characterize the spatial and temporal characteristics of this interaction as they relate to fusion events.

It is believed that the release of chemical messengers at a synapse is one of the primary mechanisms for information transfer that gives way to complex forms of learning and behavior [21]. One rationale for this, is that the great computational power of neural circuits may arise, in part, as a consequence of evoked SV release being stochastic and susceptible to change, which allows presynaptic boutons to act as filters and dynamically modify AP activity [22,23]. Thus, a great amount of focus has been placed on studying the molecular mechanisms that may impart such variability. Moreover, many studies have shown that Pr can be locally set and regulated at the level of single connections. Therefore, in addition, a lot of emphasis is placed on determining the local signaling pathways that give rise to feedback control between two connected neurons. One emerging target of local regulation is control over the partitioning of SVs among functional pools. For example,

several studies have shown that the probability of vesicle release is positively correlated to the size of the TRP, especially during high-frequency AP firing (e.g. 10-20 Hz)[24-27]. In addition, a few studies have found that there may be strong feedback control of SV partitioning by retrograde signaling [26,28]. For example, one study discovered that post-synaptic NMDA-receptor activation led to a presynaptic enhancement in neurotransmitter release caused by increasing the size of the TRP, but that this effect was blocked by inhibition of nitric-oxide synthase from the cell media [26]. Suggesting that, post-synaptic changes were met with concomitant presynaptic enhancements and that they may depend on the release or presence of a retrograde signal. In these studies, we show that Tomo1 is a strong modulator of the TRP/ResP partition and that its actions are likely controlled by Cdk5 phosphorylation (Figure 3.3, 3.4). In addition, we find that the phosphorylation state of Tomo1 is modified by neuronal activity and critically that long-term silencing of post-synaptic activity leads to compensatory enhancement in neurotransmitter release, which we find depends on Tomo1's function (Figure 3.7). This is fully consistent with previous reports showing that strong elevations or decreases in network activity lead to compensatory changes in the ResP size [29-31]. In addition, the protein levels of Tomosyn have been found to be reduced by neuronal silencing [29]; and in response to the activation of a Neurexin-Neuroligin retrograde signal in *C. elegans* [28]. Taken together, there is increasing evidence to suggest that: (1) Tomosyn proteins levels or its activation state may be regulated by neuronal activity; (2) Tomosyn proteins, may be a key target of activity-

dependent retrograde signaling; (3) activity dependent changes of presynaptic neurotransmitter release may partly rely on Tomosyn regulation of the fraction of releasable vesicles at nerve terminals.

*The potential for a molecular clamp regulating vesicle recruitment into releasable pools*

Tomosyn proteins are often characterized as inhibitors of secretion. Indeed, as shown in the studies presented here and in many before, high levels of Tomosyn expression leads to reduced secretion or reduced membrane fusion. This has been observed with *in vitro* systems [32-34]; in studies with yeast homologs of Tomosyn [18,35]; and in Tomo1 overexpression in neuronal cells [36-40] and endocrine cells [41-44]. Yet, there are a few enigmatic findings related to Tomosyn function, which suggest that Tomosyn promotes vesicle secretion. For example, knock-down of Tomosyn protein resulted in decreased neurotransmitter release at superior cervical ganglion neurons in culture [45], in reduced secretion from the rat β-cell line INS-1E [46], and in reduced numbers of SNARE complexes analyzed from Tomosyn deficient mice brain lysates[40]. In human endothelial cells, Tomosyn1 knock-out paradoxically led to increased exocytosis of vWF and P-selectin (suggesting inhibitory role), but knock-out also inhibited platelet secretion (suggesting a positive role!) [47]. Perhaps, one way to reconcile these apparent discrepancies is to view Tomosyn proteins specifically as priming clamps rather than general inhibitors, a subtle, but potentially important distinction. As defined here, a

molecular clamp, stalls or blocks priming at a specific stage without hindering or derailing progression upon clamp-relief, whereas an inhibitor may derail progression. The purpose of a clamp then is to pause and regulate. In example, Syt1 or complexin act as clamps to prevent rampant spontaneous fusion but rather direct synchronous release upon $Ca^{2+}$ influx. Perhaps, Tomosyn acts in the same way to limit priming until its clamp is relieved by yet to be identified signals. This speculation is not without warrant, as there is some evidence to suggest that a possible clamping mechanism exists for Tomosyn. These are, studies on the Tomosyn tail domain which show that it can switch its interaction between a region in the N-terminal WD40 repeats and the C-terminal R-SNARE domain [19]. When bound to the N-terminal WD40 repeats the tail domain leaves the C-teminal R-SNARE motif of Tomosyn unencumbered to inhibit secretion by binding Syntaxin1 proteins and forming non-fusiogenic SNARE complexes [19,20]. Conversely, when the tail domain is bound to an N-terminal portion of the R-SNARE motif it still permits binding to Syntaxin1 proteins but it is more amenable for displacement by VAMP proteins [20]. Thus, in this conformation, Tomosyn acts as a placeholder and using *in vitro* studies it was shown to accelerate fusion by promoting 1:1 binding stoichiometry between Syntaxin/SNAP25 [20]. Whereas in 2:1 Syntaxin/SNAP25 complexes the second Syntaxin occupies the position of VAMP thus delaying SNARE complex formation [48,49]. That being said, these studies do not fully address the functions of this tail-domain *in vivo*. Nonetheless, these studies suggest that a potential clamping mechanism could exist which triggers the inhibitory activity of

Tomosyn based on the binding of its tail region. One interesting possibility is that the GTPase activity of Rab3A serves as a potential trigger for displacing the R-SNARE motif of Tomosyn or promoting conformation change in the tail domain. Especially, when considering that few studies now have suggested that the GTP-form of Rab3A clamps secretion but that it can be relieved by transitions into GDP [50-53]

### 4.2 Limitations

*Chapter 2*

Progressive loss of insulin release from pancreatic β-cells is a central pathology associated with the development of type-2 diabetes. These deficits begin with the loss of the first phase of $K_{ATP}$/ $Ca^{2+}$-induced insulin release. Next the amplifying pathways of regulation are compromised leading to a decreasing maximal capacity of glucose-induced release. Eventually, a complete β-cell failure ensues during which insulin release is completely abrogated followed by major cell loss, requiring patients to self-monitor glucose levels and self-administer insulin [54,55]. Our studies, focused on determining the roles of Rab3A and Rab27A in regulating the first-phase of insulin secretion. Moreover, we used electrical stimulation to drive release of LDCV from β-cells. While these studies were primarily aimed on answering molecular questions, additional considerations could have led to better physiological conclusions. These notably include, the absence of assessments for the effects of loss of Rab3 and Rab27 on phase 2 of insulin release. Especially since Rab

GTPases are poised to play a critical role during the second potentiating phase of release. This is because mounting evidence suggests that this phase of insulin release is supplied by newly translocated LDCVs from the cytoplasm rather than already docked vesicles [56-58]. Therefore, given the central role of Rab GTPases in trafficking and tethering it is likely that they play a role in coordinating the second-phase of insulin release [59-61]. In a similar light, the first phase of release also appears to occur differently when stimulated by glucose vs. step-depolarizations or applications of Hi $K^+$. Again, some studies have reported that this is because different stimuli activate different vesicle pools [62]. In fact, this may be one explanation accounting for the fact that we observed no differences by TIRF microscopy in vesicle mobility in response to inhibition of the Rab GTPases (Figure 2.4). Thus, future studies would most effectively determine the role of Rab GTPases in insulin release by using more physiological stimuli, for example elevated glucose.

The strength and kinetics of vesicle pool size and refilling is strongly determined by the $Ca^{2+}$ concentration in micro and nanodomains [63]. One of our major findings indicates that Rabs differ in their ability to fill the vesicle pool associated with higher $Ca^{2+}$-sensitivity (IRP); and that Rab3A vs. Rab27A differ in their kinetics for refilling both the IRP and RRP pools. Another limitation of our study is that we did not address if Rab's functional roles depend on localized changes in $Ca^{2+}$ concentration. This could have most effectively been studied by pairing of membrane-capacitance recordings with UV flash photolysis of caged $Ca^{2+}$ leading to a rapid uniform increase in global $Ca^{2+}$ concentration.

*Chapter 3*

The data from this chapter established that Tomo1 could act as a central regulator controlling the population of SVs among the RRP, RP and TRP. For these studies we relied on optical methods for determining pools sizes. These offer the capability to directly measure presynaptic activity (compared to electrical recording at small synapses), but in some cases these are limited by the temporal sensitivity and signal detection capabilities of the equipment. This becomes particularly challenging for measuring signals with fast kinetics and small amplitudes such as the RRP size [64]. Specifically, for these studies we estimated the size of the RRP using a 20Hz, 40P stimulus (Figure 3.2). In hippocampal neurons in culture it has been established that up to 30 APs is sufficient to deplete the RRP pool [65,66]. However, RRP pools display great variability between individual release sites and the amount of asynchronous release can also affect measurements [66,67]. Thus, the most precise way to measure the RRP is to use a stimulus strong enough to empty the RRP rapidly before refilling occurs [65,68,69]. To do this via use of pHluorins combined with optical detection methods, fluorescent changes to single APs delivered in high-frequency is required [64,70]. This is because one must be able to capture the amplitude and stimulus number during which the rate of exocytosis briefly drops to 0, indicating the moment at which the RRP has been depleted but refilling has not occurred [64]. Unfortunately, our

camera was neither sensitive enough to capture fluorescent changes in response to single APs nor able to capture frames at the frequency needed; thus our measurements represent only an estimate but cannot be viewed as the true size of the RRP.

Mechanistically, our studies identified that Tomo1 is a phosphorylation substrate of Cdk5 likely directing its functional activities. Moreover, we identified via mass-spectrometry several residues that are phosphorylated *in vitro* by Cdk5. Yet, we did not establish these to be essential for Tomo1's actions. Future studies could address this by creating phosphomutants of single predicted residues and/or combinations. Likewise, we did not directly address the possibility that Cdk5 phosphorylation of Tomo1 can lead to changes in its interaction with Rab3A or Syntaxin, something that may also be learned by the production of a Tomo1 mutant that is Cdk5 phosphonull or mimetic. Finally, despite the fact that Tomo2 proteins levels in the hippocampus have been found predominantly localized to cell bodies and post-synaptic compartments, a role for Tomo2 in pool partitioning cannot be ruled out thus far [71].

### 4.3 Other experimental observations and future directions

*Presynaptic vs. Postsynaptic roles for Tomosyn proteins in the CNS*

*In situ* hybridization data gathered by the Allen Institute (http://mouse.brain-map.org) has demonstrated that Tomosyn gene expression is enriched in the hippocampus and cortex (Figure 4.1, A). These are areas that have been established as highly critical for

learning, memory and cognition [21]. Furthermore, a study using confocal and two-photon high-resolution microscopy determined that Tomo1 vs. Tomo2 displays differential expression in the mouse hippocampus [71]. In this study, Barak and his colleagues (2010) demonstrated that Tomo1 was most highly expressed in excitatory cells of the hilus and mossy fiber regions and predominantly localized to presynaptic compartments. On the other hand, Tomo2 was mainly expressed in the cell bodies of subiculum, CA1 and CA2 neurons with a postsynaptic localization. Thus, one may conclude that based on their localization to distinct compartments Tomo1 vs. Tomo2 have the potential to carry-out different cellular functions in the mouse hippocampus.

This notion is further supported by a study that assessed the developmental trajectory of the mRNA expression levels of Tomo1 and Tomo2 starting from embryonic day 10 to post-natal day 12 in the mouse brain by real-time quantitative PCR [72]. These studies concluded that Tomo1 levels were detectable earlier and were higher than Tomo2 during embryonic stages (E14-E18). Moreover, Tomo1 mRNA expression was localized to the cortical plate during the developmental stages when layering is established. In contrast, Tomo2 was more widespread, and its expression more highly elevated in postnatal stages compared to Tomo1. Given the differential regulation of Tomo mRNA it is likely that they play a developmental role in synaptic transmission. Further support for this notion is derived from a study that established a role for Tomosyn in neurite outgrowth via interactions with the Rho/RoCK pathway [73]. In this pathway, repulsive chemokines

induce Rho GTPases to bind and activate ROCK. In turn, ROCK proteins phosphorylate Syntaxin causing an increased interaction with Tomosyn and leading to inhibition of neurite outgrowth by preventing fusion of plasmalemmal precursor vesicles [73]. During the course of my investigations on Tomo1, it was noticed that overexpression and/or knockdown may have effects on (1) the density of post-synaptic spines and (2) the number of active vs. silent synapses and thus potentially play a role in structural plasticity and development (Figure 4.1).

The small protrusions emanating from dendrites of neurons are termed spines and were initially discovered by Santiago Ramon y Cajal by Golgi staining [74]. Dendritic spines are considered the functional units for synaptic integration as they represent the site of connection for the majority of excitatory presynaptic boutons [75]. Changes in the long-term activity of synapses are related to changes in spine morphology or density [76]. The Rho-ROCK pathway has been shown to be sensitive to the activity of $Ca^{2+}$/calmodulin-dependent kinase in order to promote the growth of spines during long-term potentiation of CA1 pyramidal neurons [77]. During my experiments, I found that Tomo1 knockdown was often associated with a striking enhancement in the apparent number of spines in hippocampal neurons in culture (Figure 4.1, B). At this point, inferences regarding the role of Tomosyn as a potential modulator of spines is purely speculative, but considering the following: (1) Tomosyn proteins have already been shown to interact with the Rho-ROCK

pathway and (2) Tomosyn2 is enriched post-synaptically and its protein levels increased postnatally during a time of spinogenesis they may warrant further investigation [78].

In addition, during the course of my experiment using vGpH as a measure of vesicle fusion at single boutons it also noticed that neurons overexpressing Tomo1 had many fewer "active" boutons than control, or Tomo1 knock-down neurons. That is, despite the fact a bouton contained the vGpH reporter as detected by application of $NH_4Cl$ or the mCherry reporter on VGLUT1—no fluorescence changes were detected upon stimulation at 20Hz-900P. This observation was highly akin to one reported by Kim and Ryan (2010), wherein inhibition of Cdk5 by application of roscovitine led to an unmasking of previously silent presynaptic boutons [29]. Given that our studies (Chapter 3) suggest that Tomo1 is a phosphorylation substrate of Cdk5 and that they share the same functional pathway for regulating the TRP, pilot studies were conducted to probe the role of Tomo1 in regulating silent synapse. As shown in Figure 4.1, C-D, we first replicated the findings presented by Kim and Ryan (2010) and show that inhibition of Cdk5 by roscovitine (100μM, 30 min) leads to an enhancement in the cell averaged vGpH fluorescence indicative of stronger neurotransmitter release. Next, we analyzed the number of active boutons contributing to the net vGpH signal. We defined "active" boutons as those that displayed a fluorescence change two times greater than the baseline fluorescence. The results show, that inhibition of Cdk5 lead to a ~3 fold increase in number of active boutons. Next, using some of the data from Chapter 3 (Figure 3.2), we determine the fraction of boutons that responded to the

TRP-depleting 20 Hz/900P stimulus in Tomo1 overexpressing, Tomo1 knockdown, control and control + roscovitine cells using the same criteria just described. We find that the fraction of boutons that are silent is significantly reduced in Tomo1 knockdown neurons in comparison to control and Tomo1 overexpressing neurons (Figure 4.1, E-F). These results provide strong preliminary evidence to suggest that Tomo1 plays a significant role in silencing synaptic release sites.

The possibility that Tomo1 may play a role in silencing synapses is also consistent with the findings that it is (1) presynaptically localized and (2) enriched prenatally. This is because, although the regulation of silent synapses has been recently linked to the expression of synaptic plasticity [79]; it is also recognized as an important mechanism engaged for developmentally-regulated synaptic pruning. It has been shown that the establishment of neural networks depends on massive production of neuronal connections followed by a 50% loss or pruning [80]. Moreover, it has been recently shown that the ResP size is also developmentally refined as the hippocampus matures [30]. Therefore, it is possible that, early elevations in Tomo1 level, which are enriched in cortical regions, play a significant role in pruning and neuronal integration during development.

*The tripartite complex: Setting the stop and go of vesicle trafficking to priming sites*

The results of Chapter 2 provide direct evidence for a role of Rab3A in rapid refilling of vesicle pools. One likely mechanism by which vesicles containing Rab3-GTP may be

amenable to rapid recruitment is via the formation of a tripartite complex between Rab3A-Rim-Munc13 [81]. RIM proteins have been shown to bind VGCCs directly via their PDZ domain and the priming factor Munc13-1 via an adjacent zinc-finger domain [81-83]. Importantly, RIM binding to Munc13-1 activates its priming actions since it can disassociate Munc13-1 autoinhibitory dimers [84]. Active Munc13-1 can then drive the closed (inactive) Syntaxin to open and initiate priming [62]. Munc13-1 is a multi-domain protein with additional binding domains for calmodulin, diacylglycerol (DAG), and $Ca^{2+}$.[85-88] Interestingly, DAG is an effective second-messenger for potentiating exocytosis. Its actions are mediated by protein-kinase C (PKC) and separately by Munc13-1 [89]. In regards to the Munc13-1 pathway, it is thought that potentiation occurs via increases in priming as application of β-phorbol esters (functional analogs of DAG) induces translocation of cytosolic Munc13-1 to the plasma membrane [86,90]. Based on this evidence, we conducted pilot studies in secretory PC12 cells to address if translocation of expressed Munc13-1 induced by application of β-phorbol esters could traffic RIM2/Rab3A proteins and potentially serve as a mechanism for rapid refilling of vesicle pools. As shown in Figure 4.2, A, our results suggest that 10 minute applications of 150 nM β-phorbol esters induces translocation of expressed CFP-Munc13-1 together with YFP-RIM2 proteins. The translocation of YFP-RIM2 proteins seemed to occur via direct interaction with CFP-Munc13-1 since translocation was eliminated in a YFP-RIM2 mutant (K97E/K99E) that lacks Munc13-1 binding capability (Figure 4.2, B) [81]. Furthermore, our initial studies

suggest that Rab-binding is not required for the translocation of YFP-RIM to the plasma membrane since RIM mutants deficient in Rab binding (E36A/R37S) still trafficked upon stimulation by β-phorbol esters (Figure 4.2, B) [81]. This preliminary data provides one potential mechanism by which vesicles could be rapidly refilled during periods of high-activity. Future studies should test if β-phorbol ester stimulation induces translocation of Rab3 and/or vesicles and if mutations in the DAG-binding domain of Munc13-1 hinders rapid refilling mediated by Rab3.

In addition, we assessed the effect of overexpression of these proteins in the PC12 cell line using human growth hormone (hGH) secretion assays. The co-transfection of hGH along with a protein of interest allows for specific measurements of secretion from a small fraction (~ 10% in our case) of transfected cells [91]. Figure 4.2, C-D, shows all the preliminary data gathered. In summary, we find that expression of RIM2 and/or Munc13-1 lead to an enhancement in stimulated secretion (40mM KCl, 10 minutes) relative to empty vector controls. As was shown before, we find that expression of Rab3A leads to inhibition of secretion [50]; and that co-expression of RIM2 and/or Munc13-1 is unable to remove Rab3A's clamping activity. Thus even if our hypothesis that Munc13-1 translocation may serve as a mechanism for rapid targeting of Rab3A to priming sites were to receive further experimental support, these results suggest that an additional stimulus or modulator is required to remove the Rab3A clamp. On a related note, our findings (Chapter 3) show that Tomo1 can also act as a clamp on vesicle recruitment and that it interacts with Rab3A

proteins. Similarly, studies done in *C. elegans* show that Tomosyn directly opposes the priming actions of unc13 since deficiencies in unc-13 mutants can be rescued by deletions of Tomosyn [39,92]. Taken together, these data support efforts to test a model in which rapid refilling of vesicles is promoted by the tripartite complex including Rab3/RIM/Munc13 yet opposed by the actions of Tomosyn proteins.

*Interactions between Tomosyn1 and Rab27A and potential functional roles*

The focus of this dissertation has relied heavily on the potential functional roles for RabGTPase and SNARE interactions. Mainly, it has been argued that interactions between Rab3A and Tomo1 can serve as a regulatory gate on recruitment and docking. However, pilot data collected in collaboration with Woody Hoerauf shown in Figure 4.3 presents some evidence that Tomo1 also interacts with Rab27A proteins. Our results show an IP experiment of expressed mTomo1 in HEK293 cells effectively co-precipitates expressed CFP-Rab27A (Q78L) and CFP-Rab27A (T23N), which are GTP and GDP constitutive mutants (Figure 4.3, A-B). Moreover, membrane capacitance recordings from mouse adrenal chrommafin cells show that knockdown of Tomo1 enhances the RRP size relative to a scramble-control but only when the experiments are carried out in wild-type mice (Figure 4.3, C, black trace). Conversely, knockdown of Tomo1 in Rab27A-deficient mice does not lead to an enhancement in the RRP size (Figure 4.3, C, red trace). Suggesting that Tomo1 requires Rab27 to exert inhibitory control. However, it is important to note that

loss of Rab27 alone leads to a significant decrement in the RRP size (Figure 4.3, C, compare sh-Scr condition between wt and Rab27 null). Thus, we cannot rule out the possibility that these effects are unrelated to Tomo1 function. Moreover, Rab27A has been shown to stimulate the GTPase activity of Rab3A during the acrosomal fusion reaction—therefore we also cannot rue out the possibility that these observed effects are related to Rab3 function [93].

*Final Remarks*

In summary, the data presented here hopes to have illustrated how molecular complexes associated with synaptic vesicles and SNARE proteins may act as determinants of neurotransmission modes. Decades of scientific research on vesicle fusion and secretion have shown that the strength and kinetics of release is determined by factors including but not limited to: the proximity to $Ca2^{+}$-channels, number of SNARE complexes on a primed vesicle, or the number of vesicles available to for priming. All these processes require a synaptic vesicle to interact with a specific subset of molecules, which are precisely equipped to execute a discrete function. Thus, a key node of regulation is carried-out by protein mediators that coordinate the interactions between groups of molecules largely divided into vesicle-associated proteins and plasma membrane proteins. Our studies present a strong case for one mediator being the Rab/Tomo interaction. This interaction appears especially critical since these two proteins together contain binding motifs linking them to all aspects of the vesicle cycle. We provided compelling evidence at least for their

roles in vesicle pool refilling and partitioning as well as priming. What is most critical at this point is to dissect the temporal and spatial dynamics of this interaction during the vesicle cycle (i.e. targeting, docking, priming, fusion). Learning when and where it acts will provide significant insight and focus into the exact mechanism and function.

On a more personal note, one of the major realizations gained during these studies is that $Ca^{2+}$-mediated exocytosis is a cellular gestalt. That is, as an organized whole, this process is so highly specialized and dynamic that it seems greater than the sum of its parts. Undoubtedly, many scientists that study exocytosis must share this feeling. Especially when considering that there are hundreds of molecules available whose actions in some way may synergize to guide the vesicle cycle. At times, full-comprehension of this process seems like an unattainable feat. Often leading to some dismay, at least only until the next time I find that one of my experimental perturbations somehow changed the vesicle's behavior—then I am quickly drawn back in. In a way, it seems I am also on the vesicle's cycle.

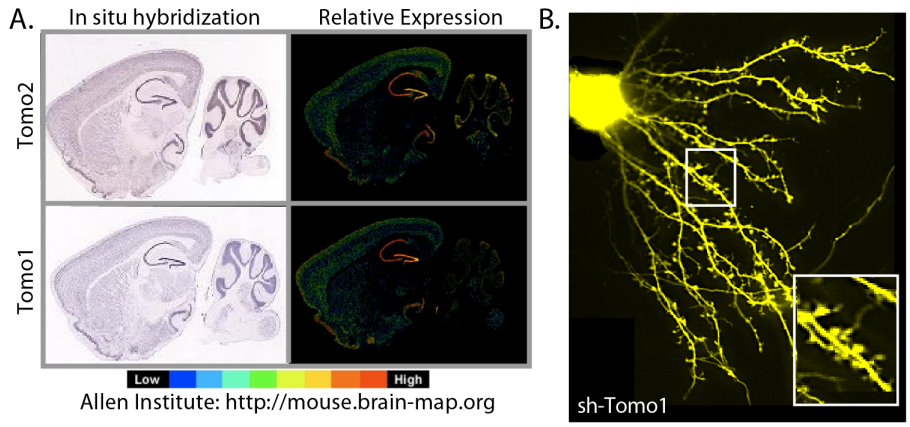
A.
In situ hybridization
Relative Expression
Tomo2
Tomo1
Low
High
Allen Institute: http://mouse.brain-map.org
B.
sh-Tomo1

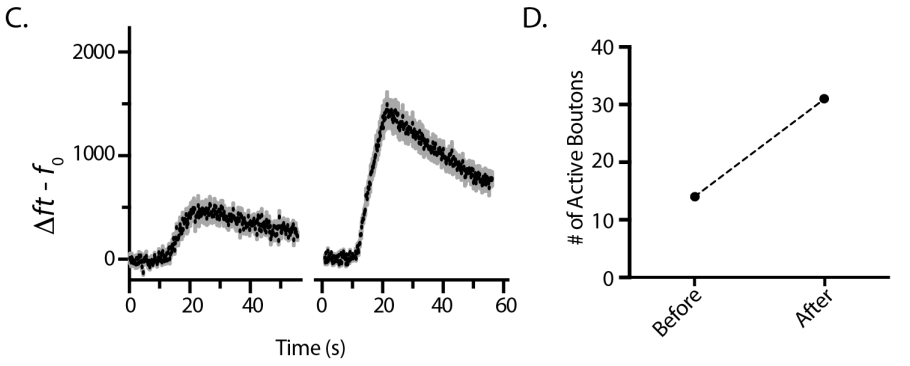
C.
2000
1000
0
Δft - f0
0
20
40
0
20
40
60
Time (s)
D.
40
30
20
10
0
# of Active Boutons
Before
After

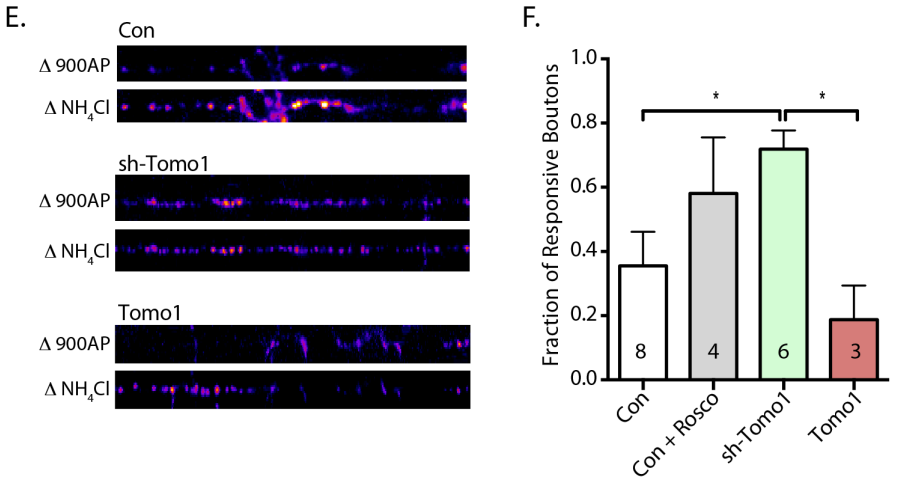
E.
Con
Δ 900AP
Δ NH4Cl
sh-Tomo1
Δ 900AP
Δ NH4Cl
Tomo1
Δ 900AP
Δ NH4Cl
F.
1.0
0.8
0.6
0.4
0.2
0.0
Fraction of Responsive Boutons
*
*
8
4
6
3
Con
Con + Rosco
sh-Tomo1
Tomo1

**Figure 4.1: Potential effects of Tomo on spine density and silent synapses.** (A) *In situ* hybridization images for Tomo1 and Tomo2 mRNA in saggital mouse brain sections, relative intensity of *in situ* signal shown on right. (B) Representative micrograph of hippocampal neuron in culture expressing mCherry and shRNA-Tomo1. (C) Averaged vGpH fluorescence in response to 100 electrical pulses delivered at 10 Hz of all boutons from a single neuron before (left) and after (right) treatment with the Cdk5 inhibitor roscovitine (100μM, 30 minutes). (D) Number of active boutons quantified from data in (C), active boutons defined as those whose peak fluorescence is twice greater than their baseline fluorescence. (D) Representative ΔF images (average of last 10 frames during stimulus – average last 10 baseline frames) for conditions indicated. (E) Quantification of the fraction of active boutons from data used in Fig. 3.2 & 3.4 shown as a fraction of the total number of boutons expressing vGpH.

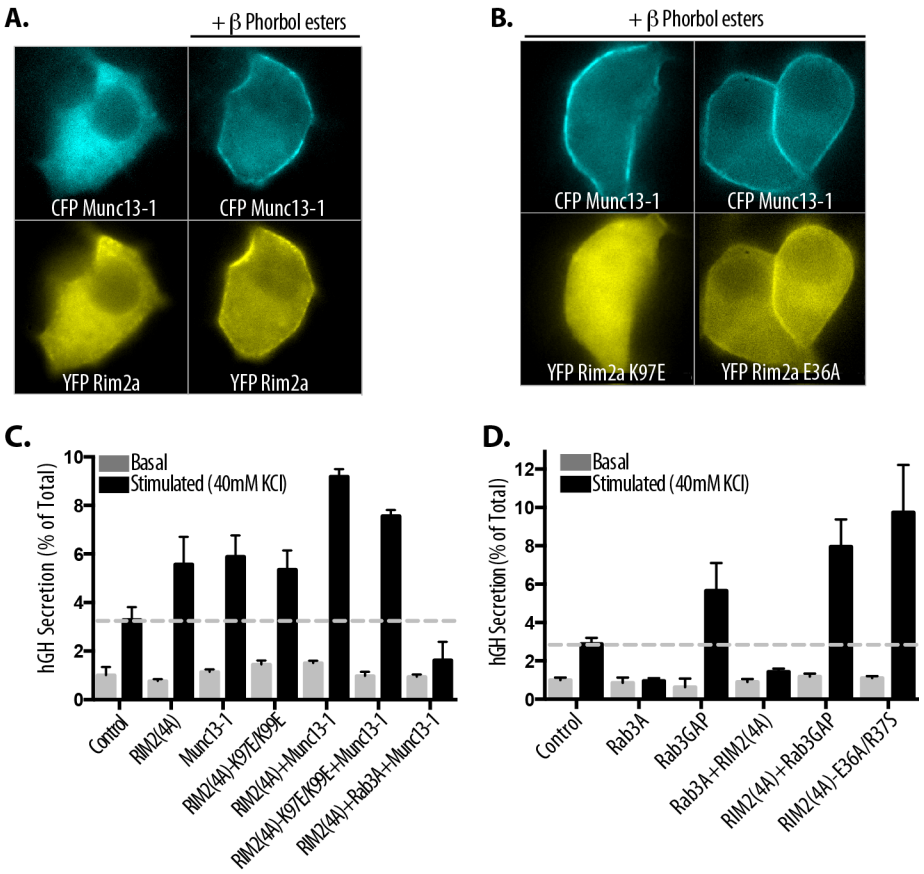
A.
+ β Phorbol esters
CFP Munc13-1
CFP Munc13-1
YFP Rim2a
YFP Rim2a
B.
+ β Phorbol esters
CFP Munc13-1
CFP Munc13-1
YFP Rim2a K97E
YFP Rim2a E36A
C.
Basal
Stimulated (40mM KCl)
hGH Secretion (% of Total)
0
2
4
6
8
10
Control
RIM2(4A)
Munc13-1
RIM2(4A)-K97E/K99E
RIM2(4A)+Munc13-1
RIM2(4A)-K97E/K99E+Munc13-1
RIM2(4A)+Rab3A+Munc13-1
D.
Basal
Stimulated (40mM KCl)
hGH Secretion (% of Total)
0
2
4
6
8
10
12
Control
Rab3A
Rab3GAP
Rab3A+RIM2(4A)
RIM2(4A)+Rab3GAP
RIM2(4A)-E36A/R37S

**Figure 4.2: β-phorbol esters induce translocation of Munc13-1 and RIM2.** (A) Representative confocal images of PC12 cells co-expressing CFP-Munc13-1 (cyan) and YFP-RIM2a (yellow) before (left) and after (right) treatment with β-phorbol esters (150 nM) for 10 minutes. B) Representative confocal images of cells expressing treated with β-phorbol esters (150 nM, 10 minutes) expressing CFP-Munc13-1 and either the RIM2a (K97E/K99E, left) that is deficient in Munc13 binding or RIM2a (E36A/R37S, right) which is deficient in Rab3 binding. (C,D) Comparison of basal (gray bars) or stimulated (40mM KCl, black bars) secretion from PC12 cells cotransfected with hGH and indicated protein(s) or an empty vector control. Secretion assays were performed 48 h following transfection. The bath solution containing the secreted hGH was collected, and cells were lysed (2% Triton X-100) to determine total hGH content. Secreted and total hGH was measured from sample aliquots using an hGH enzyme-linked immunosorbent assay kit (Roche Applied Science). bars represent mean hGH secreted relative to total hGH ±standard error of measurement.

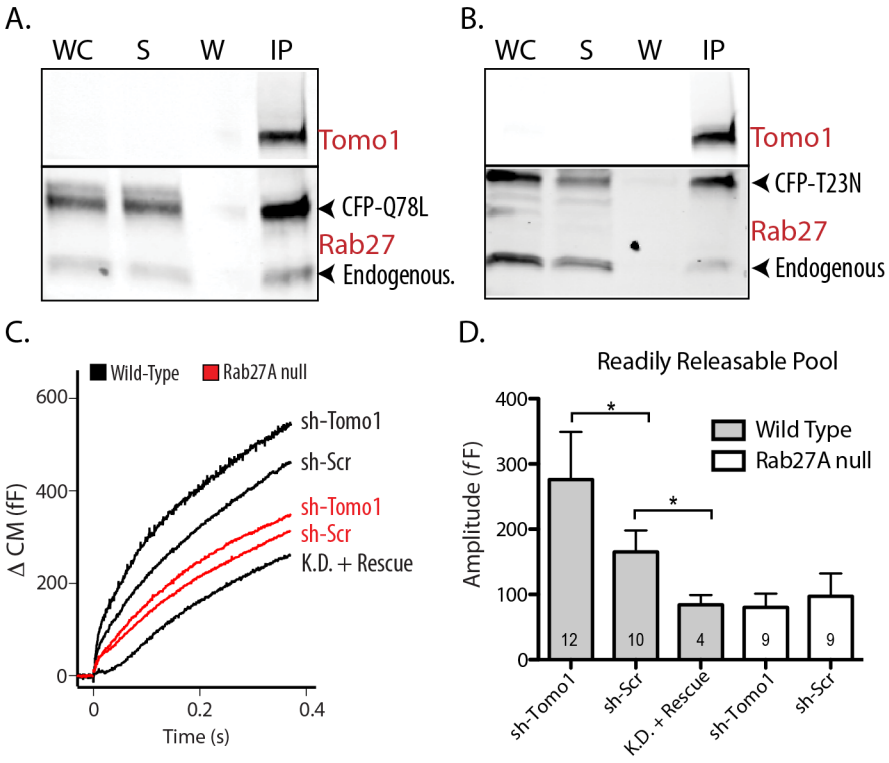
A.
WC
S
W
IP
Tomo1
CFP-Q78L
Rab27
Endogenous.
B.
WC
S
W
IP
Tomo1
CFP-T23N
Rab27
Endogenous
C.
Wild-Type
Rab27A null
600
400
200
0
Δ CM (fF)
sh-Tomo1
sh-Scr
sh-Tomo1
sh-Scr
K.D. + Rescue
0
0.2
0.4
Time (s)
D.
Readily Releasable Pool
400
300
200
100
0
Amplitude (fF)
*
*
Wild Type
Rab27A null
12
10
4
9
9
sh-Tomo1
sh-Scr
K.D. + Rescue
sh-Tomo1
sh-Scr

**Figure 4.3: Evidence for an interaction between Tomo1 and Ra27A.** Western blots showing that IP of overexpressed Tomo1 leads to co-precipitation of (A) CFP-Rab27A (Q78L) and (B) CFP-Rab27 (T23N) from HEK293 cell lysates. (C) Comparisons of mean high time resolution recordings of membrane capacitance changes in electroporated mouse chromaffin cells in response to flash photolysis of caged $Ca^{2+}$ for wild-type (black) and Rab27A null (red) mice. (D) Quantification of data in (C) by fitting curves with a double exponential for each cell, amplitude of the first kinetic phase is taken as a measurement of RRP and averaged across cell for each indicated condition with error bars representing ±standard error of measurement.

## 4.4 Bibliography


1. Rothman JE, Warren G. Implications of the SNARE hypothesis for intracellular membrane topology and dynamics. Current Biology 1994;4:220–233.

2. Söllner T, Whiteheart SW, Brunner M, Erdjument-Bromage H, Geromanos S, Tempst P, Rothman JE. SNAP receptors implicated in vesicle targeting and fusion. , Published online: 25 March 1993; | doi:101038/362318a0 1993;362:318–324.

3. Ohya T, Miaczynska M, Coskun U, Lommer B, Runge A, Drechsel D, Kalaidzidis Y, Zerial M. Reconstitution of Rab- and SNARE-dependent membrane fusion by synthetic endosomes. Nature 2009;459:1091–1097.

4. Grosshans BL, Ortiz D, Novick P. Rabs and their effectors: achieving specificity in membrane traffic. Proc Natl Acad Sci U S A [Internet] 2006;103:11821–11827. Available from: http://www.pnas.org/cgi/doi/10.1073/pnas.0601617103

5. Südhof TC. Function of Rab3 GDP-GTP exchange. 1997;18:519–522.

6. Fukuda M. Distinct Rab binding specificity of Rim1, Rim2, rabphilin, and Noc2. Identification of a critical determinant of Rab3A/Rab27A recognition by Rim2. J Biol Chem 2003;278:15373–15380.

7. Fukuda M. Rab27 and its effectors in secretory granule exocytosis: a novel docking machinery composed of a Rab27.effector complex. Biochem Soc Trans 2006;34:691–695.

8. Cheviet S, Coppola T, Haynes LP, Burgoyne RD, Regazzi R. The Rab-binding protein Noc2 is associated with insulin-containing secretory granules and is essential for pancreatic beta-cell exocytosis. Mol Endocrinol [Internet] 2004;18:117–126. Available from: http://eutils.ncbi.nlm.nih.gov/entrez/eutils/elink.fcgi?dbfrom=pubmed&id=14593078&retmode=ref&cmd=prlinks

9. Pavlos NJ, Grønborg M, Riedel D, Chua JJE, Boyken J, Kloepper TH, Urlaub H, Rizzoli SO, Jahn R. Quantitative analysis of synaptic vesicle Rabs uncovers distinct yet overlapping roles for Rab3a and Rab27b in Ca2+-triggered exocytosis. J Neurosci 2010;30:13441–13453.

10. Fischer von Mollard G, Südhof TC, Jahn R. A small GTP-binding protein dissociates from synaptic vesicles during exocytosis. Nature 1991;349:79–81.

11. Fischer von Mollard G, Stahl B, Khokhlatchev A, Südhof TC, Jahn R. Rab3C is a synaptic vesicle protein that dissociates from synaptic vesicles after stimulation of exocytosis. J Biol Chem 1994;269:10971–10974.

12. Cheng Y, Wang J, Wang Y, Ding M. Synaptotagmin 1 directs repetitive release by

coupling vesicle exocytosis to the Rab3 cycle. Elife 2015;4.

13. Pavlos NJ, Jahn R. Distinct yet overlapping roles of Rab GTPases on synaptic vesicles. Small GTPases 2011;2:77–81.

14. Kimura T, Taniguchi S, Niki I. Actin assembly controlled by GDP-Rab27a is essential for endocytosis of the insulin secretory membrane. Archives of Biochemistry and Biophysics 2010;496:33–37.

15. Handley MTW, Haynes LP, Burgoyne RD. Differential dynamics of Rab3A and Rab27A on secretory granules. Journal of Cell Science 2007;120:973–984.

16. Star EN, Newton AJ, Murthy VN. Real-time imaging of Rab3a and Rab5a reveals differential roles in presynaptic function. J Physiol (Lond) 2005;569:103–117.

17. Rossi G, Brennwald P. Yeast homologues of lethal giant larvae and type V myosin cooperate in the regulation of Rab-dependent vesicle clustering and polarized exocytosis. Mol Biol Cell 2011;22:842–857.

18. Rossi G, Watson K, Demonch M, Temple B, Brennwald P. In vitro reconstitution of Rab GTPase-dependent vesicle clustering by the yeast lethal giant larvae/tomosyn homolog, Sro7. Journal of Biological Chemistry 2015;290:612–624.

19. Yamamoto Y, Mochida S, Kurooka T, Sakisaka T. Reciprocal intramolecular interactions of tomosyn control its inhibitory activity on SNARE complex formation. J Biol Chem 2009;284:12480–12490.

20. Yamamoto Y, Fujikura K, Sakaue M, Okimura K, Kobayashi Y, Nakamura T, Sakisaka T. The tail domain of tomosyn controls membrane fusion through tomosyn displacement by VAMP2. Biochemical and Biophysical Research Communications 2010;399:24–30.

21. Kandel ER, Dudai Y, Mayford MR. The Molecular and Systems Biology of Memory. Cell 2014;157:163–186.

22. Abbott LF, Regehr WG. Synaptic computation. Nature 2004;431:796–803.

23. Feldman DE. The Spike-Timing Dependence of Plasticity. 2012;75:556–571.

24. Jack Waters SJS. Vesicle pool partitioning influences presynaptic diversity and weighting in rat hippocampal synapses. J Physiol (Lond) 2002;541:811–823.

25. Mozhayeva MG, Sara Y, Liu X, Kavalali ET. Development of vesicle pools during maturation of hippocampal synapses. J Neurosci 2002;22:654–665.

26. Ratnayaka A, Marra V, Bush D, Burden JJ, Branco T, Staras K. Recruitment of resting vesicles into recycling pools supports NMDA receptor-dependent synaptic potentiation in cultured hippocampal neurons. J Physiol (Lond) 2012;590:1585–

1597.

27. Ryan TA, Reuter H, Smith SJ. Optical detection of a quantal presynaptic membrane turnover. Nature 1997;388:478–482.

28. Hu Z, Hom S, Kudze T, Tong XJ, Choi S, Aramuni G, Zhang W, Kaplan JM. Neurexin and Neuroligin Mediate Retrograde Synaptic Inhibition in C. elegans. Science 2012;337:980–984.

29. Kim SH, Ryan TA. CDK5 serves as a major control point in neurotransmitter release. 2010;67:797–809.

30. Rose T, Schoenenberger P, Jezek K, Oertner TG. Developmental refinement of vesicle cycling at schaffer collateral synapses. 2013;77:1109–1121.

31. Virmani T, Atasoy D, Kavalali ET. Synaptic vesicle recycling adapts to chronic changes in activity. J Neurosci 2006;26:2197–2206.

32. Yu H, Rathore SS, Gulbranson DR, Shen J. The N- and C-terminal domains of tomosyn play distinct roles in soluble N-ethylmaleimide-sensitive factor attachment protein receptor binding and fusion regulation. Journal of Biological Chemistry 2014;289:25571–25580.

33. Widberg CH, Bryant NJ, Girotti M, Rea S, James DE. Tomosyn interacts with the t-SNAREs syntaxin4 and SNAP23 and plays a role in insulin-stimulated GLUT4 translocation. J Biol Chem 2003;278:35093–35101.

34. Hatsuzawa K, Lang T, Fasshauer D, Bruns D, Jahn R. The R-SNARE motif of tomosyn forms SNARE core complexes with syntaxin 1 and SNAP-25 and down-regulates exocytosis. J Biol Chem 2003;278:31159–31166.

35. Lehman K, Rossi G, Adamo JE, Brennwald P. Yeast homologues of tomosyn and lethal giant larvae function in exocytosis and are associated with the plasma membrane SNARE, Sec9. J Cell Biol 1999;146:125–140.

36. Barak B, Okun E, Ben-Simon Y, Lavi A, Shapira R, Madar R, Wang Y, Norman E, Sheinin A, Pita MA, Yizhar O, Mughal MR, Stuenkel E, van Praag H, Mattson MP, Ashery U. Neuron-specific expression of tomosyn1 in the mouse hippocampal dentate gyrus impairs spatial learning and memory. Neuromolecular medicine 2013;15:351–363.

37. Chen K, Richlitzki A, Featherstone DE, Schwärzel M, Richmond JE. Tomosyn-dependent regulation of synaptic transmission is required for a late phase of associative odor memory. Proceedings of the National Academy of Sciences 2011;108:18482–18487.

38. Gracheva EO, Burdina AO, Holgado AM, Berthelot-Grosjean M, Ackley BD, Hadwiger

G, Nonet ML, Weimer RM, Richmond JE. Tomosyn inhibits synaptic vesicle priming in Caenorhabditis elegans. PLoS Biol 2006;4:e261.

39. McEwen JM, Madison JM, Dybbs M, Kaplan JM. Antagonistic regulation of synaptic vesicle priming by Tomosyn and UNC-13. 2006;51:303–315.

40. Sakisaka T, Yamamoto Y, Mochida S, Nakamura M, Nishikawa K, Ishizaki H, Okamoto-Tanaka M, Miyoshi J, Fujiyoshi Y, Manabe T, Takai Y. Dual inhibition of SNARE complex formation by tomosyn ensures controlled neurotransmitter release. J Cell Biol 2008;183:323–337.

41. Nagano K, Takeuchi H, Gao J, Mori Y, Otani T, Wang D, Hirata M. Tomosyn is a novel Akt substrate mediating insulin-dependent GLUT4 exocytosis. International Journal of Biochemistry and Cell Biology 2015;62:62–71.

42. Yizhar O, Lipstein N, Gladycheva SE, Matti U, Ernst SA, Rettig J, Stuenkel EL, Ashery U. Multiple functional domains are involved in tomosyn regulation of exocytosis. J Neurochem 2007;103:604–616.

43. Yizhar O, Matti U, Melamed R, Hagalili Y, Bruns D, Rettig J, Ashery U. Tomosyn inhibits priming of large dense-core vesicles in a calcium-dependent manner. Proc Natl Acad Sci U S A 2004;101:2578–2583.

44. Zhang W, Lilja L, Mandic SA, Gromada J, Smidt K, Janson J, Takai Y, Bark C, Berggren P-O, Meister B. Tomosyn is expressed in beta-cells and negatively regulates insulin exocytosis. Diabetes 2006;55:574–581.

45. Baba T, Sakisaka T, Mochida S, Takai Y. PKA-catalyzed phosphorylation of tomosyn and its implication in Ca2+-dependent exocytosis of neurotransmitter. J Cell Biol 2005;170:1113–1125.

46. Cheviet S, Bezzi P, Ivarsson R, Renström E, Viertl D, Kasas S, Catsicas S, Regazzi R. Tomosyn-1 is involved in a post-docking event required for pancreatic beta-cell exocytosis. Journal of Cell Science 2006;119:2912–2920.

47. Zhu Q, Yamakuchi M, Ture S, la Luz Garcia-Hernandez de M, Ko KA, Modjeski KL, LoMonaco MB, Johnson AD, O'Donnell CJ, Takai Y, Morrell CN, Lowenstein CJ. Syntaxin-binding protein STXBP5 inhibits endothelial exocytosis and promotes platelet secretion. J Clin Invest 2014;124:4503–4516.

48. Fasshauer D, Otto H, Eliason WK, Jahn R, Brünger AT. Structural changes are associated with soluble N-ethylmaleimide-sensitive fusion protein attachment protein receptor complex formation. J Biol Chem 1997;272:28036–28041.

49. Pobbati AV, Stein A, Fasshauer D. N- to C-terminal SNARE complex assembly promotes rapid membrane fusion. Science 2006;313:673–676.

50. Holz RW, Brondyk WH, Senter RA, Kuizon L, Macara IG. Evidence for the involvement of Rab3A in Ca(2+)-dependent exocytosis from adrenal chromaffin cells. J Biol Chem 1994;269:10229–10234.

51. Müller M, Pym ECG, Tong A, Davis GW. Rab3-GAP Controls the Progression of Synaptic Homeostasis at a Late Stage of Vesicle Release. Neuron 2011;69:749–762.

52. L Johannes PMLMRJDVJPHFD. The GTPase Rab3a negatively controls calcium-dependent exocytosis in neuroendocrine cells. EMBO J 1994;13:2029.

53. Lin CG, Pan CY, Kao L-S. Rab3A delayed catecholamine secretion from bovine adrenal chromaffin cells. Biochemical and Biophysical Research Communications 1996;221:675–681.

54. Porte D, Kahn SE. beta-cell dysfunction and failure in type 2 diabetes: potential mechanisms. Diabetes 2001;50 Suppl 1:S160–3.

55. Seino S, Takahashi H, Takahashi T, Shibasaki T. Treating diabetes today: a matter of selectivity of sulphonylureas. Diabetes Obes Metab 2012;14 Suppl 1:9–13.

56. Izumi T. Heterogeneous modes of insulin granule exocytosis: molecular determinants. Front Biosci (Landmark Ed) 2011;16:360–367.

57. Ohara-Imaizumi M, Nagamatsu S. Insulin exocytotic mechanism by imaging technique. J Biochem 2006;140:1–5.

58. Kashima Y, Miki T, Shibasaki T, Ozaki N, Miyazaki M, Yano H, Seino S. Critical role of cAMP-GEFII--Rim2 complex in incretin-potentiated insulin secretion. J Biol Chem 2001;276:46046–46053.

59. Fukuda M. Versatile Role of Rab27 in Membrane Trafficking: Focus on the Rab27 Effector Families. J Biochem 2005;137:9–16.

60. Zerial M, McBride H. Rab proteins as membrane organizers. Nat Rev Mol Cell Biol 2001;2:107–117.

61. Regazzi R, Ravazzola M, Iezzi M, Lang J, Zahraoui A, Andereggen E, Morel P, Takai Y, Wollheim CB. Expression, localization and functional role of small GTPases of the Rab3 family in insulin-secreting cells. Journal of Cell Science 1996;109 ( Pt 9):2265–2273.

62. Yasuda T, Shibasaki T, Minami K, Takahashi H, Mizoguchi A, Uriu Y, Numata T, Mori Y, Miyazaki J-I, Miki T, Seino S. Rim2alpha determines docking and priming states in insulin granule exocytosis. Cell Metab 2010;12:117–129.

63. Neher E, Sakaba T. Multiple roles of calcium ions in the regulation of neurotransmitter release. 2008;59:861–872.

64. Ariel P, Ryan TA. Optical mapping of release properties in synapses. Front Neural Circuits 2010;4.

65. Rosenmund C, Stevens CF. Definition of the readily releasable pool of vesicles at hippocampal synapses. 1996;16:1197–1207.

66. Stevens CF, Williams JH. Discharge of the readily releasable pool with action potentials at hippocampal synapses. 2007;98:3221–3229. Available from: http://jn.physiology.org/cgi/doi/10.1152/jn.00857.2007

67. Dobrunz LE, Stevens CF. Heterogeneity of release probability, facilitation, and depletion at central synapses. 1997;18:995–1008.

68. Moulder KL, Mennerick S. Reluctant vesicles contribute to the total readily releasable pool in glutamatergic hippocampal neurons. J Neurosci 2005;25:3842–3850.

69. Rizzoli SO, Betz WJ. Synaptic vesicle pools. Nat Rev Neurosci 2005;6:57–69.

70. Ariel P, Hoppa MB, Ryan TA. Intrinsic variability in Pv, RRP size, Ca(2+) channel repertoire, and presynaptic potentiation in individual synaptic boutons. Front Syn Neurosci 2012;4:9.

71. Barak B, Williams A, Bielopolski N, Gottfried I, Okun E, Brown MA, Matti U, Rettig J, Stuenkel EL, Ashery U. Tomosyn Expression Pattern in the Mouse Hippocampus Suggests Both Presynaptic and Postsynaptic Functions. Front Neuroanat 2010;4.

72. Groffen AJA, Jacobsen L, Schut D, Verhage M. Two distinct genes drive expression of seven tomosyn isoforms in the mammalian brain, sharing a conserved structure with a unique variable domain. J Neurochem 2005;92:554–568.

73. Sakisaka T, Baba T, Tanaka S, Izumi G, Yasumi M, Takai Y. Regulation of SNAREs by tomosyn and ROCK: implication in extension and retraction of neurites. J Cell Biol 2004;166:17–25.

74. Yuste R. The discovery of dendritic spines by Cajal. Front Neuroanat 2015;9.

75. Yuste R, Denk W. Dendritic spines as basic functional units of neuronal integration. Nature 1995;375:682–684.

76. Matsuzaki M, Honkura N, Ellis-Davies GCR, Kasai H. Structural basis of long-term potentiation in single dendritic spines. Nature 2004;429:761–766.

77. Murakoshi H, Wang H, Yasuda R. Local, persistent activation of Rho GTPases during plasticity of single dendritic spines. - PubMed - NCBI. Nature 2011;472:100–104.

78. Dailey ME, Smith SJ. The dynamics of dendritic structure in developing hippocampal slices. Journal of Neuroscience 1996;16:2983–2994.

79. Crawford DC, Mennerick S. Presynaptically silent synapses: dormancy and awakening of presynaptic vesicle release. Neuroscientist 2012;18:216–223.

80. Joan Stiles TLJ. The Basics of Brain Development. Neuropsychology Review 2010;20:327–348.

81. Dulubova I, Lou X, Lu J, Huryeva I, Alam A, Schneggenburger R, Südhof TC, Rizo J. A Munc13/RIM/Rab3 tripartite complex: from priming to plasticity? EMBO J 2005;24:2839–2850.

82. Kaeser PS, Deng L, Wang Y, Dulubova I, Liu X, Rizo J, Südhof TC. RIM proteins tether Ca2+ channels to presynaptic active zones via a direct PDZ-domain interaction. Cell 2011;144:282–295.

83. Han Y, Kaeser PS, Südhof TC, Schneggenburger R. RIM determines $Ca^2$+ channel density and vesicle docking at the presynaptic active zone. 2011;69:304–316.

84. Deng L, Kaeser PS, Xu W, Südhof TC. RIM Proteins Activate Vesicle Priming by Reversing Autoinhibitory Homodimerization of Munc13. 2011;69:317–331.

85. Basu J, Betz A, Brose N, Rosenmund C. Munc13-1 C1 domain activation lowers the energy barrier for synaptic vesicle fusion. J Neurosci 2007;27:1200–1210.

86. BETZ A, Ashery U, Rickmann M, Augustin I, NEHER E, Südhof TC, Rettig J, Brose N. Munc13-1 is a presynaptic phorbol ester receptor that enhances neurotransmitter release. 1998;21:123–136.

87. Shin O-H, Lu J, Rhee J-S, Tomchick DR, Pang ZP, Wojcik SM, Camacho-Perez M, Brose N, Machius M, Rizo J, Rosenmund C, Südhof TC. Munc13 C2B domain is an activity-dependent Ca2+ regulator of synaptic exocytosis. Nat Struct Mol Biol 2010;17:280–288.

88. Junge HJ, Rhee J-S, Jahn O, Varoqueaux F, Spiess J, Waxham MN, Rosenmund C, Brose N. Calmodulin and Munc13 Form a Ca2+ Sensor/Effector Complex that Controls Short-Term Synaptic Plasticity. Cell 2004;118:389–401.

89. Wierda KDB, Toonen RFG, de Wit H, Brussaard AB, Verhage M. Interdependence of PKC-Dependent and PKC-Independent Pathways for Presynaptic Plasticity. 2007;54:275–290.

90. Rhee J-S, Betz A, Pyott S, Reim K, Varoqueaux F, Augustin I, Hesse D, Südhof TC, Takahashi M, Rosenmund C, Brose N. Beta phorbol ester- and diacylglycerol-induced augmentation of transmitter release is mediated by Munc13s and not by PKCs. Cell 2002;108:121–133.

91. Wick PF, Senter RA, Parsels LA, Uhler MD, Holz RW. Transient transfection studies of secretion in bovine chromaffin cells and PC12 cells. Generation of kainate-sensitive

chromaffin cells. J Biol Chem 1993;268:10983–10989.

92. Hu Z, Tong X-J, Kaplan JM. UNC-13L, UNC-13S, and Tomosyn form a protein code for fast and slow neurotransmitter release in Caenorhabditis elegans. Elife 2013;2:e00967.

93. Bustos MA, Lucchesi O, Ruete MC, Mayorga LS, Tomes CN. Rab27 and Rab3 sequentially regulate human sperm dense-core granule exocytosis. Proceedings of the National Academy of Sciences 2012;109:E2057–66.